A Comprehensive Introduction to Superconductivity

Mollie Reichert

First Edition, 2012

ISBN 978-81-323-4059-1

Published by:
White Word Publications
4735/22 Prakashdeep Bldg,
Ansari Road, Darya Ganj,
Delhi - 110002
Email: info@wtbooks.com

Table of Contents

Chapter 1

Superconductivity

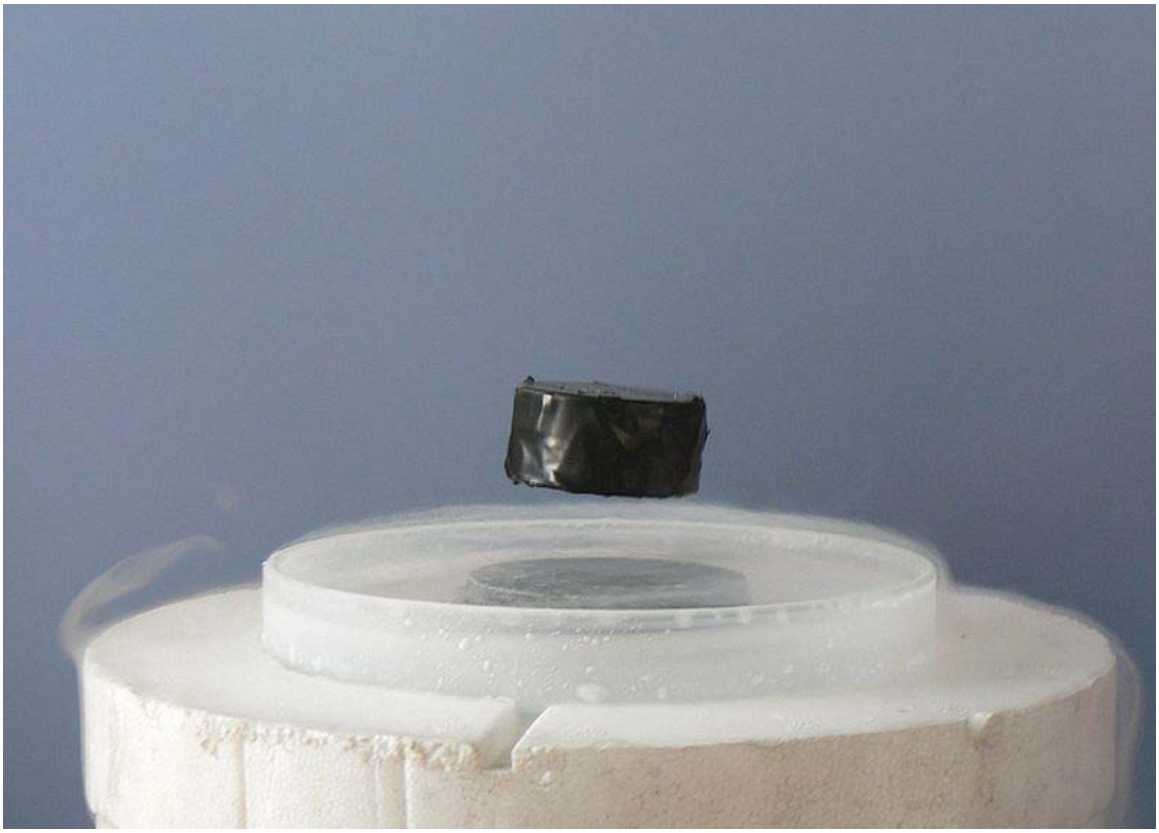

A magnet levitating above a high-temperature superconductor, cooled with liquid nitrogen. Persistent electric current flows on the surface of the superconductor, acting to exclude the magnetic field of the magnet (the Faraday's law of induction). This current effectively forms an electromagnet that repels the magnet.

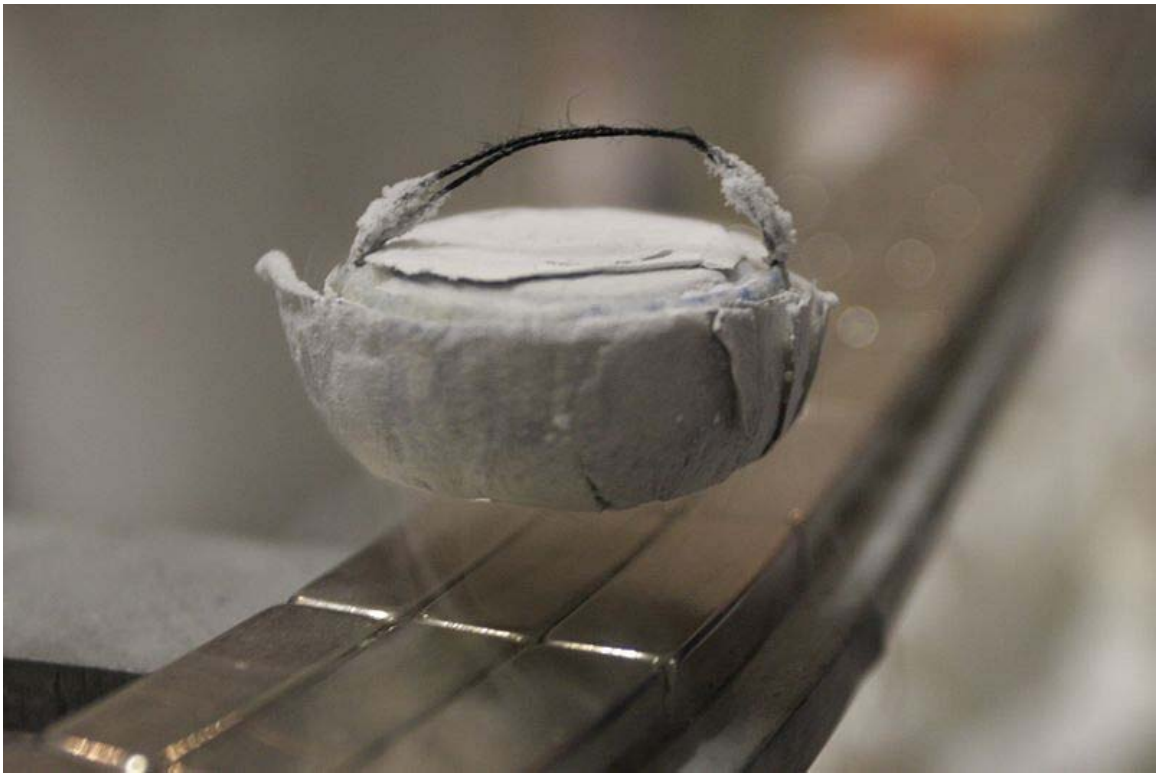

A high-temperature superconductor levitating above a magnet

Superconductivity is an electrical resistance of exactly zero which occurs in certain materials below a characteristic temperature. It was discovered by Heike Kamerlingh Onnes on April 8, 1911 in Leiden. Like ferromagnetism and atomic spectral lines, superconductivity is a quantum mechanical phenomenon. It is also characterized by a phenomenon called the Meissner effect, the ejection of any sufficiently weak magnetic field from the interior of the superconductor as it transitions into the superconducting state. The occurrence of the Meissner effect indicates that superconductivity cannot be understood simply as the idealization of *perfect conductivity* in classical physics.

The electrical resistivity of a metallic conductor decreases gradually as the temperature is lowered. However, in ordinary conductors such as copper and silver, this decrease is limited by impurities and other defects. Even near absolute zero, a real sample of copper shows some resistance. Despite these imperfections, in a superconductor the resistance drops abruptly to zero when the material is cooled below its critical temperature. An electric current flowing in a loop of superconducting wire can persist indefinitely with no power source.

In 1986, it was discovered that some cuprate-perovskite ceramic materials have critical temperatures above 90 K (−183 °C). These high-temperature superconductors renewed interest in the topic because of the prospects for improvement and potential room-temperature superconductivity. From a practical perspective, even 90 K is relatively easy to reach with readily available liquid nitrogen (which has a boiling point of 77 K), resulting in more experiments and applications.

Classification

There is not just one criterion to classify superconductors. The most common are

- **By their physical properties**: they can be *Type I* (if their phase transition is of first order) or *Type II* (if their phase transition is of second order).
- **By the theory to explain them**: they can be *conventional* (if they are explained by the BCS theory or its derivatives) or *unconventional* (if not).
- **By their critical temperature**: they can be *high temperature* (generally considered if they reach the superconducting state just cooling them with liquid nitrogen, that is, if $T_c > 77$ K), or *low temperature* (generally if they need other techniques to be cooled under their critical temperature).
- **By material**: they can be chemical elements (as mercury or lead), alloys (as niobium-titanium or germanium-niobium), ceramics (as YBCO or the magnesium diboride), or organic superconductors (as fullerenes or carbon nanotubes, which technically might be included among the chemical elements as they are made of carbon).

Elementary properties of superconductors

Most of the physical properties of superconductors vary from material to material, such as the heat capacity and the critical temperature, critical field, and critical current density at which superconductivity is destroyed.

On the other hand, there is a class of properties that are independent of the underlying material. For instance, all superconductors have *exactly* zero resistivity to low applied currents when there is no magnetic field present or if the applied field does not exceed a critical value. The existence of these "universal" properties implies that superconductivity is a thermodynamic phase, and thus possesses certain distinguishing properties which are largely independent of microscopic details.

Zero electrical DC resistance

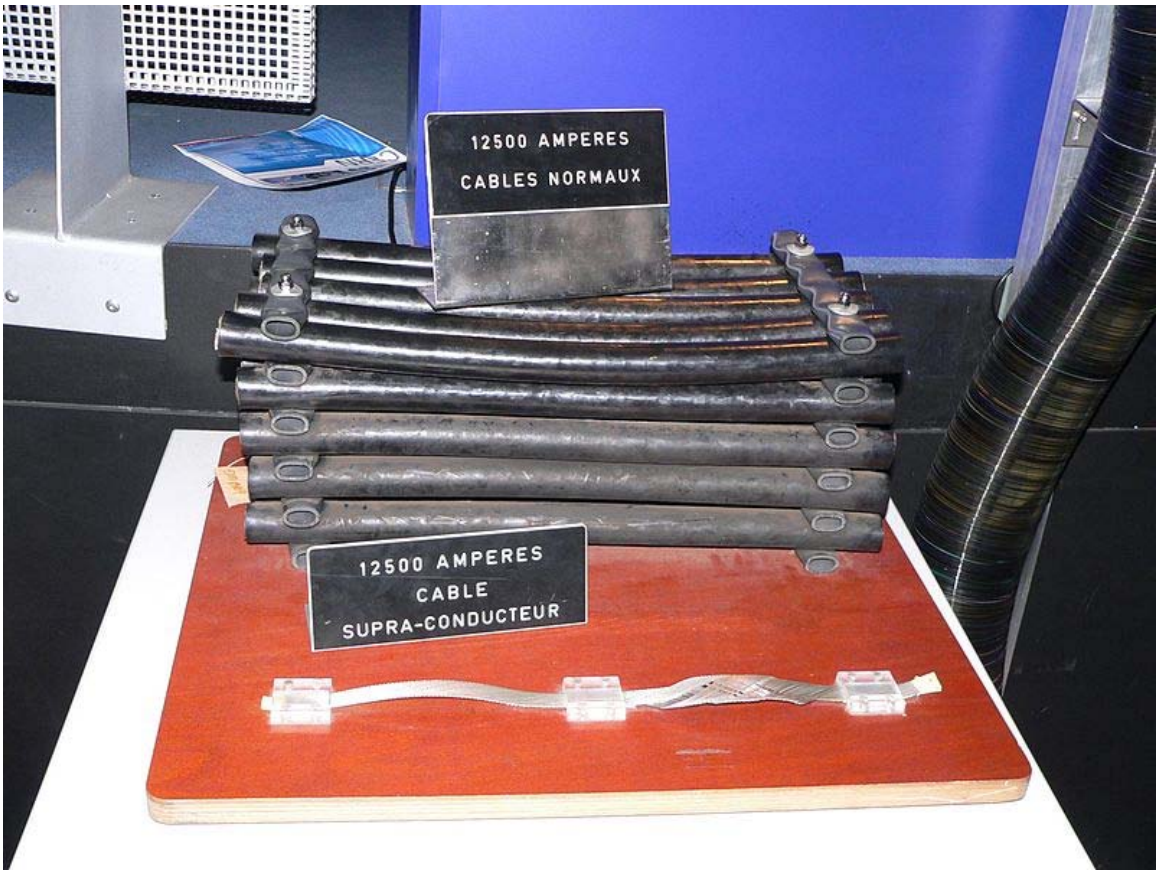

Electric cables for accelerators at CERN: top, regular cables for LEP; bottom, superconducting cables for the LHC.

The simplest method to measure the electrical resistance of a sample of some material is to place it in an electrical circuit in series with a current source I and measure the resulting voltage V across the sample. The resistance of the sample is given by Ohm's law as $R = V/I$. If the voltage is zero, this means that the resistance is zero and that the sample is in the superconducting state.

Superconductors are also able to maintain a current with no applied voltage whatsoever, a property exploited in superconducting electromagnets such as those found in MRI machines. Experiments have demonstrated that currents in superconducting coils can persist for years without any measurable degradation. Experimental evidence points to a current lifetime of at least 100,000 years. Theoretical estimates for the lifetime of a persistent current can exceed the estimated lifetime of the universe, depending on the wire geometry and the temperature.

In a normal conductor, an electric current may be visualized as a fluid of electrons moving across a heavy ionic lattice. The electrons are constantly colliding with the ions in the lattice, and during each collision some of the energy carried by the current is absorbed by the lattice and converted into heat, which is essentially the vibrational kinetic

energy of the lattice ions. As a result, the energy carried by the current is constantly being dissipated. This is the phenomenon of electrical resistance.

The situation is different in a superconductor. In a conventional superconductor, the electronic fluid cannot be resolved into individual electrons. Instead, it consists of bound *pairs* of electrons known as Cooper pairs. This pairing is caused by an attractive force between electrons from the exchange of phonons. Due to quantum mechanics, the energy spectrum of this Cooper pair fluid possesses an *energy gap*, meaning there is a minimum amount of energy ΔE that must be supplied in order to excite the fluid. Therefore, if ΔE is larger than the thermal energy of the lattice, given by kT, where k is Boltzmann's constant and T is the temperature, the fluid will not be scattered by the lattice. The Cooper pair fluid is thus a superfluid, meaning it can flow without energy dissipation.

In a class of superconductors known as type II superconductors, including all known high-temperature superconductors, an extremely small amount of resistivity appears at temperatures not too far below the nominal superconducting transition when an electric current is applied in conjunction with a strong magnetic field, which may be caused by the electric current. This is due to the motion of vortices in the electronic superfluid, which dissipates some of the energy carried by the current. If the current is sufficiently small, the vortices are stationary, and the resistivity vanishes. The resistance due to this effect is tiny compared with that of non-superconducting materials, but must be taken into account in sensitive experiments. However, as the temperature decreases far enough below the nominal superconducting transition, these vortices can become frozen into a disordered but stationary phase known as a "vortex glass". Below this vortex glass transition temperature, the resistance of the material becomes truly zero.

Superconducting phase transition

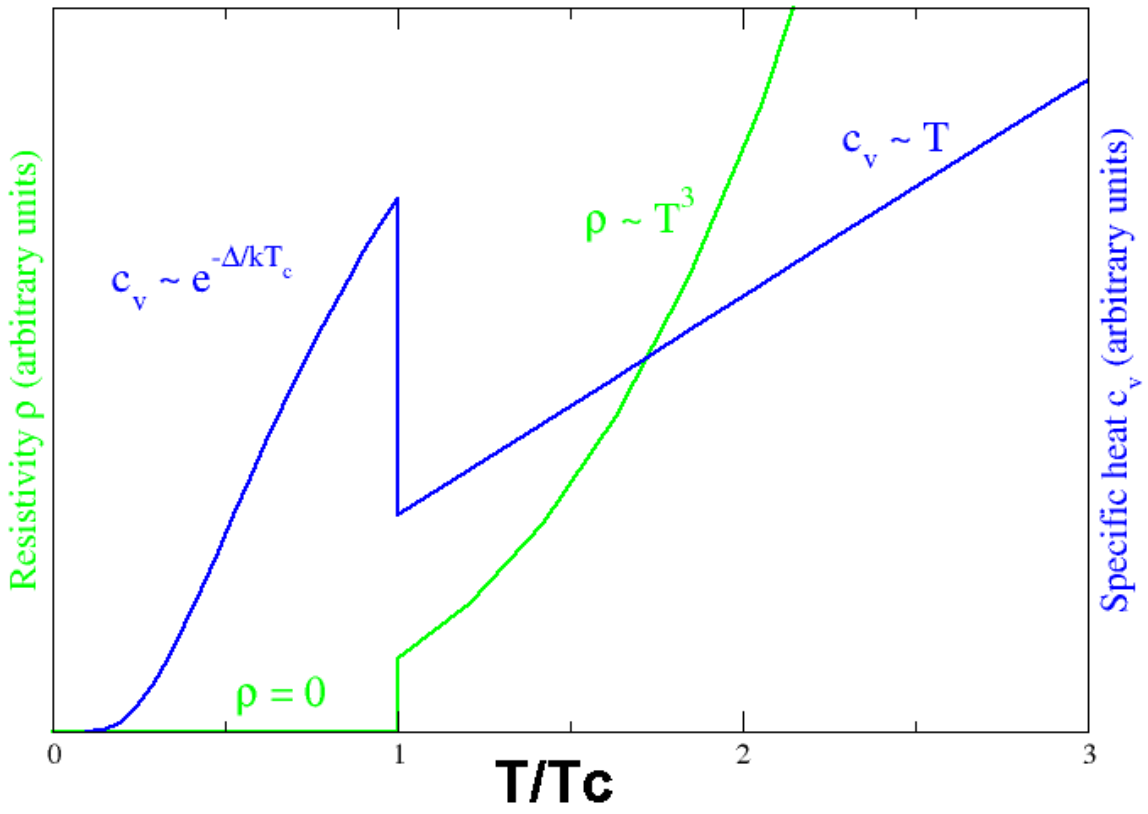

Behavior of heat capacity (c_v, blue) and resistivity (ρ, green) at the superconducting phase transition

In superconducting materials, the characteristics of superconductivity appear when the temperature *T* is lowered below a **critical temperature** T_c. The value of this critical temperature varies from material to material. Conventional superconductors usually have critical temperatures ranging from around 20 K to less than 1 K. Solid mercury, for example, has a critical temperature of 4.2 K. As of 2009, the highest critical temperature found for a conventional superconductor is 39 K for magnesium diboride (MgB_2), although this material displays enough exotic properties that there is some doubt about classifying it as a "conventional" superconductor. Cuprate superconductors can have much higher critical temperatures: $YBa_2Cu_3O_7$, one of the first cuprate superconductors to be discovered, has a critical temperature of 92 K, and mercury-based cuprates have been found with critical temperatures in excess of 130 K. The explanation for these high critical temperatures remains unknown. Electron pairing due to phonon exchanges explains superconductivity in conventional superconductors, but it does not explain superconductivity in the newer superconductors that have a very high critical temperature.

Similarly, at a fixed temperature below the critical temperature, superconducting materials cease to superconduct when an external magnetic field is applied which is greater than the *critical magnetic field*. This is because the Gibbs free energy of the

superconducting phase increases quadratically with the magnetic field while the free energy of the normal phase is roughly independent of the magnetic field. If the material superconducts in the absence of a field, then the superconducting phase free energy is lower than that of the normal phase and so for some finite value of the magnetic field (proportional to the square root of the difference of the free energies at zero magnetic field) the two free energies will be equal and a phase transition to the normal phase will occur. More generally, a higher temperature and a stronger magnetic field lead to a smaller fraction of the electrons in the superconducting band and consequently a longer London penetration depth of external magnetic fields and currents. The penetration depth becomes infinite at the phase transition.

The onset of superconductivity is accompanied by abrupt changes in various physical properties, which is the hallmark of a phase transition. For example, the electronic heat capacity is proportional to the temperature in the normal (non-superconducting) regime. At the superconducting transition, it suffers a discontinuous jump and thereafter ceases to be linear. At low temperatures, it varies instead as $e^{-\alpha/T}$ for some constant, α. This exponential behavior is one of the pieces of evidence for the existence of the energy gap.

The order of the superconducting phase transition was long a matter of debate. Experiments indicate that the transition is second-order, meaning there is no latent heat. However in the presence of an external magnetic field there is latent heat, as a result of the fact that the superconducting phase has a lower entropy below the critical temperature than the normal phase. It has been experimentally demonstrated that, as a consequence, when the magnetic field is increased beyond the critical field, the resulting phase transition leads to a decrease in the temperature of the superconducting material.

Calculations in the 1970s suggested that it may actually be weakly first-order due to the effect of long-range fluctuations in the electromagnetic field. In the 1980s it was shown theoretically with the help of a disorder field theory, in which the vortex lines of the superconductor play a major role, that the transition is of second order within the type II regime and of first order (i.e., latent heat) within the type I regime, and that the two regions are separated by a tricritical point. The results were confirmed by Monte Carlo computer simulations.

Meissner effect

When a superconductor is placed in a weak external magnetic field **H**, and cooled below its transition temperature, the magnetic field is ejected. The Meissner effect does not cause the field to be completely ejected but instead the field penetrates the superconductor but only to a very small distance, characterized by a parameter λ, called the London penetration depth, decaying exponentially to zero within the bulk of the material. The Meissner effect is a defining characteristic of superconductivity. For most superconductors, the London penetration depth is on the order of 100 nm.

The Meissner effect is sometimes confused with the kind of diamagnetism one would expect in a perfect electrical conductor: according to Lenz's law, when a *changing*

magnetic field is applied to a conductor, it will induce an electric current in the conductor that creates an opposing magnetic field. In a perfect conductor, an arbitrarily large current can be induced, and the resulting magnetic field exactly cancels the applied field.

The Meissner effect is distinct from this—it is the spontaneous expulsion which occurs during transition to superconductivity. Suppose we have a material in its normal state, containing a constant internal magnetic field. When the material is cooled below the critical temperature, we would observe the abrupt expulsion of the internal magnetic field, which we would not expect based on Lenz's law.

The Meissner effect was given a phenomenological explanation by the brothers Fritz and Heinz London, who showed that the electromagnetic free energy in a superconductor is minimized provided

$$\nabla^2 \mathbf{H} = \lambda^{-2} \mathbf{H}$$

where **H** is the magnetic field and λ is the London penetration depth.

This equation, which is known as the London equation, predicts that the magnetic field in a superconductor decays exponentially from whatever value it possesses at the surface.

A superconductor with little or no magnetic field within it is said to be in the Meissner state. The Meissner state breaks down when the applied magnetic field is too large. Superconductors can be divided into two classes according to how this breakdown occurs. In Type I superconductors, superconductivity is abruptly destroyed when the strength of the applied field rises above a critical value H_c. Depending on the geometry of the sample, one may obtain an intermediate state consisting of a baroque pattern of regions of normal material carrying a magnetic field mixed with regions of superconducting material containing no field. In Type II superconductors, raising the applied field past a critical value H_{c1} leads to a mixed state (also known as the vortex state) in which an increasing amount of magnetic flux penetrates the material, but there remains no resistance to the flow of electric current as long as the current is not too large. At a second critical field strength H_{c2}, superconductivity is destroyed. The mixed state is actually caused by vortices in the electronic superfluid, sometimes called fluxons because the flux carried by these vortices is quantized. Most pure elemental superconductors, except niobium, technetium, vanadium and carbon nanotubes, are Type I, while almost all impure and compound superconductors are Type II.

London moment

Conversely, a spinning superconductor generates a magnetic field, precisely aligned with the spin axis. The effect, the London moment, was put to good use in Gravity Probe B. This experiment measured the magnetic fields of four superconducting gyroscopes to determine their spin axes. This was critical to the experiment since it is one of the few ways to accurately determine the spin axis of an otherwise featureless sphere.

Theories of superconductivity

Since the discovery of superconductivity, great efforts have been devoted to finding out how and why it works. During the 1950s, theoretical condensed matter physicists arrived at a solid understanding of "conventional" superconductivity, through a pair of remarkable and important theories: the phenomenological Ginzburg-Landau theory (1950) and the microscopic BCS theory (1957). Generalizations of these theories form the basis for understanding the closely related phenomenon of superfluidity, because they fall into the Lambda transition universality class, but the extent to which similar generalizations can be applied to unconventional superconductors as well is still controversial. The four-dimensional extension of the Ginzburg-Landau theory, the Coleman-Weinberg model, is important in quantum field theory and cosmology.

History of superconductivity

Superconductivity was discovered on April 8, 1911 by Heike Kamerlingh Onnes, who was studying the resistance of solid mercury at cryogenic temperatures using the recently-produced liquid helium as a refrigerant. At the temperature of 4.2 K, he observed that the resistance abruptly disappeared. In the same experiment, he also observed the superfluid transition of helium at 2.2 K, without recognizing its significance. (The precise date and circumstances of the discovery were only reconstructed a century later, when Onnes's notebook was found.) In subsequent decades, superconductivity was observed in several other materials. In 1913, lead was found to superconduct at 7 K, and in 1941 niobium nitride was found to superconduct at 16 K.

The next important step in understanding superconductivity occurred in 1933, when Meissner and Ochsenfeld discovered that superconductors expelled applied magnetic fields, a phenomenon which has come to be known as the Meissner effect. In 1935, F. and H. London showed that the Meissner effect was a consequence of the minimization of the electromagnetic free energy carried by superconducting current.

In 1950, the phenomenological Ginzburg-Landau theory of superconductivity was devised by Landau and Ginzburg. This theory, which combined Landau's theory of second-order phase transitions with a Schrödinger-like wave equation, had great success in explaining the macroscopic properties of superconductors. In particular, Abrikosov showed that Ginzburg-Landau theory predicts the division of superconductors into the two categories now referred to as Type I and Type II. Abrikosov and Ginzburg were awarded the 2003 Nobel Prize for their work (Landau had received the 1962 Nobel Prize for other work, and died in 1968).

Also in 1950, Maxwell and Reynolds *et al.* found that the critical temperature of a superconductor depends on the isotopic mass of the constituent element. This important discovery pointed to the electron-phonon interaction as the microscopic mechanism responsible for superconductivity.

The complete microscopic theory of superconductivity was finally proposed in 1957 by Bardeen, Cooper and Schrieffer. Independently, the superconductivity phenomenon was explained by Nikolay Bogolyubov. This BCS theory explained the superconducting current as a superfluid of Cooper pairs, pairs of electrons interacting through the exchange of phonons. For this work, the authors were awarded the Nobel Prize in 1972.

The BCS theory was set on a firmer footing in 1958, when Bogolyubov showed that the BCS wavefunction, which had originally been derived from a variational argument, could be obtained using a canonical transformation of the electronic Hamiltonian. In 1959, Lev Gor'kov showed that the BCS theory reduced to the Ginzburg-Landau theory close to the critical temperature.

In 1962, the first commercial superconducting wire, a niobium-titanium alloy, was developed by researchers at Westinghouse, allowing the construction of the first practical superconducting magnets. In the same year, Josephson made the important theoretical prediction that a supercurrent can flow between two pieces of superconductor separated by a thin layer of insulator. This phenomenon, now called the Josephson effect, is exploited by superconducting devices such as SQUIDs. It is used in the most accurate available measurements of the magnetic flux quantum $\Phi_0 = \frac{h}{2e}$, and thus (coupled with the quantum Hall resistivity) for Planck's constant *h*. Josephson was awarded the Nobel Prize for this work in 1973.

In 2008, it was discovered that the same mechanism that produces superconductivity could produce a superinsulator state in some materials, with almost infinite electrical resistance.

High-temperature superconductivity

Until 1986, physicists had believed that BCS theory forbade superconductivity at temperatures above about 30 K. In that year, Bednorz and Müller discovered superconductivity in a lanthanum-based cuprate perovskite material, which had a transition temperature of 35 K (Nobel Prize in Physics, 1987). It was soon found that replacing the lanthanum with yttrium (i.e., making YBCO) raised the critical temperature to 92 K, which was important because liquid nitrogen could then be used as a refrigerant (at atmospheric pressure, the boiling point of nitrogen is 77 K). This is important commercially because liquid nitrogen can be produced cheaply on-site from air, and is not prone to some of the problems (for instance solid air plugs) of helium in piping. Many other cuprate superconductors have since been discovered, and the theory of superconductivity in these materials is one of the major outstanding challenges of theoretical condensed matter physics.

From about 1993, the highest temperature superconductor was a ceramic material consisting of thallium, mercury, copper, barium, calcium and oxygen ($HgBa_2Ca_2Cu_3O_{8+\delta}$) with T_c = 138 K.

In February 2008, an iron-based family of high-temperature superconductors was discovered. Hideo Hosono, of the Tokyo Institute of Technology, and colleagues found lanthanum oxygen fluorine iron arsenide ($LaO_{1-x}F_xFeAs$), an oxypnictide that superconducts below 26 K. Replacing the lanthanum in $LaO_{1-x}F_xFeAs$ with samarium leads to superconductors that work at 55 K.

Crystal structure of high-temperature ceramic superconductors

The structure of a high-T_c superconductor is closely related to perovskite structure, and the structure of these compounds has been described as a distorted, oxygen deficient multi-layered perovskite structure. One of the properties of the crystal structure of oxide superconductors is an alternating multi-layer of CuO_2 planes with superconductivity taking place between these layers. The more layers of CuO_2 the higher T_c. This structure causes a large anisotropy in normal conducting and superconducting properties, since electrical currents are carried by holes induced in the oxygen sites of the CuO_2 sheets. The electrical conduction is highly anisotropic, with a much higher conductivity parallel to the CuO_2 plane than in the perpendicular direction. Generally, Critical temperatures depend on the chemical compositions, cations substitutions and oxygen content. They can be classified as superstripes; i.e., particular realizations of superlattices at atomic limit made of superconducting atomic layers, wires, dots separated by spacer layers, that gives multiband and multigap superconductivy.

YBCO superconductors

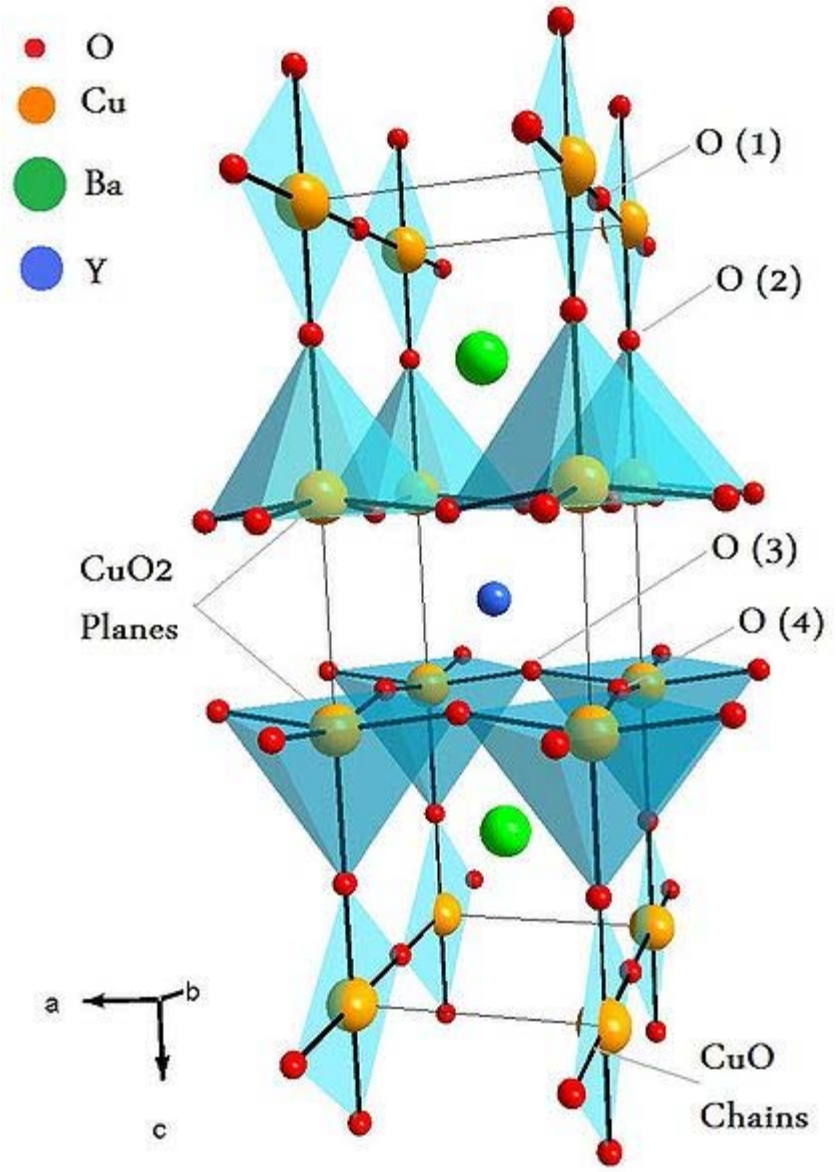

YBCO unit cell

The first superconductor found with $T_c > 77$ K (liquid nitrogen boiling point) is yttrium barium copper oxide ($YBa_2Cu_3O_{7-x}$), the proportions of the 3 different metals in the $YBa_2Cu_3O_7$ superconductor are in the mole ratio of 1 to 2 to 3 for yttrium to barium to copper respectively. Thus, this particular superconductor is often referred to as the 123 superconductor.

The unit cell of $YBa_2Cu_3O_7$ consists of three pseudocubic elementary perovskite unit cells. Each perovskite unit cell contains a Y or Ba atom at the center: Ba in the bottom unit cell, Y in the middle one, and Ba in the top unit cell. Thus, Y and Ba are stacked in

the sequence [Ba–Y–Ba] along the c-axis. All corner sites of the unit cell are occupied by Cu, which has two different coordinations, Cu(1) and Cu(2), with respect to oxygen. There are four possible crystallographic sites for oxygen: O(1), O(2), O(3) and O(4). The coordination polyhedra of Y and Ba with respect to oxygen are different. The tripling of the perovskite unit cell leads to nine oxygen atoms, whereas $YBa_2Cu_3O_7$ has seven oxygen atoms and, therefore, is referred to as an oxygen-deficient perovskite structure. The structure has a stacking of different layers: $(CuO)(BaO)(CuO_2)(Y)(CuO_2)(BaO)(CuO)$. One of the key feature of the unit cell of $YBa_2Cu_3O_{7-x}$ (YBCO) is the presence of two layers of CuO_2. The role of the Y plane is to serve as a spacer between two CuO_2 planes. In YBCO, the Cu–O chains are known to play an important role for superconductivity. T_c is maximal near 92 K when $x \approx 0.15$ and the structure is orthorhombic. Superconductivity disappears at $x \approx 0.6$, where the structural transformation of YBCO occurs from orthorhombic to tetragonal.

Bi-, Tl- and Hg-based high-T_c superconductors

The crystal structure of Bi-, Tl- and Hg-based high-T_c superconductors are very similar. Like YBCO, the perovskite-type feature and the presence of CuO_2 layers also exist in these superconductors. However, unlike YBCO, Cu–O chains are not present in these superconductors. The YBCO superconductor has an orthorhombic structure, whereas the other high-T_c superconductors have a tetragonal structure.

The **Bi–Sr–Ca–Cu–O** system has three superconducting phases forming a homologous series as $Bi_2Sr_2Ca_{n-1}Cu_nO_{4+2n+x}$ (n = 1, 2 and 3). These three phases are Bi-2201, Bi-2212 and Bi-2223, having transition temperatures of 20, 85 and 110 K, respectively, where the numbering system represent number of atoms for Bi, Sr, Ca and Cu respectively. The two phases have a tetragonal structure which consists of two sheared crystallographic unit cells. The unit cell of these phases has double Bi–O planes which are stacked in a way that the Bi atom of one plane sits below the oxygen atom of the next consecutive plane. The Ca atom forms a layer within the interior of the CuO_2 layers in both Bi-2212 and Bi-2223; there is no Ca layer in the Bi-2201 phase. The three phases differ with each other in the number of CuO_2 planes; Bi-2201, Bi-2212 and Bi-2223 phases have one, two and three CuO_2 planes, respectively. The c axis of these phases increases with the number of CuO_2 planes (see table below). The coordination of the Cu atom is different in the three phases. The Cu atom forms an octahedral coordination with respect to oxygen atoms in the 2201 phase, whereas in 2212, the Cu atom is surrounded by five oxygen atoms in a pyramidal arrangement. In the 2223 structure, Cu has two coordinations with respect to oxygen: one Cu atom is bonded with four oxygen atoms in square planar configuration and another Cu atom is coordinated with five oxygen atoms in a pyramidal arrangement.

Tl–Ba–Ca–Cu–O superconductor: The first series of the Tl-based superconductor containing one Tl–O layer has the general formula $TlBa_2Ca_{n-1}Cu_nO_{2n+3}$, whereas the second series containing two Tl–O layers has a formula of $Tl_2Ba_2Ca_{n-1}Cu_nO_{2n+4}$ with n = 1, 2 and 3. In the structure of $Tl_2Ba_2CuO_6$ (Tl-2201), there is one CuO_2 layer with the stacking sequence (Tl–O) (Tl–O) (Ba–O) (Cu–O) (Ba–O) (Tl–O) (Tl–O). In $Tl_2Ba_2CaCu_2O_8$ (Tl-2212), there are two Cu–O layers with a Ca layer in between. Similar

to the $Tl_2Ba_2CuO_6$ structure, Tl–O layers are present outside the Ba–O layers. In $Tl_2Ba_2Ca_2Cu_3O_{10}$ (Tl-2223), there are three CuO2 layers enclosing Ca layers between each of these. In Tl-based superconductors, T_c is found to increase with the increase in CuO_2 layers. However, the value of T_c decreases after four CuO_2 layers in $TlBa_2Ca_{n-1}Cu_nO_{2n+3}$, and in the $Tl_2Ba_2Ca_{n-1}Cu_nO_{2n+4}$ compound, it decreases after three CuO_2 layers.

Hg–Ba–Ca–Cu–O superconductor: The crystal structure of $HgBa_2CuO_4$ (Hg-1201), $HgBa_2CaCu_2O_6$ (Hg-1212) and $HgBa_2Ca_2Cu_3O_8$ (Hg-1223) is similar to that of Tl-1201, Tl-1212 and Tl-1223, with Hg in place of Tl. It is noteworthy that the T_c of the Hg compound (Hg-1201) containing one CuO_2 layer is much larger as compared to the one-CuO_2-layer compound of thallium (Tl-1201). In the Hg-based superconductor, T_c is also found to increase as the CuO_2 layer increases. For Hg-1201, Hg-1212 and Hg-1223, the values of T_c are 94, 128 and 134 K respectively, as shown in table below. The observation that the T_c of Hg-1223 increases to 153 K under high pressure indicates that the T_c of this compound is very sensitive to the structure of the compound.

Critical temperature (T_c), crystal structure and lattice constants of some high-T_c superconductors

Formula	Notation	T_c (K)	No. of Cu-O planes in unit cell	Crystal structure
$YBa_2Cu_3O_7$	123	92	2	Orthorhombic
$Bi_2Sr_2CuO_6$	Bi-2201	20	1	Tetragonal
$Bi_2Sr_2CaCu_2O_8$	Bi-2212	85	2	Tetragonal
$Bi_2Sr_2Ca_2Cu_3O_6$	Bi-2223	110	3	Tetragonal
$Tl_2Ba_2CuO_6$	Tl-2201	80	1	Tetragonal
$Tl_2Ba_2CaCu_2O_8$	Tl-2212	108	2	Tetragonal
$Tl_2Ba_2Ca_2Cu_3O_{10}$	Tl-2223	125	3	Tetragonal
$TlBa_2Ca_3Cu_4O_{11}$	Tl-1234	122	4	Tetragonal
$HgBa_2CuO_4$	Hg-1201	94	1	Tetragonal
$HgBa_2CaCu_2O_6$	Hg-1212	128	2	Tetragonal
$HgBa_2Ca_2Cu_3O_8$	Hg-1223	134	3	Tetragonal

Preparation of high-T_c superconductors

The simplest method for preparing high-T_c superconductors is a solid-state thermochemical reaction involving mixing, calcination and sintering. The appropriate amounts of precursor powders, usually oxides and carbonates, are mixed thoroughly using a ball mill. Solution chemistry processes such as coprecipitation, freeze-drying and sol–gel methods are alternative ways for preparing a homogenous mixture. These powders are calcined in the temperature range from 800 °C to 950 °C for several hours. The powders are cooled, reground and calcined again. This process is repeated several times to get homogenous material. The powders are subsequently compacted to pellets and sintered. The sintering environment such as temperature, annealing time, atmosphere

and cooling rate play a very important role in getting good high-T_c superconducting materials. The $YBa_2Cu_3O_{7-x}$ compound is prepared by calcination and sintering of a homogenous mixture of Y_2O_3, $BaCO_3$ and CuO in the appropriate atomic ratio. Calcination is done at 900–950 °C, whereas sintering is done at 950 °C in an oxygen atmosphere. The oxygen stoichiometry in this material is very crucial for obtaining a superconducting $YBa_2Cu_3O_{7-x}$ compound. At the time of sintering, the semiconducting tetragonal $YBa_2Cu_3O_6$ compound is formed, which, on slow cooling in oxygen atmosphere, turns into superconducting $YBa_2Cu_3O_{7-x}$. The uptake and loss of oxygen are reversible in $YBa_2Cu_3O_{7-x}$. A fully oxidized orthorhombic $YBa_2Cu_3O_{7-x}$ sample can be transformed into tetragonal $YBa_2Cu_3O_6$ by heating in a vacuum at temperature above 700 °C.

The preparation of Bi-, Tl- and Hg-based high-T_c superconductors is difficult compared to YBCO. Problems in these superconductors arise because of the existence of three or more phases having a similar layered structure. Thus, syntactic intergrowth and defects such as stacking faults occur during synthesis and it becomes difficult to isolate a single superconducting phase. For Bi–Sr–Ca–Cu–O, it is relatively simple to prepare the Bi-2212 ($T_c \approx 85$ K) phase, whereas it is very difficult to prepare a single phase of Bi-2223 ($T_c \approx 110$ K). The Bi-2212 phase appears only after few hours of sintering at 860–870 °C, but the larger fraction of the Bi-2223 phase is formed after a long reaction time of more than a week at 870 °C. Although the substitution of Pb in the Bi–Sr–Ca–Cu–O compound has been found to promote the growth of the high-T_c phase, a long sintering time is still required.

Applications

Superconducting magnets are some of the most powerful electromagnets known. They are used in MRI and NMR machines, mass spectrometers, and the beam-steering magnets used in particle accelerators. They can also be used for magnetic separation, where weakly magnetic particles are extracted from a background of less or non-magnetic particles, as in the pigment industries.

In the 1950s and 1960s, superconductors were used to build experimental digital computers using cryotron switches. More recently, superconductors have been used to make digital circuits based on rapid single flux quantum technology and RF and microwave filters for mobile phone base stations.

Superconductors are used to build Josephson junctions which are the building blocks of SQUIDs (superconducting quantum interference devices), the most sensitive magnetometers known. SQUIDs are used in scanning SQUID microscopes and magnetoencephalography. Series of Josephson devices are used to realize the SI volt. Depending on the particular mode of operation, a Josephson junction can be used as a photon detector or as a mixer. The large resistance change at the transition from the normal- to the superconducting state is used to build thermometers in cryogenic micro-calorimeter photon detectors.

Other early markets are arising where the relative efficiency, size and weight advantages of devices based on high-temperature superconductivity outweigh the additional costs involved.

Promising future applications include high-performance smart grid, electric power transmission, transformers, power storage devices, electric motors (e.g. for vehicle propulsion, as in vactrains or maglev trains), magnetic levitation devices, fault current limiters, nanoscopic materials such as buckyballs, nanotubes, composite materials and superconducting magnetic refrigeration. However, superconductivity is sensitive to moving magnetic fields so applications that use alternating current (e.g. transformers) will be more difficult to develop than those that rely upon direct current.

Chapter 2

SQUID

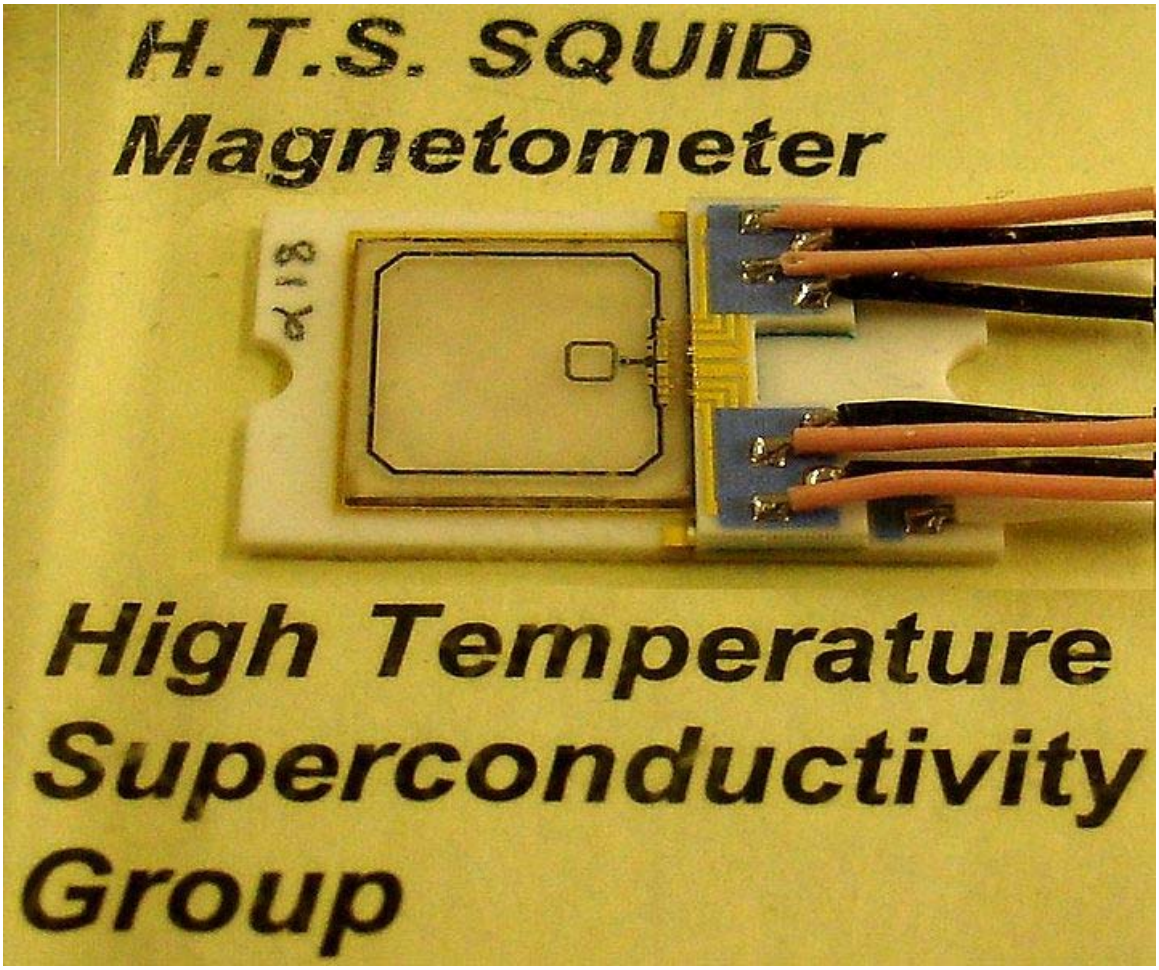

Sensing element of the SQUID

A **SQUID** (for **superconducting quantum interference device**) is a very sensitive magnetometer used to measure extremely weak magnetic fields, based on superconducting loops containing Josephson junctions.

SQUIDs are sensitive enough to measure fields as low as 5 aT (5×10^{-18} T) within a few days of averaged measurements. Their noise levels are as low as 3 $fT\cdot Hz^{-½}$. For comparison, a typical refrigerator magnet produces 0.01 tesla (10^{-2} T), and some processes in animals produce very small magnetic fields between 10^{-9} T and 10^{-6} T. Recently invented SERF atomic magnetometers are potentially more sensitive and do not require cryogenic refrigeration but are orders of magnitude larger in size (~1 cm^3) and must be operated in a near-zero magnetic field.

History and design

There are two main types of SQUID: direct current (DC) and radio frequency (RF). RF SQUIDs can work with only one Josephson junction, which might make them cheaper to produce, but are less sensitive.

DC SQUID

The DC SQUID was invented in 1964 by Robert Jaklevic, John J. Lambe, James Mercereau, and Arnold Silver of Ford Research Labs after Brian David Josephson postulated the Josephson effect in 1962 and the first Josephson Junction was made by John Rowell and Philip Anderson at Bell Labs in 1963. It has two Josephson junctions in parallel in a superconducting loop. It is based on the DC Josephson effect. In the absence of any external magnetic field, the input current I splits into the two branches equally. Now, consider if a small amount of external flux is applied to the superconducting loop. This results in the screening currents that generate the magnetic field to cancel this applied external flux. The current in one of the branches of the superconducting loop is in the direction of I, and is equal to $I/2 + I_s/2$ and in the second branch is in the opposite direction of I and is equal to $I/2 - I_s/2$. As soon as the current in any one of the branches exceeds the critical current for the Josephson junction, the superconducting ring becomes resistive and a voltage appears across the junction. Now consider if the external flux is further increased and it now exceeds $\Phi_0/2$. Since the flux enclosed by the superconducting loop must be an integral number of the flux quanta, in this case the SQUID instead of screening the flux, energetically prefers to increase it to Φ_0. The screening current now flows in the opposite direction. Thus the screening current changes direction every time the flux increases by half integer multiples of Φ_0. Thus the critical current oscillates as a function of the applied flux. If the input current is more than I_c, then the SQUID always operates in the resistive mode. The voltage in this case is thus a function of the applied magnetic field and the period equal to Φ_0. Since the current-voltage characteristics of the DC SQUID is hysteritic, a shunt resistance, R is connected across the junction to eliminate the hysteresis (in the case of copper oxide based high temperature superconductors the junction's own intrinsic resistance is usually sufficient). The screening current is the applied flux divided by the self inductance of the ring. Thus $\Delta\Phi$ can be estimated as the function of ΔV (flux to voltage converter).

$\Delta V = R\,\Delta I$
$2I = 2\,\Delta\Phi/L$, where L is the self inductance of the superconducting ring
$\Delta V = (R/L)\,\Delta\Phi$

RF SQUID

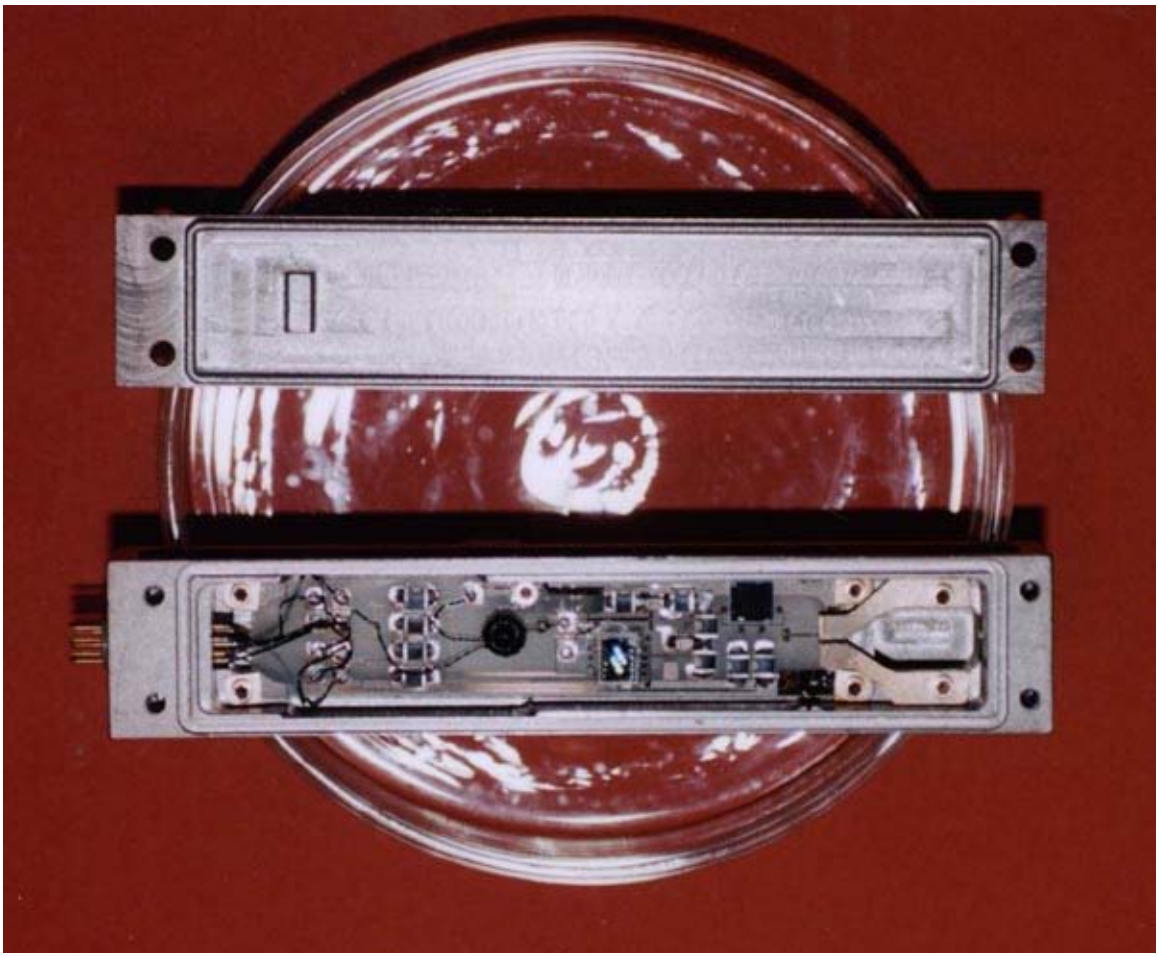

A prototype of a semiconductor SQUID

The RF SQUID was invented in 1965 by Robert Jaklevic, John J. Lambe, Arnold Silver, and James Edward Zimmerman at Ford. It is based on the AC Josephson effect and uses only one Josephson junction. It is less sensitive compared to DC SQUID but is cheaper and easier to manufacture in smaller quantities. The major part of fundamental measurements in biomagnetism even of extremely small signals have been performed, using RF SQUIDS (Tonotopic representation of the auditory cortex by Romani and Williamson 1980, brainstem auditory evoced magnetic field by Erné et al. 1987). The RF SQUID is inductively coupled to a resonant tank circuit. Depending on the external magnetic field, as the SQUID operates in the resistive mode, the effective inductance of the tank circuit changes, thus changing the resonant frequency of the tank circuit. These frequency measurements can be easily done and thus the losses which appear as the voltage across the load resistor in the circuit are a periodic function of the applied magnetic flux with a period of Φ_0. For a precise mathematical description refer to the original paper by Erné et al.

The traditional superconducting materials for SQUIDs are pure niobium or a lead alloy with 10% gold or indium, as pure lead is unstable when its temperature is repeatedly changed. To maintain superconductivity, the entire device needs to operate within a few degrees of absolute zero, cooled with liquid helium.

"High temperature" SQUID sensors are more recent; they are made of high temperature superconductors, particularly YBCO, and are cooled by liquid nitrogen which is cheaper and more easily handled than liquid helium. They are less sensitive than conventional "low temperature" SQUIDs but good enough for many applications.

Uses

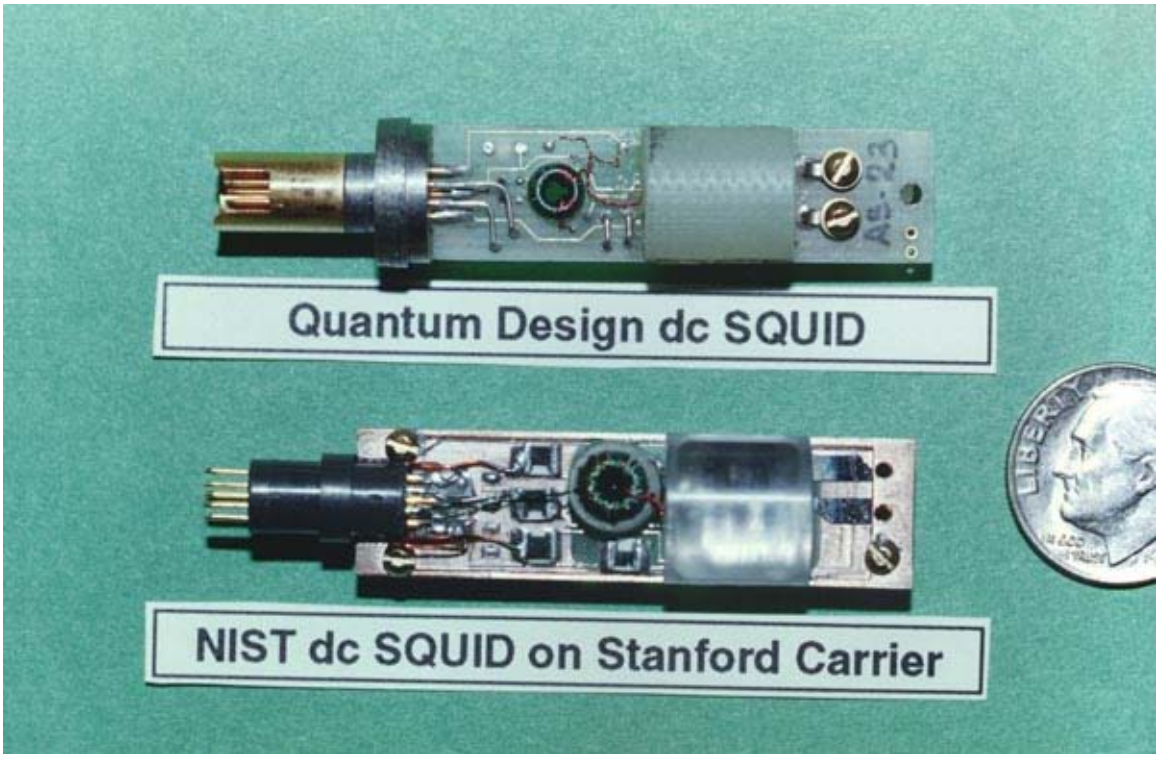

The inner workings of an early SQUID

The extreme sensitivity of SQUIDs makes them ideal for studies in biology. Magnetoencephalography (MEG), for example, uses measurements from an array of SQUIDs to make inferences about neural activity inside brains. Because SQUIDs can operate at acquisition rates much higher than the highest temporal frequency of interest in the signals emitted by the brain (kHz), MEG achieves good temporal resolution. Another area where SQUIDs are used is magnetogastrography, which is concerned with recording the weak magnetic fields of the stomach. A novel application of SQUIDs is the magnetic marker monitoring method, which is used to trace the path of orally applied drugs. In the clinical environment SQUIDs are used in cardiology for magnetic field imaging (MFI), which detects the magnetic field of the heart for diagnosis and risk stratification.

Probably the most common use of SQUIDs is in magnetic property measurement systems (MPMS). These are turn-key systems, made by several manufacturers, that measure the magnetic properties of a material sample. This is typically done over a temperature range from that of 4 K to roughly 190 K, though higher temperatures mean less precision.

For example, SQUIDs are being used as detectors to perform magnetic resonance imaging (MRI). While high field MRI uses precession fields of one to several teslas, SQUID-detected MRI uses measurement fields that lie in the microtesla regime. Since the MRI signal drops off as the square of the magnetic field, a SQUID is used as the detector because of its extreme sensitivity. The SQUID coupled to a second-order gradiometer and input circuit, along with the application of gradients are the fundamental entities which allows a research group to retrieve noninvasive images. SQUID-detected MRI has advantages over high field MRI systems such as the low cost required to build such a system and its compactness. The principle has been proven by imaging human extremities, and its future application may involve tumor screening.

Another application is the scanning SQUID microscope, which uses a SQUID immersed in liquid helium as the probe. The use of SQUIDs in oil prospecting, mineral exploration, earthquake prediction and geothermal energy surveying is becoming more widespread as superconductor technology develops; they are also used as precision movement sensors in a variety of scientific applications, such as the detection of gravitational waves. Four SQUIDs were employed on Gravity Probe B in order to test the limits of the theory of general relativity.

It has also been suggested that they might be implemented in a quantum computer. These are the only macroscopic devices that have been cited as possible qubits in this context.

Chapter 3

Superconducting Magnet

A **superconducting magnet** is an electromagnet made from coils of superconducting wire. They must be cooled to cryogenic temperatures during operation. Superconducting magnets can produce greater magnetic fields than all but the strongest electromagnets and can be cheaper to operate because no energy is dissipated as heat in the windings.

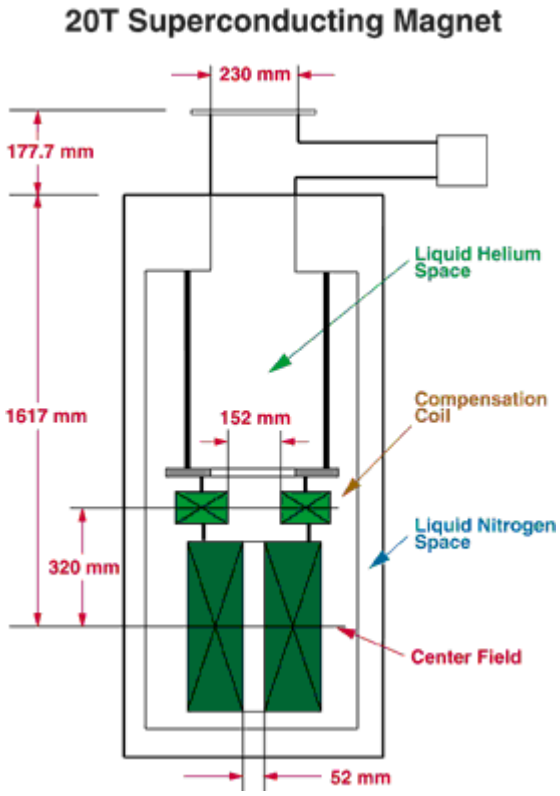

Schematic of a 20 tesla superconducting magnet with vertical bore

Construction

Cooling

During operation, the magnet windings must be cooled below their critical temperature; the temperature at which the winding material changes from the normal resistive state and becomes a superconductor. Liquid helium is used as a coolant for most superconductive windings, even those with critical temperatures far above its boiling point of 4.2 K. This is because the lower the temperature, the better superconductive windings work—the higher the currents and magnetic fields they can stand without returning to their nonsuperconductive state. The magnet and coolant are contained in a thermally insulated container (dewar) called a cryostat. To keep the helium from boiling away, the cryostat is usually constructed with an outer jacket containing (significantly cheaper) liquid nitrogen at 77 K. One of the goals of the search for high temperature superconductors is to build magnets that can be cooled by liquid nitrogen alone. At temperatures above about 20 K cooling can be achieved without boiling off cryogenic liquids.

Materials

The maximum magnetic field achievable in a superconducting magnet is limited by the field at which the winding material ceases to be superconducting, its 'critical field', H_c, which for type-II superconductors is its upper critical field. Another limiting factor is the 'critical current', I_c at which the winding material also ceases to be superconducting. Advances in magnets have focused on creating better winding materials.

The superconducting portions of most current magnets are composed of niobium-titanium. This material has critical temperature of 10 kelvins and can superconduct at up to about 15 teslas. More expensive magnets can be made of niobium-tin (Nb_3Sn). These have a T_c of 18 K. When operating at 4.2 K they are able to withstand a much higher magnetic field intensity, up to 25 to 30 teslas. Unfortunately, it is far more difficult to make the required filaments from this material. This is why sometimes a combination of Nb_3Sn for the high field sections and Nb_3Ti for the lower field sections is used. Vanadium-gallium is another material used for the high field inserts.

High temperature superconductors (e.g. BSCCO or YBCO) may be used for high-field inserts when magnetic fields are required which are higher than Nb_3Sn can manage. BSCCO, YBCO or magnesium diboride may also be used for current leads, conducting high currents from room temperature into the cold magnet without an accompanying large heat leak from resistive leads.

Coil windings

The coil windings of a superconducting magnet are made of wires or tapes of Type II superconductors (e.g.niobium-titanium or niobium-tin). The wire or tape itself may be made of tiny filaments (about 20 micrometers thick) of superconductor in a copper

matrix. The copper is needed to add mechanical stability, and to provide a low resistance path for the large currents in case the temperature rises above T_c or the current rises above I_c and superconductivity is lost. These filaments need to be this small *because in this type of superconductor the current only flows skin-deep.* The coil must be carefully designed to withstand (or counteract) magnetic pressure and Lorentz forces that could otherwise cause wire fracture or crushing of insulation between adjacent turns.

Operation

7 T horizontal bore superconducting magnet, part of a mass spectrometer. The magnet itself is inside the cylindrical cryostat.

Power supply

The current to the coil windings is provided by a high current, very low voltage DC power supply, since in steady state the only voltage across the magnet is due to the resistance of the feeder wires. Any change to the current through the magnet must be

done very slowly, first because electrically the magnet is a large inductor and an abrupt current change will result in a large voltage spike across the windings, and more importantly because fast changes in current can cause eddy currents and mechanical stresses in the windings that can precipitate a quench (see below). So the power supply is usually microprocessor-controlled, programmed to accomplish current changes gradually, in gentle ramps. It usually takes several minutes to energize or de-energize a laboratory-sized magnet.

Persistent mode

An alternate operating mode, once the magnet has been energized, is to short-circuit the windings with a piece of superconductor. The windings become a closed superconducting loop, the power supply can be turned off, and persistent currents will flow for months, preserving the magnetic field. The advantage of this *persistent mode* is that stability of the magnetic field is better than is achievable with the best power supplies, and no energy is needed to power the windings. The short circuit is made by a 'persistent switch', a piece of superconductor inside the magnet connected across the winding ends, attached to a small heater. In normal mode, the switch wire is heated above its transition temperature, so it is resistive. Since the winding itself has no resistance, no current flows through the switch wire. To go to persistent mode, the current is adjusted until the desired magnetic field is obtained, then the heater is turned off. The persistent switch cools to its superconducting temperature, short circuiting the windings. The current and the magnetic field will not actually persist forever, but will decay slowly according to a normal L/R time constant:

$$H = H_0 e^{-(R/L)t}$$

where $R$is a small residual resistance in the superconducting windings due to joints or a phenomenon called flux motion resistance. Nearly all commercial superconducting magnets are equipped with persistent switches.

Magnet quench

A quench is an abnormal termination of magnet operation that occurs when part of the superconducting coil enters the normal (resistive) state. This can occur because the field inside the magnet is too large, the rate of change of field is too large (causing eddy currents and resultant heating in the copper support matrix), or a combination of the two. More rarely a defect in the magnet can cause a quench. When this happens, that particular spot is subject to rapid Joule heating, which raises the temperature of the surrounding regions. This pushes those regions into the normal state as well, which leads to more heating in a chain reaction. The entire magnet rapidly becomes normal (this can take several seconds, depending on the size of the superconducting coil). This is accompanied by a loud bang as the energy in the magnetic field is converted to heat, and rapid boil-off of the cryogenic fluid. The abrupt decrease of current can result in kilovolt inductive voltage spikes and arcing. Permanent damage to the magnet is rare, but components can be damaged by localized heating or large mechanical forces. In practice, magnets usually

have safety devices to stop or limit the current when the beginning of a quench is detected. If a large magnet undergoes a quench, the inert vapor formed by the evaporating cryogenic fluid can present a significant asphyxiation hazard to operators by displacing breathable air. A large section of the superconducting magnets in CERN's Large Hadron Collider unexpectedly quenched during start-up operations in 2008, necessitating a replacement of a number of magnets.

History

Although the idea of making electromagnets with superconducting wire was proposed by Heike Kamerlingh Onnes shortly after he discovered superconductivity in 1911, a practical superconducting electromagnet had to await the discovery of type-II superconductors that could stand high magnetic fields. The first successful superconducting magnet was built by George Yntema in 1954 using niobium wire and achieved a field of 0.71 T at 4.2 K. Widespread interest was sparked by Kunzler's 1961 discovery of the advantages of niobium-tin as a high H_c, high current winding material.

In 1986, the discovery of high temperature superconductors by Georg Bednorz and Karl Muller energized the field, raising the possibility of magnets that could by cooled by liquid nitrogen instead of the more difficult to work with helium.

In 2007 a magnet with windings of YBCO achieved a world record field of 26.8 teslas. The US National Research Council has a goal of creating a 30 tesla superconducting magnet.

Uses

An MRI machine that uses a superconducting magnet. The magnet is inside the doughnut-shaped housing, and can create a 3 tesla field inside the central hole.

Superconducting magnets have a number of advantages over resistive electromagnets. They can achieve an order of magnitude stronger field than ordinary ferromagnetic-core electromagnets, which are limited to fields of around 2 T. The field is generally more stable, resulting in less noisy measurements. They can be smaller, and the area at the center of the magnet where the field is created is empty rather than being occupied by an iron core. Most importantly, for large magnets they can consume much less power. In the persistent state (above), the only power the magnet consumes is that needed for any refrigeration equipment to preserve the cryogenic temperature. Higher fields, however can be achieved with special cooled resistive electromagnets, as superconducting coils will enter the normal (non-superconducting) state at high fields.

Superconducting magnets are widely used in MRI machines, NMR equipment, mass spectrometers, magnetic separation processes, and particle accelerators.

One of the most challenging use of SC magnets is in the LHC particle accelerator . The niobium-titanium (Nb-Ti) magnets operate at 1.9 K to allow them to run safely at 8.3 T. Each magnet stores 7 MJ. In total the magnets store 10.4 GJ. Once or twice a day, as the

protons are accelerated from 450 GeV to 7 TeV, the field of the superconducting bending magnets will be increased from 0.54 T to 8.3 T.

The central solenoid and toroidal field superconducting magnets designed for the ITER fusion reactor use niobium-tin (Nb_3Sn) as a superconductor. The Central Solenoid coil will carry 46 kA and produce a field of 13.5 teslas. The 18 Toroidal Field coils at max field of 11.8 T will store 41 GJ (total?). They have been tested at a record 80 kA. Other lower field ITER magnets (PF and CC) will use niobium-titanium. Most of the ITER magnets will have their field varied many times per hour.

Chapter 4

Superconducting Magnetic Energy Storage

Superconducting Magnetic Energy Storage (SMES) systems store energy in the magnetic field created by the flow of direct current in a superconducting coil which has been cryogenically cooled to a temperature below its superconducting critical temperature.

A typical SMES system includes three parts: superconducting coil, power conditioning system and cryogenically cooled refrigerator. Once the superconducting coil is charged, the current will not decay and the magnetic energy can be stored indefinitely.

The stored energy can be released back to the network by discharging the coil. The power conditioning system uses an inverter/rectifier to transform alternating current (AC) power to direct current or convert DC back to AC power. The inverter/rectifier accounts for about 2–3% energy loss in each direction. SMES loses the least amount of electricity in the energy storage process compared to other methods of storing energy. SMES systems are highly efficient; the round-trip efficiency is greater than 95%.

Due to the energy requirements of refrigeration and the high cost of superconducting wire, SMES is currently used for short duration energy storage. Therefore, SMES is most commonly devoted to improving power quality. If SMES were to be used for utilities it would be a diurnal storage device, charged from baseload power at night and meeting peak loads during the day.

Advantages over other energy storage methods

There are several reasons for using superconducting magnetic energy storage instead of other energy storage methods. The most important advantage of SMES is that the time delay during charge and discharge is quite short. Power is available almost instantaneously and very high power output can be provided for a brief period of time.

Other energy storage methods, such as pumped hydro or compressed air have a substantial time delay associated with the energy conversion of stored mechanical energy back into electricity. Thus if a customer's demand is immediate, SMES is a viable option. Another advantage is that the loss of power is less than other storage methods because electric currents encounter almost no resistance. Additionally the main parts in a SMES are motionless, which results in high reliability.

Current use

There are several small SMES units available for commercial use and several larger test bed projects. Several 1 MW·h units are used for power quality control in installations around the world, especially to provide power quality at manufacturing plants requiring ultra-clean power, such as microchip fabrication facilities.

These facilities have also been used to provide grid stability in distribution systems. SMES is also used in utility applications. In northern Wisconsin, a string of distributed SMES units was deployed to enhance stability of a transmission loop. The transmission line is subject to large, sudden load changes due to the operation of a paper mill, with the potential for uncontrolled fluctuations and voltage collapse. Developers of such devices include American Superconductor.

The Engineering Test Model is a large SMES with a capacity of approximately 20 MW·h, capable of providing 400 MW of power for 100 seconds or 10 MW of power for 2 hours.

Calculation of stored energy

The magnetic energy stored by a coil carrying a current is given by one half of the inductance of the coil times the square of the current.

$$E = \frac{1}{2} L I^2$$

Where

E = energy measured in joules
L = inductance measured in henries
I = current measured in amperes

Now let’s consider a cylindrical coil with conductors of a rectangular cross section. The mean radius of coil is R. a and b are width and depth of the conductor. f is called form function which is different for different shapes of coil. ξ (xi) and δ (delta) are two parameters to characterize the dimensions of the coil. We can therefore write the magnetic energy stored in such a cylindrical coil as shown below. This energy is a function of coil dimensions, number of turns and carrying current.

$$E = \frac{1}{2} R N^2 I^2 f(\xi, \delta)$$

Where

E = energy measured in joules
I = current measured in amperes
f(ξ,δ) = form function, joules per ampere-meter
N = number of turns of coil

Solenoid versus toroid

Besides the properties of the wire, the configuration of the coil itself is an important issue from a mechanical engineering aspect. There are three factors which affect the design and the shape of the coil - they are: Inferior strain tolerance, thermal contraction upon cooling and lorentz forces in a charged coil. Among them, the strain tolerance is crucial not because of any electrical effect, but because it determines how much structural material is needed to keep the SMES from breaking. For small SMES systems, the optimistic value of 0.3% strain tolerance is selected. Toroidal geometry can help to lessen the external magnetic forces and therefore reduces the size of mechanical support needed. Also, due to the low external magnetic field, toroidal SMES can be located near a utility or customer load.

For small SMES, solenoids are usually used because they are easy to coil and no pre-compression is needed. In toroidal SMES, the coil is always under compression by the outer hoops and two disks, one of which is on the top and the other is on the bottom to avoid breakage. Currently, there is little need for toroidal geometry for small SMES, but as the size increases, mechanical forces become more important and the toroidal coil is needed.

The older large SMES concepts usually featured a low aspect ratio solenoid approximately 100 m in diameter buried in earth. At the low extreme of size is the concept of micro-SMES solenoids, for energy storage range near 1 MJ.

Low-temperature versus high-temperature superconductors

Under steady state conditions and in the superconducting state, the coil resistance is negligible. However, the refrigerator necessary to keep the superconductor cool requires electric power and this refrigeration energy must be considered when evaluating the efficiency of SMES as an energy storage device.

Although the high-temperature superconductor (HTSC) has higher critical temperature, flux lattice melting takes place in moderate magnetic fields around a temperature lower than this critical temperature. The heat loads that must be removed by the cooling system include conduction through the support system, radiation from warmer to colder surfaces, AC losses in the conductor(during charge and discharge), and losses from the cold–to-

warm power leads that connect the cold coil to the power conditioning system. Conduction and radiation losses are minimized by proper design of thermal surfaces. Lead losses can be minimized by good design of the leads. AC losses depend on the design of the conductor, the duty cycle of the device and the power rating.

The refrigeration requirements for HTSC and low-temperature superconductor (LTSC) toroidal coils for the baseline temperatures of 77 K, 20 K, and 4.2 K, increases in that order. The refrigeration requirements here is defined as electrical power to operate the refrigeration system. As the stored energy increases by a factor of 100, refrigeration cost only goes up by a factor of 20. Also, the savings in refrigeration for an HTSC system is larger (by 60% to 70%) than for an LTSC systems.

Cost

Whether HTSC or LTSC systems are more economical depends because there are other major components determining the cost of SMES: Conductor consisting of superconductor and copper stabilizer and cold support are major costs in themselves. They must be judged with the overall efficiency and cost of the device. Other components, such as vacuum vessel insulation, has been shown to be a small part compared to the large coil cost. The combined costs of conductors, structure and refrigerator for toroidal coils are dominated by the cost of the superconductor. The same trend is true for solenoid coils. HTSC coils cost more than LTSC coils by a factor of 2 to 4. We expect to see a cheaper cost for HTSC due to lower refrigeration requirements but this is not the case. So, why is the HTSC system more expensive?

To gain some insight consider a breakdown by major components of both HTSC and LTSC coils corresponding to three typical stored energy levels, 2, 20 and 200 MW·h. The conductor cost dominates the three costs for all HTSC cases and is particularly important at small sizes. The principal reason lies in the comparative current density of LTSC and HTSC materials. The critical current (J_c) of HTSC wire is lower than LTSC wire generally in the operating magnetic field, about 5 to 10 teslas (T). Assume the wire costs are the same by weight. Because HTSC wire has lower (J_c) value than LTSC wire, it will take much more wire to create the same inductance. Therefore, the cost of wire is much higher than LTSC wire. Also, as the SMES size goes up from 2 to 20 to 200 MW·h, the LTSC conductor cost also goes up about a factor of 10 at each step. The HTSC conductor cost rises a little slower but is still by far the costliest item.

The structure costs of either HTSC or LTSC go up uniformly (a factor of 10) with each step from 2 to 20 to 200 MW·h. But HTSC structure cost is higher because the strain tolerance of the HTSC (ceramics cannot carry much tensile load) is less than LTSC, such as Nb_3Ti or Nb_3Sn, which demands more structure materials. Thus, in the very large cases, the HTSC cost can not be offset by simply reducing the coil size at a higher magnetic field.

It is worth noting here that the refrigerator cost in all cases is so small that there is very little percentage savings associated with reduced refrigeration demands at high

temperature. This means that if a HTSC, BSCCO for instance, works better at a low temperature, say 20K, it will certainly be operated there. For very small SMES, the reduced refrigerator cost will have a more significant positive impact.

Clearly, the volume of superconducting coils increases with the stored energy. Also, we can see that the LTSC torus maximum diameter is always smaller for a HTSC magnet than LTSC due to higher magnetic field operation. In the case of solenoid coils, the height or length is also smaller for HTSC coils, but still much higher than in a toroidal geometry (due to low external magnetic field).

An increase in peak magnetic field yields a reduction in both volume (higher energy density) and cost (reduced conductor length). Smaller volume means higher energy density and cost is reduced due to the decrease of the conductor length. There is an optimum value of the peak magnetic field, about 7 T in this case. If the field is increased past the optimum, further volume reductions are possible with minimal increase in cost. The limit to which the field can be increased is usually not economic but physical and it relates to the impossibility of bringing the inner legs of the toroid any closer together and still leave room for the bucking cylinder.

The superconductor material is a key issue for SMES. Superconductor development efforts focus on increasing Jc and strain range and on reducing the wire manufacturing cost.

Technical challenges

The energy content of current SMES systems is usually quite small. Methods to increase the energy stored in SMES often resort to large-scale storage units. As with other superconducting applications, cryogenics are a necessity. A robust mechanical structure is usually required to contain the very large Lorentz forces generated by and on the magnet coils. The dominant cost for SMES is the superconductor, followed by the cooling system and the rest of the mechanical structure.

- *Mechanical support* - Needed because of lorentz forces.
- *Size* - To achieve commercially useful levels of storage, around 1 GW·h (3.6 TJ), a SMES installation would need a loop of around 100 miles (160 km). This is traditionally pictured as a circle, though in practice it could be more like a rounded rectangle. In either case it would require access to a significant amount of land to house the installation, and to contain the health effects noted below.
- *Manufacturing* - There are two manufacturing issues around SMES. The first is the fabrication of bulk cable suitable to carry the current. Most of the superconducting materials found to date are relatively delicate ceramics, making it difficult to use established techniques to draw extended lengths of superconducting wire. Much research has focussed on layer deposit techniques, applying a thin film of material onto a stable substrate, but this is currently only suitable for small-scale electrical circuits.

- *Infrastructure* - The second problem is the infrastructure required for an installation. Until room-temperature superconductors are found, the 100 mile (160 km) loop of wire would have to be contained within a vacuum flask of liquid nitrogen. This in turn would require stable support, most commonly envisioned by burying the installation.
- *Critical current* - In general power systems look to maximize the current they are able to handle. This makes any losses due to inefficiencies in the system relatively insignificant. Unfortunately the superconducting properties of most materials break down as current increases, at a level known as the critical current. Current materials struggle, therefore, to carry sufficient current to make a commercial storage facility economically viable.
- *Critical magnetic field* - Related to critical current, there is a similar limitation to superconductivity linked to the magnetic field induced in the wire, and this too is a factor at commercial storage levels
- *Possible Adverse Health effects* - A potential concern with SMES, beyond obvious accidents (such as a break in the containment of liquid nitrogen), is the very large magnetic fields that would be created by a commercial installation. If long term exposure to such fields is found to be hazardous, any installation would likely require a suitable buffer zone around it to mitigate potential effects.

Current lack of representation in industry

Several issues at the onset of the technology have hindered its proliferation:

1. As current is passed through a superconductor, the superconductivity was destroyed by the created magnetic field before appreciable values for a utility application could be reached.
2. Expensive refrigeration units and high power cost to maintain operating temperatures
3. Existence and continued development of adequate technologies using normal conductors

These still pose problems for superconducting applications but are improving over time. Advances have been made in the performance of superconducting materials. Furthermore,the reliability and efficiency of refrigeration systems has improved significantly to the point that some devices are now able to operate on electrical power systems

Chapter 5

Superconducting Radio Frequency

The Cornell storage ring 500 MHz SRF cavity.

Superconducting Radio Frequency (SRF) science and technology involves the application of electrical superconductors to radio frequency devices. The ultra-low electrical loss of the superconductor yields RF resonators with extremely high quality factors, or Q. For example, it is commonplace for a 1.3 GHz niobium SRF resonant cavity at 1.8 kelvins to obtain $Q=5\times10^{10}$. Such a very high Q resonator and its narrow bandwidth can then be exploited for a variety of applications.

Introduction

A comparison often cited to gauge the minute amount of loss in an SRF resonant cavity is that if one of the first investigators of pendulous motion, Galileo Galilei, had experimented with a 1 Hz mechanical resonator that had a Q that is achieved by today's SRF cavities, and had left one of his pendulums swinging since the early 17th century in a sepulchered lab, then it would still be swinging today with about half of its original amplitude!

Photograph of the Cornell storage ring 500 MHz SRF cavity being lifted out of a cryogenic test dewar while still cold.

The largest application of superconducting RF by far is in particle accelerators, where resonant RF cavities are formed from, or coated with, superconducting materials. Electromagnetic fields are excited in the cavity by coupling in an RF source with an antenna. When the RF frequency fed by the antenna is the same as that of a cavity mode, the fields resonantly build to high amplitudes. Particles passing through small apertures in the cavity are then accelerated by the electric fields and deflected by the magnetic fields. The resonant frequency driven in SRF cavities typically ranges from 200 MHz to 3 GHz, depending on the particle species to be accelerated. The most common fabrication technology for such SRF cavities is to form thin walled (1–3 mm) shell components from pure niobium sheets by pressing or other exotic techniques, and then electron beam welding them together to form a cavity. One such finished product is pictured above.

A simplified diagram of the key elements of an SRF cavity setup is shown below. The cavity is immersed in a liquid helium bath, which is pumped to remove helium vapor boil-off as well as to reduce the bath temperature. In fact, the helium vessel is often pumped to a pressure below helium's superfluid lambda point to take advantage of superfluid's thermal properties and its absence of boiling, which would cause mechanical perturbations of the cavity. An antenna is needed in the setup to couple RF power to the cavity fields and any passing particle beam. And the cold portions of the setup need to be extremely well insulated, which is best accomplished by a vacuum vessel surrounding the

helium vessel and all ancillary cold components. The terminology for the full SRF cavity setup, including the vacuum vessel and many details not discussed here, is a "Cryomodule".

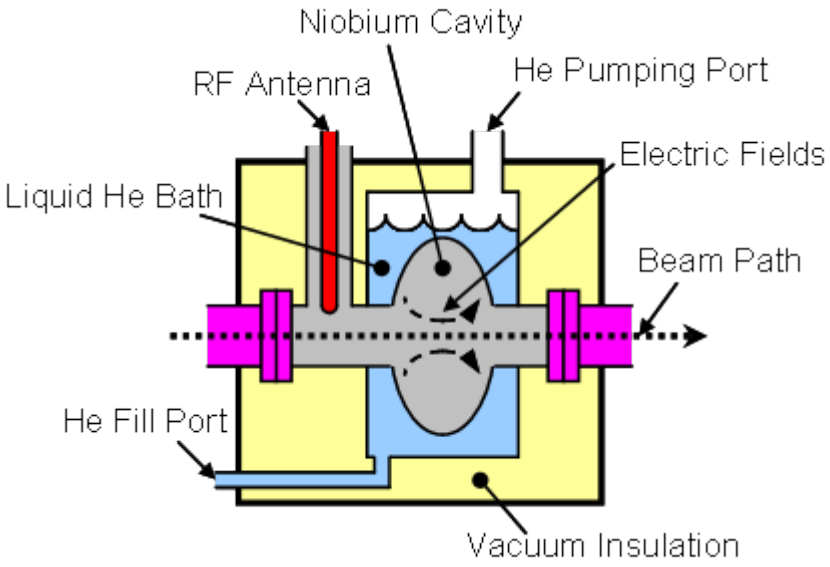

A simplified diagram of an SRF cavity in a helium bath with RF coupling and a passing particle beam.

Entry into superconducting RF technology can incur more complexity, expense, and time than normal-conducting RF cavity strategies. SRF requires chemical facilities for harsh cavity treatments, a low-particulate cleanroom for high-pressure water rinsing and assembly of components, and complex engineering for the cryomodule vessel and cryogenics. And a vexing aspect of SRF is the as-yet elusive ability to consistently produce high-quality cavities in high volume production, as would be required for a large linear collider. Nevertheless, for many applications the benefits provided by SRF cavities are the only solution available to meet the host of the application's demanding performance requirements.

Several extensive treatments of SRF physics and technology are available, many of them free of charge and online. There are the proceedings of CERN accelerator schools, a scientific paper giving a thorough presentation of the many aspects of an SRF cavity to be used in the International Linear Collider, bi-annual International Conferences on RF Superconductivity held at varying global locations in odd numbered years, and tutorials presented at the conferences.

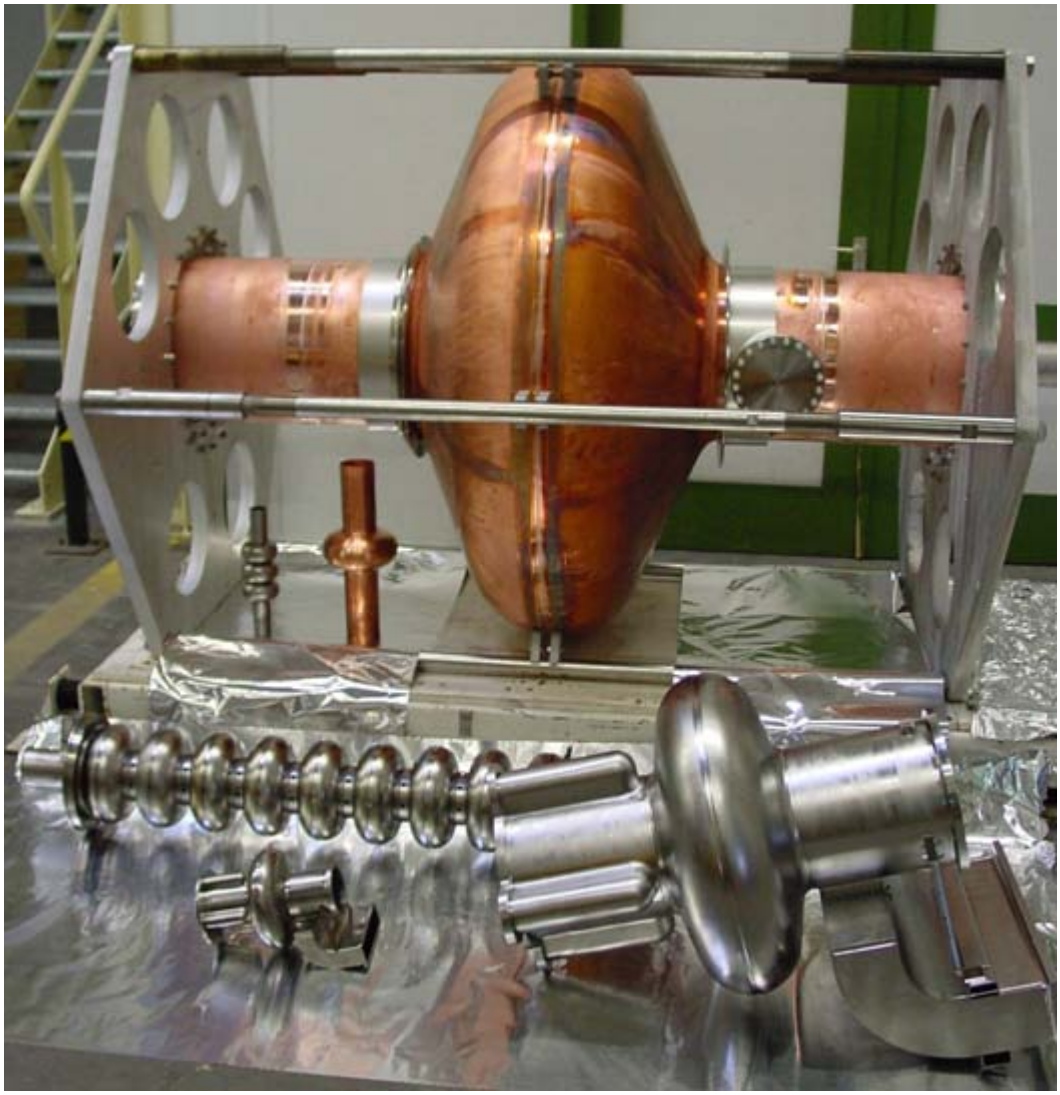

A collection of SRF cavities developed at Cornell University with frequencies spanning 200 MHz to 3 GHz.

SRF cavity application in particle accelerators

A large variety of RF cavities are utilized in particle accelerators. Historically they have been made of copper, a good electrical conductor, and operated near room temperature with water cooling. The water cooling is necessary to remove the heat generated by the electrical loss in the cavity. In the past two decades, though, there has been a growing number of accelerator facilities for which superconducting cavities were deemed more suitable, or necessary, for the accelerator than normal-conducting copper versions. The motivation for using superconductors in RF cavities is *not* to achieve a net power savings. Though superconductors have very small electrical resistance, the little power that they do dissipate is done so at very low temperatures, typically in a liquid helium bath at 1.6 K to 4.5 K. The refrigeration power to maintain the cryogenic bath at low temperature in the presence of heat from small RF power dissipation is dictated by the Carnot efficiency,

and can easily be comparable to the normal-conductor power dissipation of a room-temperature copper cavity. The motivations for using superconducting RF cavities, are instead, the following:

- **High duty cycle or cw operation**. SRF cavities allow the excitation of high electromagnetic fields at high duty cycle, or even cw, in such regimes that a copper cavity's electrical loss could *melt* the copper, even with robust water cooling.
- **Low beam impedance**. The low electrical loss in an SRF cavity allows their geometry to have large beampipe apertures while still maintaining a high accelerating field along the beam axis. Normal-conducting cavities need small beam apertures to concentrate the electric field as compensation for power losses in wall currents. However, the small apertures can be deleterious to a particle beam due to their spawning of larger wakefields, which are quantified by the accelerator parameters termed "beam impedance" and "loss parameter".
- **Nearly all RF power goes to the beam**. The RF source driving the cavity need only provide the RF power that is absorbed by the particle beam being accelerated, since the RF power dissipated in the SRF cavity walls is negligible. This is in contrast to normal-conducting cavities where the wall power loss can easily equal or exceed the beam power consumption. The RF power budget is important since the RF source technologies, such as a Klystron, Inductive output tube (IOT), or solid state amplifier, have costs that increase dramatically with increasing power.

When future superconducting material advances occur to obtain higher superconducting critical temperatures T_c and consequently higher SRF bath temperatures, then the better efficiencies of the refrigerator could yield a significant net power savings by SRF over the normal conducting approach to RF cavities. There are other issues that would have to be considered with a higher bath temperature, though, such as the absence of superfluidity that is presently exploited with liquid helium that would not be present with, e.g., liquid nitrogen. At present, none of the "high T_c" superconducting materials are suitable for RF applications. Shortcomings of these materials arise due to their underlying physics as well as their bulk mechanical properties not being amenable to fabricating accelerator cavities. However, depositing films of promising materials onto other mechanically amenable cavity materials could provide a viable option for exotic materials serving SRF applications. At presnt, the de facto choice of SRF material remains to be pure niobium, which has a critical temperature of 9.3 K and functions as a superconductor nicely in a liquid helium bath of 4.2 K or lower.

Physics of SRF cavities

The physics of Superconducting RF can be complex and lengthy. A few simple approximations derived from the complex theories, though, can serve to provide some of the important parameters of SRF cavities.

By way of background, some of the pertinent parameters of RF cavities are itemized as follows. A resonator's quality factor is defined by

$$Q_o = \frac{\omega U}{P_d},$$

where:

ω is the resonant frequency in [rad/s],
U is the energy stored in [J], and
P_d is the power dissipated in [W] in the cavity to maintain the energy U.

The energy stored in the cavity is given by the integral of field energy density over its volume,

$$U = \frac{\mu_0}{2} \int |\vec{H}|^2 dV,$$

where:

H is the magnetic field in the cavity and
μ_0 is the permeability of free space.

The power dissipated is given by the integral of resistive wall losses over its surface,

$$P_d = \frac{R_s}{2} \int |\vec{H}|^2 dS,$$

where:

R_s is the surface resistance which will be discussed below.

The integrals of the electromagnetic field in the above expressions are generally not solved analytically, since the cavity boundaries rarely lie along axes of common coordinate systems. Instead, the calculations are performed by any of a variety of computer programs that solve for the fields for non-simple cavity shapes, and then numerically integrate the above expressions.

An RF cavity parameter known as the Geometry Factor ranks the cavity's effectiveness of providing accelerating electric field due to the influence of its shape alone, which excludes specific material wall loss. The Geometry Factor is given by

$$G = \frac{\omega \mu_0 \int |\vec{H}|^2 dV}{\int |\vec{H}|^2 dS},$$

and then

$$Q_o = \frac{G}{R_s}.$$

The geometry factor is quoted for cavity designs to allow comparison to other designs independent of wall loss, since wall loss for SRF cavities can vary substantially depending on material preparation, cryogenic bath temperature, electromagnetic field level, and other highly variable parameters. The Geometry Factor is also independent of cavity size, it is constant as a cavity shape is scaled to change its frequency.

As an example of the above parameters, a typical 9-cell SRF cavity for the International Linear Collider (a.k.a, a TESLA cavity) would have G=270 Ω and R_s= 10 nΩ, giving Q_o=2.7×10^{10}.

The critical parameter for SRF cavities in the above equations is the surface resistance R_s, and is where the complex physics comes into play. For normal-conducting copper cavities operating near room temperature, R_s is simply determined by the empirically measured bulk electrical conductivity σ by

$$R_{s\ normal} = \sqrt{\frac{\omega\mu_0}{2\sigma}}.$$

For copper at 300 K, σ=5.8×10^7 (Ω·m)$^{-1}$ and at 1.3 GHz, $R_{s\ copper}$= 9.4 mΩ.

For Type II superconductors in RF fields, R_s can be viewed as the sum of the superconducting BCS resistance and temperature-independent "residual resistances",

$$R_s = R_{BCS} + R_{res}\ .$$

The *BCS resistance* derives from BCS theory. One way to view the nature of the BCS RF resistance is that the superconducting cooper pairs, which have zero resistance for DC current, have finite mass and momentum which has to alternate sinusoidally for the AC currents of RF fields, thus giving rise to a small energy loss. The BCS resistance for niobium can be approximated when the temperature is less than half of niobium's superconducting critical temperature, $T<T_c/2$, by

$$R_{BCS} \simeq 2 \times 10^{-4} \left(\frac{f}{1.5 \times 10^9}\right)^2 \frac{e^{-17.67/T}}{T}\ [\Omega],$$

where:

f is the frequency in [Hz],
T is the temperature in [K], and

T_c=9.3 K for niobium, so that this approximation is valid for T<4.65 K.

Note that for superconductors, the BCS resistance increases quadratically with frequency, $\sim f^2$, whereas for normal conductors the surface resistance increases as the root of frequency, $\sim\sqrt{f}$. For this reason, the majority of superconducting cavity applications favor lower frequencies, <3 GHz, and normal-conducting cavity applications favor higher frequencies, >0.5 GHz, there being some overlap depending on the application.

The superconductor's *residual resistance* arises from several sources, such as random material defects, hydrides that can form on the surface due to hot chemistry and slow cool-down, and others that are yet to be identified. One of the quantifiable residual resistance contributions is due to an external magnetic field pinning magnetic fluxons in a Type II superconductor. The pinned fluxon cores create small normal-conducting regions in the niobium that can be summed to estimate their net resistance. For niobium, the magnetic field contribution to R_s can be approximated by

$$R_H = \frac{H_{ext}}{2H_{c2}} R_n \approx 9.49 \times 10^{-12} H_{ext} \sqrt{f}_{[\Omega]},$$

where:

H_{ext} is any external magnetic field in [Oe],
H_{c2} is the Type II superconductor magnetic quench field, which is 2400 Oe (190 kA/m) for niobium, and
R_n is the normal-conducting resistance of niobium in ohms.

The Earth's nominal magnetic flux of 0.5 gauss (50 μT) translates to a magnetic field of 0.5 Oe (40 A/m) and would produce a residual surface resistance in a superconductor that is orders of magnitude greater than the BCS resistance, rendering the superconductor too lossy for practical use. For this reason, superconducting cavities are surrounded by magnetic shielding to reduce the field permeating the cavity to typically <10 mOe (0.8 A/m).

Using the above approximations for a niobium a SRF cavity at 1.8 K, 1.3 GHz, and assuming a magnetic field of 10 mOe (0.8 A/m), the surface resistance components would be

R_{BCS} = 4.55 nΩ and
R_{res} = R_H = 3.42 nΩ, giving a net surface resistance
R_s = 7.97 nΩ. If for this cavity
G = 270 Ω then the ideal quality factor would be
Q_o = 3.4×10^{10}.

The Q_o just described can be further improved by up to a factor of 2 by performing a mild vacuum bake of the cavity. Empirically, the bake seems to reduce the BCS resistance by

50%, but increases the residual resistance by 30%. The plot below shows the ideal Q_o values for a range of residual magnetic field for a baked and unbaked cavity.

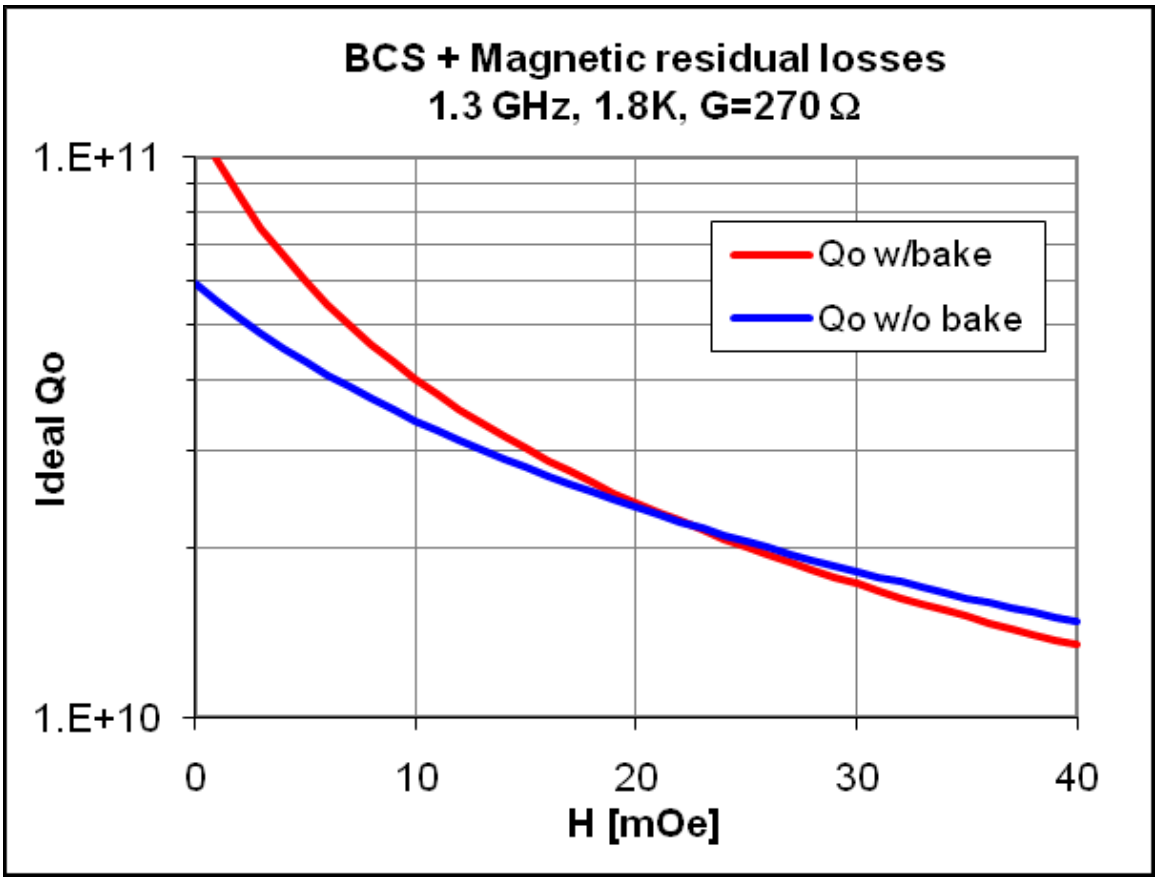

Plot of SRF cavity ideal Q_o vs external DC magnetic field for the same cavity frequency, temperature, and geometry factor as used in the text.

In general, much care and attention to detail must be exercised in the experimental setup of SRF cavities so that there is not Q_o degradation due to RF losses in ancillary components, such as stainless steel vacuum flanges that are too close to the cavity's evanescent fields. However, careful SRF cavity preparation and experimental configuration have achieved the ideal Q_o not only for low field amplitudes, but up to cavity fields that are typically 75% of the magnetic field quench limit. Few cavities make it to the magnetic field quench limit since residual losses and vanishingly small defects heat up localized spots, which eventually exceed the superconducting critical temperature and lead to a thermal quench.

Q *vs* E

When using superconducting RF cavities in particle accelerators, the field level in the cavity should generally be as high as possible to most efficiently accelerate the beam passing through it. The Q_o values described by the above calculations tend to degrade as the fields increase, which is plotted for a given cavity as a "Q vs E" curve, where "E"

refers to the accelerating electric field of the TM_{01} mode. Ideally, the cavity Q_o would remain constant as the accelerating field is increased all the way up to the point of a magnetic quench field, as indicated by the "ideal" dashed line in the plot below. In reality, though, even a well prepared niobium cavity will have a Q vs E curve that lies beneath the ideal, as shown by the "good cavity" curve in the plot.

There are many phenomena that can occur in an SRF cavity to degrade its Q vs E performance, such as impurities in the niobium, hydrogen contamination due to excessive heat during chemistry, and a rough surface finish. After a couple decades of development, a necessary prescription for successful SRF cavity production is emerging. This includes:

- Eddy-current scanning of the raw niobium sheet for impurities,
- Good quality control of electron beam welding parameters,
- Maintain a low cavity temperature during acid chemistry to avoid hydrogen contamination,
- Electropolish of the cavity interior to achieve a very smooth surface,
- High pressure rinse (HPR) of the cavity interior in a clean room with filtered water to remove particulate contamination,
- Careful assembly of the cavity to other vacuum apparatus in a clean room with clean practices,
- A vacuum bake of the cavity at 120 °C for 48 hours, which typically improves Q_o by a factor of 2.

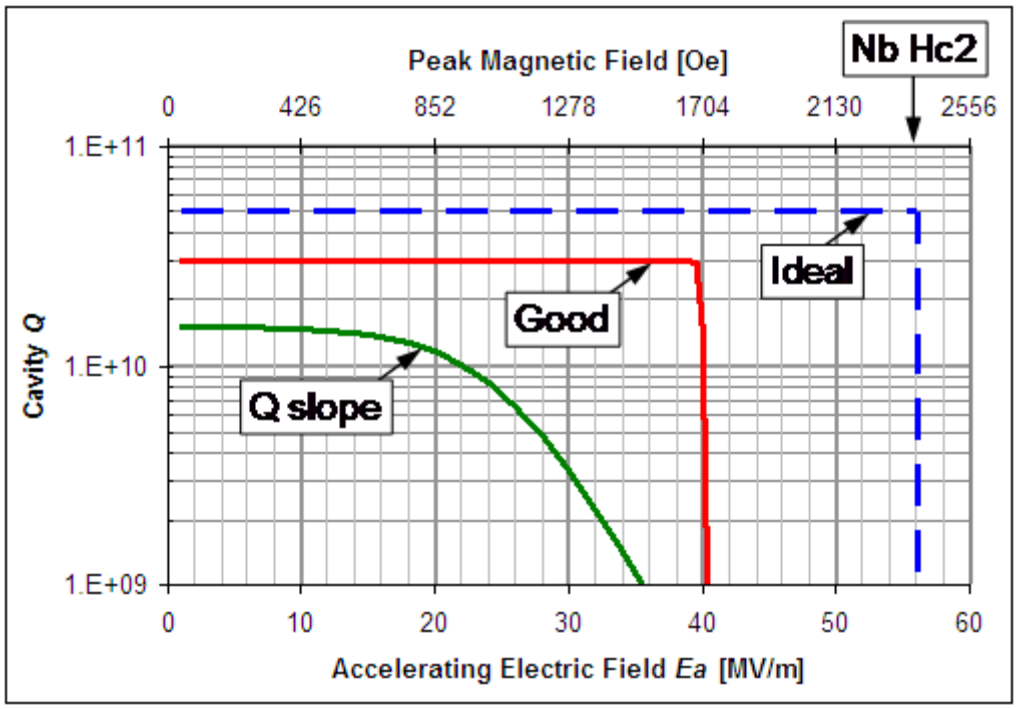

Example plots of SRF cavity Q_o vs the accelerating electric field E_a and peak magnetic field of the TM_{01} mode.

There remains some uncertainty as to the root cause of why some of these steps lead to success, such as the electropolish and vacuum bake. However, if this prescription is not followed, the Q vs E curve often shows an excessive degradation of Q_o with increasing field, as shown by the "Q slope" curve in the plot below. Finding the root causes of Q slope phenomena is the subject of ongoing fundamental SRF research. The insight gained could lead to simpler cavity fabrication processes as well as benefit future material development efforts to find higher T_c alternatives to niobium.

Wakefields and higher order modes (HOMs)

One of the main reasons for using SRF cavities in particle accelerators is that their large apertures result in low beam impedance and higher thresholds of deleterious beam instabilities. As a charged particle beam passes through a cavity, its electromagnetic radiation field is perturbed by the sudden increase of the conducting wall diameter in the transition from the small-diameter beampipe to the large hollow RF cavity. A portion of the particle's radiation field is then "clipped off" upon re-entrance into the beampipe and left behind as wakefields in the cavity. The wakefields are simply superimposed upon the externally driven accelerating fields in the cavity. The spawning of electromagnetic cavity modes as wakefields from the passing beam is analogous to a drumstick striking a drumhead and exciting many resonant mechanical modes.

The beam wakefields in an RF cavity excite a subset of the spectrum of the many electromagnetic modes, including the externally driven TM_{01} mode. There are then a host of beam instabilities that can occur as the repetitive particle beam passes through the RF cavity, each time adding to the wakefield energy in a collection of modes.

For a particle bunch with charge q, a length much shorter than the wavelength of a given cavity mode, and traversing the cavity at time t=0, the amplitude of the wakefield voltage left behind in the cavity in a given mode is given by

$$V_{wake} = \frac{q\omega_o R}{2Q_o}\, e^{j\omega_o t}\, e^{-\frac{\omega t}{2Q_L}} = kq\, e^{j\omega_o t}\, e^{-\frac{\omega t}{2Q_L}},$$

where:

R is the "shunt impedance" of the cavity mode defined by

$$R = \frac{\left(\int \vec{E} \cdot dl\right)^2}{P_d} = \frac{V^2}{P_d},$$

E is the electric field of the RF mode,
P_d is the power dissipated in the cavity to produce the electric field E,
Q_L is the "loaded Q" of the cavity, which takes into account energy leakage out of the coupling antenna,
ω_o is the angular frequency of the mode,
the imaginary exponential is the mode's sinusoidal time variation,

the real exponential term quantifies the decay of the wakefield with time, and

$$k = \frac{\omega_o R}{2Q_o}$$ is termed the *loss parameter* of the RF mode.

The shunt impedance R can be calculated from the solution of the electromagnetic fields of a mode, typically by a computer program that solves for the fields. In the equation for V_{wake}, the ratio R/Q_o serves as a good comparative measure of wakefield amplitude for various cavity shapes, since the other terms are typically dictated by the application and are fixed. Mathematically,

$$\frac{R}{Q_o} = \frac{V^2}{\omega U} = \frac{2\left(\int \vec{E} \cdot dl\right)^2}{\omega \mu_o \int |\vec{H}|^2 dV} = \frac{2k}{\omega_o},$$

where relations defined above have been used. R/Q_o is then a parameter that factors out cavity dissipation and is viewed as measure of the cavity geometry's effectiveness of producing accelerating voltage per stored energy in its volume. The wakefield being proportional to R/Q_o can be seen intuitively since a cavity with small beam apertures concentrates the electric field on axis and has high R/Q_o, but also clips off more of the particle bunch's radiation field as deleterious wakefields.

The calculation of electromagnetic field buildup in a cavity due to wakefields can be complex and depends strongly on the specific accelerator mode of operation. For the straightforward case of a storage ring with repetitive particle bunches spaced by time interval T_b and a bunch length much shorter than the wavelength of a given mode, the long term steady state wakefield voltage presented to the beam by the mode is given by

$$V_{ss\ wake} = V_{wake}\left(\frac{1}{1 - e^{-\tau} e^{j\delta}} - \frac{1}{2}\right),$$

where:

$$\tau = \frac{\omega T_b}{2Q_L}$$ is the decay of the wakefield between bunches, and
δ is the phase shift of the wakefield mode between bunch passages through the cavity.

As an example calculation, let the phase shift $\delta=0$, which would be close to the case for the TM_{01} mode by design and unfortunately likely to occur for a few HOM's. Having $\delta=0$ (or an integer multiple of an RF mode's period, $\delta=n2\pi$) gives the worse-case wakefield build-up, where successive bunches are maximally decelerated by previous bunches' wakefields and give up even more energy than with only their "self wake". Then, taking $\omega = 2\pi$ 500 MHz, T_b=1 μs, and $Q_L=10^6$, the buildup of wakefields would be $V_{ss\ wake}=637\times V_{wake}$. A pitfall for any accelerator cavity would be the presence of what is

termed a "trapped mode". This is an HOM that does not leak out of the cavity and consequently has a Q_L that can be orders of magnitude larger than used in this example. In this case, the buildup of wakefields of the trapped mode would likely cause a beam instability. The beam instability implications due to the $V_{ss\ wake}$ wakefields is thus addressed differently for the fundamental accelerating mode TM_{01} and all other RF modes, as described next.

Fundamental accelerating mode TM_{01}

The complex calculations treating wakefield-related beam stability for the TM_{01} mode in accelerators show that there are specific regions of phase between the beam bunches and the driven RF mode that allow stable operation at the highest possible beam currents. At some point of increasing beam current, though, just about any accelerator configuration will become unstable. As pointed out above, the beam wakefield amplitude is proportional to the cavity parameter R/Q_o, so this is typically used as a comparative measure of the likelihood of TM_{01} related beam instabilities. A comparison of R/Q_o and R for 500 MHz superconducting and normal-conducting cavities is shown below. The accelerating voltage provided by both is comparable for a given net power consumption, including refrigeration for SRF. The R/Q_o for the SRF cavity is 15 times less than the normal-conducting version, and thus less beam instability susceptible. This one of the main reasons such SRF cavities are chosen for use in high-current storage rings.

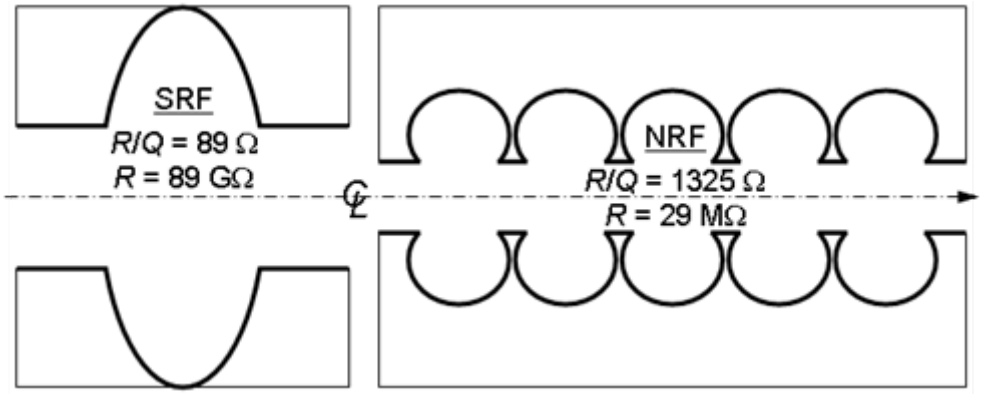

Comparison of superconducting and normal-conducting RF cavity shapes and their R/Q_o.

Higher order modes (HOMs)

In addition to the fundamental accelerating TM_{01} mode of an RF cavity, numerous higher frequency modes and a few lower-frequency dipole modes are excited by charged particle beam wakefields, all generally denoted higher order modes (HOMs). These modes serve no useful purpose for accelerator particle beam dynamics, only giving rise to beam instabilities, and are best heavily damped to have as low a Q_L as possible. The damping is accomplished by preferentially allowing dipole and all HOMs to leak out of the SRF cavity, and then coupling them to resistive RF loads. The leaking out of undesired RF modes occurs along the beampipe, and results from a careful design of the cavity aperture shapes. The aperture shapes are tailored to keep the TM_{01} mode "trapped" with high Q_o

inside of the cavity and allow HOMs to propagate away. The flutes present an effectively larger beampipe diameter to asymmetric RF modes, allowing them to easily propagate away from the cavity, while presenting an effectively small diameter to the axisymmetric TM_{01} mode and hindering its propagation.

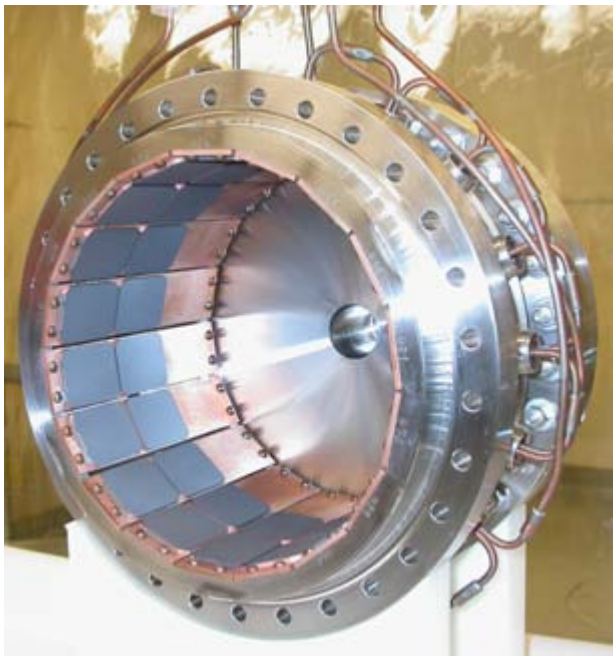

Photograph of the Cornell electron storage ring beamline HOM load.

The resistive load for HOMs can be implemented by having loop antennas located at apertures on the side of the beampipe, with coaxial lines routing the RF to outside of the cryostat to standard RF loads. Another approach is to place the HOM loads directly on the beampipe as hollow cylinders with RF lossy material attached to the interior surface, as shown in the image to the right. This "beamline load" approach can be more technically challenging, since the load must absorb high RF power while preserving a high-vacuum beamline environment in close proximity to a contamination-sensitive SRF cavity. Further, such loads must sometimes operate at cryogenic temperatures to avoid large thermal gradients along the beampipe from the cold SRF cavity. The benefit of the beamline HOM load configuration, however, is a greater absorptive bandwidth and HOM attenuation as compared to antenna coupling. This benefit can be the difference between a stable vs. an unstable particle beam for high current accelerators.

Cryogenics

A significant part of SRF technology is cryogenic engineering. The SRF cavities tend to be thin-walled structures immersed in a bath of liquid helium having temperature 1.6 K to 4.5 K. Careful engineering is then required to insulate the helium bath from the room-temperature external environment. This is accomplished by:

- A vacuum chamber surrounding the cold components to eliminate convective heat transfer by gases.
- Multi-layer insulation wrapped around cold components. This insulation is composed of dozens of alternating layers of aluminized mylar and thin fiberglass sheet, which reflects infrared radiation that shines through the vacuum insulation from the 300 K exterior walls.
- Low thermal conductivity mechanical connections between the cold mass and the room temperature vacuum vessel. These connections are required, for example, to support the mass of the helium vessel inside the vacuum vessel and to connect the apertures in the SRF cavity to the accelerator beamline. Both types of connections transition from internal cryogenic temperatures to room temperature at the vacuum vessel boundary. The thermal conductivity of these parts is minimized by having small cross sectional area and being composed of low thermal conductivity material, such as stainless steel for the vacuum beampipe and fiber reinforced epoxies (G10) for mechanical support. The vacuum beampipe also requires good electrical conductivity on its interior surface to propagate the image currents of the beam, which is accomplished by about 100 μm of copper plating on the interior surface.

The major cryogenic engineering challenge of SRF technology is the refrigeration plant for the liquid helium. The small power that is dissipated in an SRF cavity and the heat leak to the vacuum vessel are both heat loads at very low temperature. The refrigerator must replenish this loss with an inherent poor efficiency, given by the product of the Carnot efficiency η_C and a "practical" efficiency η_p. The Carnot efficiency derives from the second law of thermodynamics and can be quite low. It is given by

$$\eta_C = \begin{cases} \frac{T_{cold}}{T_{warm} - T_{cold}}, & \text{if } T_{cold} < T_{warm} - T_{cold} \\ 1, & \text{otherwise} \end{cases}$$

where

T_{cold} is the temperature of the cold load, which is the helium vessel in this case, and
T_{warm} is the temperature of the refrigeration heat sink, usually room temperature.

In most cases T_{warm} =300 K, so for T_{cold} ≥150 K the Carnot efficiency is unity. The practical efficiency is a catch-all term that accounts for the many mechanical non-idealities that come into play in a refrigeration system aside from the fundamental physics of the Carnot efficiency. For a large refrigeration installation there is some economy of scale, and it is possible to achieve η_p in the range of 0.2–0.3. The wall-plug power consumed by the refrigerator is then

$$P_{warm} = \frac{P_{cold}}{\eta_C \, \eta_p},$$

where

P_{cold} is the power dissipated at temperature T_{cold} .

As an example, if the refrigerator delivers 1.8 K helium to the cryomodule where the cavity and heat leak dissipate P_{cold}=10 W, then the refrigerator having T_{warm}=300 K and η_p=0.3 would have η_C=0.006 and a wall-plug power of P_{warm}=5.5 kW. Of course, most accelerator facilities have numerous SRF cavities, so the refrigeration plants can get to be very large installations.

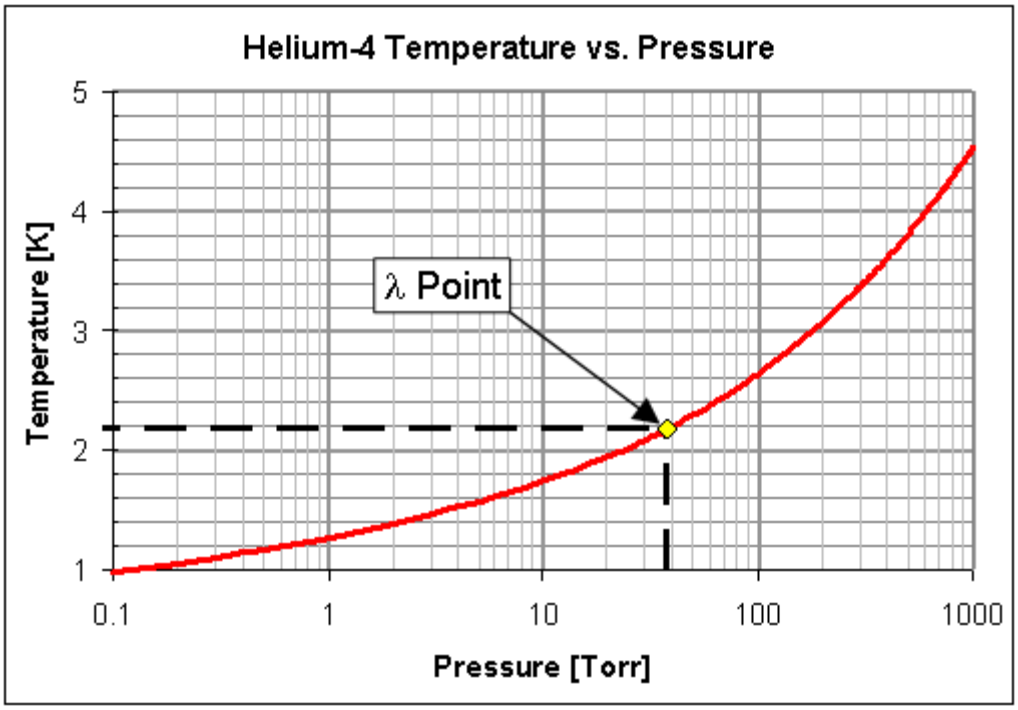

Plot of helium-4 temperature vs. pressure, with the superfluid λ point indicated.

The temperature of operation of an SRF cavity is typically selected as a minimization of wall-plug power for the entire SRF system. The plot to the right then shows the pressure to which the helium vessel must be pumped to obtain the desired liquid helium temperature. Atmospheric pressure is 760 Torr (101.325 kPa), corresponding to 4.2 K helium. The superfluid λ point occurs at about 38 Torr (5.1 kPa), corresponding to 2.18 K helium. Most SRF systems either operate at atmospheric pressure, 4.2 K, or below the λ point at a system efficiency optimum usually around 1.8 K, corresponding to about 12 Torr (1.6 kPa).

Chapter 6

Superconductor Insulator Transition and Superconductor-Insulator-Superconductor

Superconductor Insulator Transition

The **Superconductor Insulator Transition** is an example of a quantum phase transition, whereupon tuning some parameter in the Hamiltonian, a dramatic change in the behavior of the electrons occurs. The nature of how this transition occurs is disputed, and many studies seek to understand how the order parameter, $\Psi = \Delta\exp(i\theta)$, changes. Here Δ is the amplitude of the order parameter, and θ is the phase. Most theories involve either the destruction of the amplitude of the order parameter - by a reduction in the density of states at the Fermi surface, or by destruction of the phase coherence; which results from the proliferation of vortices.

Destruction of superconductivity

In two dimensions, the subject of superconductivity becomes very interesting because the existence of true long-range order is not possible. How then is superconductivity obtained? In the 70's, Kosterlitz and Thouless (along with Berezinski) showed that a different kind of long-range order could exist - topological order - which showed power law correlations (meaning that by measuring the two-point correlation function $\langle \Psi(0)\Psi(r)\rangle \propto r^{-\gamma}$ it decays algebraically).

This picture changes if disorder is included. Kosterlitz-Thouless behavior can be obtained, but the fluctuations of the order parameter are greatly enhanced, and the transition temperature is suppressed.

The model to keep in mind in terms of understanding how superconductivity occurs in a two-dimensional disordered superconductor is the following. At high temperatures, the

system is in the normal state. As the system is cooled towards its transition temperature, superconducting grains begin to fluctuate in and out of existence. When one of these grains "pops" into existence, it is accelerated without dissipation for a time τ before decaying back into the normal state. This has the effect of increasing the conductivity even before the system has condensed into the superconducting state. This increased conductivity above T_{c0} is referred to as paraconductivity, or fluctuation conductivity, and was first correctly described by Aslamazov and Larkin. As the system is cooled further, the lifetime of these fluctuations increase, and becomes comparable to the Ginzburg-Landau time $\tau_{GL} = \frac{\pi}{\hbar(T - T_{c0})}$. Eventually, the amplitude Δ of the order parameter becomes well defined (it is non-zero wherever there are superconducting patches), and it can begin to support phase fluctuations. These phase fluctuations set in at a lower temperature, and are caused by vortices - which are topological defects in the order parameter. It is the motion of vortices that gives rise to finite resistance below T_{c0}. Eventually the system is cooled further, below the Kosterlitz-Thouless temperature T_c, all of the free vortices become bound into vortex-antivortex pairs, and the systems attains a state with zero resistance.

Finite magnetic field

Cooling the system to $T = 0$ and turn on a magnetic field has certain effects. For very small fields ($B < B_{c1}$) the magnetic field is shielded from the interior of the sample. Above B_{c1} however, the energy cost to keep out the external field becomes too great, and the superconductor allows the field to penetrate in quantized fluxons. Now the superconductor has transitioned into the "mixed state", in which there is a superfluid along with vortices - which now have only one circulation.

Increasing the field adds vortices to the system. In a conventional bulk superconductor, eventually the density of vortices becomes so large that they overlap. The core of the vortex contains normal electrons (i.e. the amplitude of the superconducting order parameter is zero), so when they overlap, superconductivity is killed by destroying the amplitude of the order parameter. Increasing the field further leads to a very interesting possibility - in two-dimensions where the fluctuations are enhanced - that the vortices may condense into a Bose-condensate, which localizes the superconducting pairs.

Superconductor-Insulator-Superconductor

Superconductor-insulator-superconductor, also known as SIS tunnel junction or just SIS, is a two-terminal (diode) electronic device consisting of two superconductors separated by a very thin layer of insulating material. The device is typically fabricated epitaxially on silicon or other insulating substrates. Some common structures are Pb-PbO-Pb and Nb-Al_2O_3-Nb. Many variations on the SIS have been tried based on almost

all metallic and alloy superconductors. With a thin enough insulating layer, the electronic response time of this device can be measured in picoseconds, allowing it to be used in circuits where logic or radio signals above 100 GHz are processed. In operation, the SIS must be cooled to a temperature significantly lower than the superconducting transition temperature of its electrodes. For lead- and niobium-based devices, it is typical to operate at temperatures close to that of liquid helium, about 4.2 kelvins.

All currents flowing through an SIS must somehow get "through" the insulating layer. The insulator is made thin enough so that the dominant method of conduction is quantum tunnelling. There are two important components to the tunneling currents. First are the Josephson Effect currents, due to the tunneling of Cooper pairs of electrons. Second, are single electron or quasiparticle currents. These arise when the voltage across the insulating barrier is large enough to pull the Cooper pairs apart.

In many applications, the SIS is shunted by a resistor. In this configuration, only the Cooper pair or Josephson currents through the SIS are significant, while normal (or single) electrons can flow through the resistor. The SIS-resistor pair operate as a nearly ideal resistively shunted junction (RSJ). As part of an RSJ, the SIS is the primary active element in RSFQ fast logic circuits, SQUIDs and the Josephson Voltage Standard which defines the international standard volt.

SIS quasiparticle currents enable their use as extremely low noise receivers for radio astronomy in the 100 GHz to 1000 GHz frequency range. In this application, the SIS is dc biased at a voltage just below what is needed to break Cooper pairs into quasiparticles. Radio waves from the astronomical objects of interest are focussed on to the SIS, along with a local oscillator radio source. Radio frequency photons are absorbed by the SIS. For each photon absorbed in the SIS, one Cooper pair is broken and an electron crosses the insulator by "photon-assisted tunneling." This is a description of an SIS heterodyne receiver.. These receivers are so sensitive that the physical theory of the devices must take into account quantum noise to properly describe their performance.

Chapter 7

Superdiamagnetism and Technological Applications of Superconductivity

Superdiamagnetism

Superdiamagnetism (or **perfect diamagnetism**) is a phenomenon occurring in certain materials at low temperatures, characterised by the complete absence of magnetic permeability (i.e. a magnetic susceptibility $\chi_v = -1$) and the exclusion of the interior magnetic field. Superdiamagnetism is a feature of superconductivity. It was identified in 1933, by Walter Meissner and Robert Ochsenfeld (the Meissner effect).

Superdiamagnetism established that the superconductivity of a material was a stage of phase transition. Superconducting magnetic levitation is due to superdiamagnetism, which repels a permanent magnet, and flux pinning, which prevents the magnet floating away.

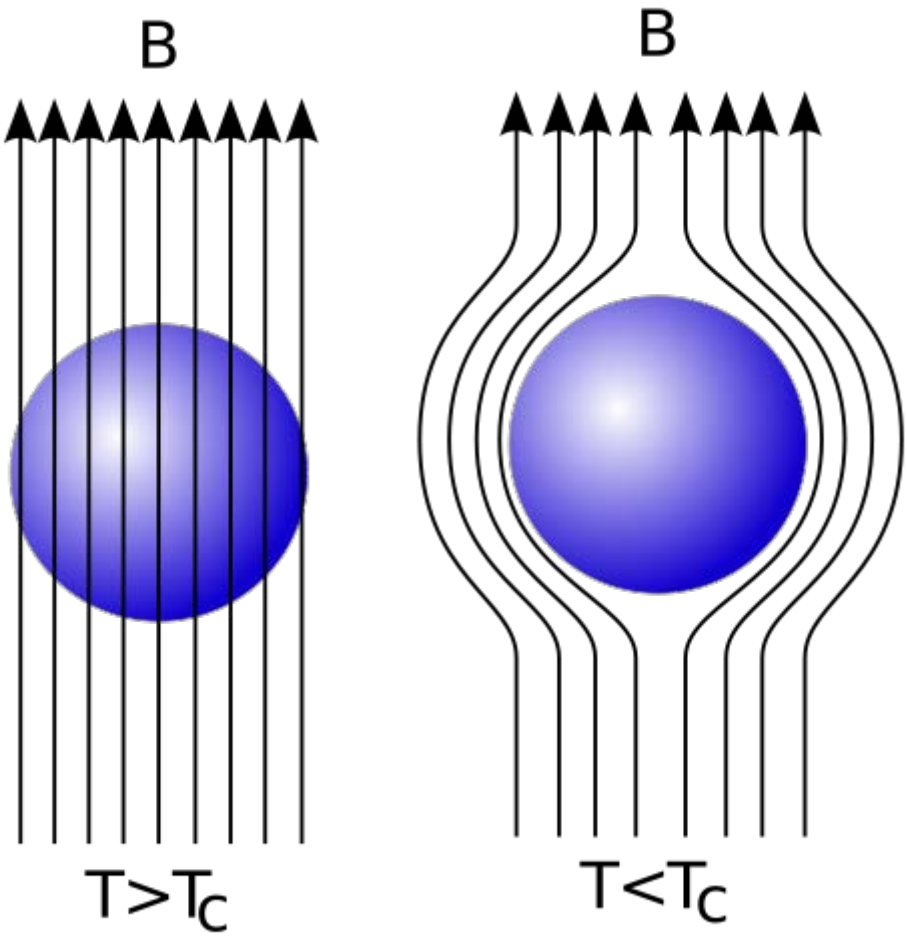

Diagram of the Meissner effect. Magnetic field lines, are excluded from a superconductor when it is below its critical temperature.

Theory

Fritz London and Heinz London developed the theory that the exclusion of magnetic flux is brought about by electrical screening currents that flow at the surface of the superconducting material and which generate a magnetic field that exactly cancels the externally applied field inside the superconductor. These screening currents are generated whenever a superconducting material is brought inside a magnetic field. This can be understood by the fact that a superconductor has zero electrical resistance, so that "eddy currents", induced by the motion of the material inside a magnetic field, will not decay. Fritz, at the Royal Society in 1935, stated that the thermodynamic state would be described by a single wave function.

"Screening currents" also appear in a situation wherein an initially normal, conducting metal is placed inside a magnetic field. As soon as the metal is cooled below the

appropriate transition temperature, it becomes superconducting. This expulsion of magnetic field upon the cooling of the metal cannot be explained any longer by merely assuming zero resistance and is called *the Meissner effect*. It shows that the superconducting state does not depend on the history of preparation, only upon the present values of temperature, pressure and magnetic field, and therefore is a true thermodynamic state.

Technological applications of superconductivity

Some of the **technological applications of superconductivity** include :

- the production of sensitive magnetometers based on SQUIDs,
- fast digital circuits (including those based on Josephson junctions and rapid single flux quantum technology),
- powerful superconducting electromagnets used in maglev trains, Magnetic Resonance Imaging (MRI) and Nuclear magnetic resonance (NMR) machines, magnetic confinement fusion reactors (e.g. tokamaks), and the beam-steering and focusing magnets used in particle accelerators,
- low-loss power cables,
- RF and microwave filters (e.g., for mobile phone base stations, as well as, military ultra-sensitive/selective receivers),
- fast fault current limiters
- railgun and coilgun magnets.
- Electric motors and generators

Magnetic Resonance Imaging (MRI) and Nuclear Magnetic Resonance (NMR)

The biggest application right now for superconductivity is in producing the large volume, stable magnetic fields required for MRI and NMR. This represents a multi-billion US$ market for companies such as Oxford Instruments, Siemens etc. The magnets typically use low temperature superconductors (LTS) because high-temperature superconductors are not yet cheap enough to cost effectively deliver the high, stable and large volume fields required, notwithstanding the need to cool LTS instruments to liquid helium temperatures. Superconductors are also used in high field scientific magnets *because copper has a limit to the field strength it can produce*.

High-temperature superconductivity (HTS)

The commercial applications so far for high-temperature superconductors (HTS) have been limited.

HTS superconduct at temperatures up to the boiling point of liquid nitrogen which makes them cheaper to cool than low temperature superconductors (LTS). However the problem with HTS technology is that the currently known high-temperature superconductors are brittle ceramics which are expensive to manufacture and not easily turned into wires or other useful shapes. Therefore the applications for HTS have been where it has some other intrinsic advantage i.e. in

- low thermal loss current leads for LTS devices (low thermal conductivity),
- RF and microwave filters (low resistance to RF), and
- increasingly in specialist scientific magnets, particularly where size and electricity consumption are critical (while HTS wire is much more expensive than LTS in these applications this can be offset by the relative cost and convenience of cooling); the ability to ramp field is desired (the higher and wider range of HTS's operating temperature means faster changes in field can be managed); or cryogen free operation is desired (LTS generally requires liquid helium that is becoming more scarce and expensive).

HTS-based systems

HTS has application in scientific and industrial magnets, including use in NMR and MRI systems. Commercial systems are now available in each category.

Also one intrinsic attribute of HTS is that it can withstand much higher magnetic fields than LTS, so HTS at liquid helium temperatures are being explored for very high-field inserts inside LTS magnets.

Promising future industrial and commercial HTS applications include Induction heaters, transformers, fault current limiters, power storage, motors and generators, fusion reactors and magnetic levitation devices.

Early applications will be where the benefit of smaller size, lower weight or the ability to rapidly switch current (fault current limiters) outweighs the added cost. Longer-term as conductor price falls HTS systems should be competitive in a much wider range of applications on energy efficiency grounds alone.

Holbrook Superconductor Project

The Holbrook Superconductor Project is a project to design and build the world's first production superconducting transmission power cable. The cable was commissioned in late June 2008. The suburban Long Island electrical substation is fed by about 600-meter-long underground cable system consists of about 99 miles of high-temperature

superconductor wire manufactured by American Superconductor, installed underground and chilled with liquid nitrogen greatly reducing the costly right-of-way required to deliver additional power.

Tres Amigas Project

American Superconductor was chosen for The Tres Amigas Project, the United States' first renewable energy market hub. The Tres Amigas renewable energy market hub will be a multi-mile, triangular electricity pathway of Superconductor Electricity Pipelines capable of transferring and balancing many gigawatts of power between three U.S. power grids (the Eastern Interconnection, the Western Interconnection and the Texas Interconnection). Unlike traditional powerlines, it will transfer power as DC instead of AC current. It will be located in Clovis, New Mexico.

Magnesium diboride

Magnesium diboride is a much cheaper superconductor than either BSCCO or YBCO in terms of cost per current-carrying capacity per length (cost/(kA*m)), in the same ballpark as LTS, and on this basis many manufactured wires are already cheaper than copper. Furthermore, MgB_2 superconducts at temperatures higher than LTS (its critical temperature is 39 K, compared with less than 10 K for NbTi and 18.3 K for Nb_3Sn), introducing the possibility of using it at 10-20 K in cryogen-free magnets or perhaps eventually in liquid hydrogen. However MgB_2 is limited in the magnetic field it can tolerate at these higher temperatures, so further research is required to demonstrate its competitiveness in higher field applications.

Chapter 8

Type-1.5 Superconductor and Type-II Superconductor

Type-1.5 superconductor

The term **type-1.5 superconductor** refers to a *multicomponent* superconductor which *simultaneously* has several magnetic properties of Type I superconductor (such as positive superconductor to normal metal interface energy and characteristic length scales associated with modulation of the condensate density larger than magnetic field penetration length) and Type-II superconductor (such as negative superconductor to normal metal interface energy and a different characteristic length scales associated with modulation of the condensate density smaller than magnetic field penetration length).

Properties of type-1.5 superconductor

	Type-I superconductor	Type-II superconductor	Type-1.5 superconductor
Characteristic length scales	The characteristic magnetic field variation length scale is smaller than the characteristic length scale of condensate density variation (coherence length) $\lambda<\sqrt{2}\xi$	The characteristic magnetic field variation length scale is larger than the characteristic length scale of the condensate density variation (coherence length) $\lambda<\sqrt{2}\xi$	Two characteristic length scales of condensates density variation ξ_1, ξ_2. Characteristic magnetic field variation length scale is smaller than one of the characteristic length scales of density variation and larger than another characteristic length scale of density variation $\sqrt{2}\xi_2<\lambda<\sqrt{2}\xi$
Intervortex interaction	Attractive	Repulsive	Attractive at long range and repulsive at short range
Phases in magnetic field of a clean bulk superconductor	(1) Meissner state at low fields; (2) Macroscopically large normal domains at larger fields. First order phase transition between the states (1) and (2)	(1) Meissner state at low fields, (2) vortex lattices/liquids at larger fields.	(1) Meissner state at low fields (2) "Semi-Meissner state": vortex clusters coexisting with Meissner domains at intermediate fields (3) Vortex lattices/liquids at larger fields.
Phases transitions	First order phase transition between the states (1) and (2)	Second order phase transition between the states (1) and (2) and second order phase transition between from the state (2) to normal state	First order phase transition between the states (1) and (2) and second order phase transition between from the state (2) to normal state.

Energy of Superconducting/normal boundary	Positive	Negative	Negative energy of superconductor/normal interface inside a vortex cluster, positive energy at the boundary of vortex cluster
Weakest magnetic field required to form a vortex	Larger than thermodynamical critical magnetic field	Smaller than thermodynamical critical magnetic field	In some cases larger than critical magnetic field for single vortex but smaller than critical magnetic field for a vortex cluster
Energy E(N) of N-quanta axially symmetric vortex solutions	E(N)/N < E(N–1)/(N–1) for all N, i.e. N-quanta vortex does not decay in 1-quanta vortices	E(N)/N > E(N–1)/(N–1) for all N, i.e. N-quanta vortex decays in 1-quanta vortices	There is a characteristic number of flux quanta Nc such that E(N)/N < E(N–1)/(N–1) for N<Nc and E(N)/N > E(N–1)/(N–1) for N>Nc, N-quanta vortex decays into vortex cluster

Traditionally superconductors were divided into two classes: type-I and type-II according to their behavior in magnetic field.

Type-I superconductors completely expel external magnetic fields if the strength of the applied field is sufficiently low this state is called the Meissner state. However at elevated magnetic field, when the magnetic field energy becomes comparable with the superconducting condensation energy, the superconductivity is destroyed.

Type-II superconductors besides the Meissner state, possess another state: a sufficiently strong applied magnetic field can produce quantum vortices which can carry magnetic flux through the interior of the superconductor. These quantum vortices repel each other and thus tend to form uniform vortex lattices or liquids . Formally, vortex solutions exist also in models of type-I superconductivity, but the interaction between vortices is purely attractive so a system of many vortices is unstable against a collapse onto a state of a single giant macroscopic vortex. More importantly, the vortices in type-I superconductor are energetically unfavorable. To produce them it would require to apply magnetic field with strength larger than what a superconducting condensate can withstand. In the usual Ginzburg–Landau theory, only the quantum vortices with purely repulsive interaction are energetically cheap enough to be induced by applied magnetic field.

However it was later predicted that the type-I/type-II dichotomy is broken in two component superconductors. A two component superconductor is described by the following Ginzburg-Landau model

$$F=\sum_{i,j=1,2}\frac{1}{2m}|(\nabla-ieA)\psi_i|^2+\alpha_i|\psi_i|^2+\beta_i|\psi_i|^4-\eta(\psi_1\psi_2^*+\psi_1^*\psi_2)+\gamma[(\nabla-ieA)\psi_1\cdot(\nabla+ieA)\psi_2^*+(\nabla+ieA)\psi_1^*\cdot(\nabla-ieA)\psi_2]+\nu|\psi_1|^2|\psi_2|^2+\frac{1}{2}(\nabla\times A)^2$$

where $\psi_i=|\psi_i|e^{i\phi_i},i=1,2$ are two superconducting condensates. In systems with U(1)xU(1) symmetry η = γ = 0, in multiband superconductors quite generically $\eta\neq 0,\gamma\neq 0$. In case if the condensates are coupled only electromagnetically, i.e. by A the model has three length scales: the London penetration length $\lambda=\frac{1}{e\sqrt{|\psi_1|^2+|\psi_2|^2}}$ and two coherence lengths $\xi_1=\frac{1}{\sqrt{2\alpha_1}},\xi_2=\frac{1}{\sqrt{2\alpha_2}}$. The necessary but not sufficient condition for occurrence of type-1.5 regime is $\xi_1 > \lambda > \xi_2$. Additional condition of thermodynamic stability should be satisfied.

When $\eta \neq 0, \gamma \neq 0, \nu \neq 0$three length scales of the problem are the London penetration length and two characteristic length scales associated with normal modes of coupled density fluctuations rather than coherence lengths. In that case the generalized $\tilde{\xi}_1(\alpha_1, \beta_1, \alpha_2, \beta_2, \eta, \gamma, \nu), \tilde{\xi}_2(\alpha_1, \beta_1, \alpha_2, \beta_2, \eta, \gamma, \nu)$are attributed to "mixed" combinations of density fields.

An example of two-component superconductivity is the two-band superconductor magnesium diboride. There, one can distinguish two superconducting components associated with electrons belong to different bands. A different example of two component systems is the projected superconducting states of liquid metallic hydrogen or deuterium where mixtures of superconducting electrons and superconducting protons or deuterons were theoretically predicted.

In two-component system new vortex solutions were found with interaction which has a nonmonotonic character: such vortices attract each other at large distances and repel each other at short distances. It was further shown that there is a range of parameters where these vortices are energetically favorable enough to be excitable by external field, attractive interaction part notwithstanding. These vortices are endowed with a number of exotic properties and result into a formation of new superconducting phase in low magnetic fields dubbed "Semi-Meissner" state in . The vortices, whose density is controlled by the strength of applied magnetic field, instead of forming a regular structure, should have a tendency to form "vortex" droplets because of their long-range attractive interaction caused by condensate density suppression in the area around the vortex. Such vortex clusters should coexist with the areas of vortex-less two-component Meissner domains.

In 2009, experimental results have been reported indicating that magnesium diboride may fall into this new class of superconductivity. The term type-1.5 superconductor was coined for this state. Further experimental data backing this conclusion was reported in . More recent theoretical works show that the type-1.5 may be more general phenomenon because it does not require a material with two truly superconducting bands, but can also happen as a result of even very small interband proximity effect and is robust in the presence of various inter-band couplings such as interband Josephson coupling .

Animations of type-1.5 superconducting behavior

Movies from numerical simulations of the Semi-Meissner state where Meissner domains coexist with clusters where vortex droplets form in one superconducting components and macroscopic normal domains in the other**.**

Type-II superconductor

A **Type-II superconductor** is a superconductor characterized by its gradual transition from the superconducting to the normal state within an increasing magnetic field. Typically they superconduct at higher temperatures and magnetic fields than Type-I superconductors. This allows them to conduct higher currents and makes them useful for strong electromagnets.

The possibility of type-II superconductivity was theoretically predicted by Alexei Alexeyevich Abrikosov, for which a Nobel Prize in Physics was awarded in 2003.

Materials

Type-II superconductors are usually made of metal alloys or complex oxide ceramics, whereas most superconducting pure metals are Type-I superconductors. All high temperature superconductors are Type-II superconductors, and (as of early 2008) comprise mostly complex copper oxide ceramics. While most pure metal or pure element superconductors are Type-I, niobium, vanadium, and technetium are pure element Type-II superconductors. Boron-doped diamond and silicon are also Type-II superconductors. Metal alloy superconductors also exhibit Type-II behavior (*e.g.* niobium-titanium, niobium-tin).

Niobium-tin was discovered in 1954.

Other Type-II examples are the cuprate-perovskite ceramic materials which have achieved the highest temperatures to reach the superconducting state. These include $La_{1.85}Ba_{0.15}CuO_4$, BSCCO, and YBCO (Yttrium-Barium-Copper-Oxide), which is famous as the first material to achieve superconductivity above the boiling point of liquid nitrogen.

In 2001 Magnesium diboride was discovered to be a type-II SC with useful properties. Until the discovery of the iron-arsenide family, It was the highest temperature superconductor not containing copper.

Important uses

Strong superconducting electromagnets (used in MRI scanners, NMR machines, and particle accelerators) often use niobium-titanium or, for higher fields, niobium-tin.

Critical temperatures and critical fields

In comparison to the (theoretically) sharp transition of a Type-I superconductor above the lower temperature T_{c1}, magnetic flux from external fields is no longer completely expelled, and the superconductor exists in a mixed state. Above the higher temperature T_{c2}, the superconductivity is completely destroyed, and the material exists in a normal

state. Both of these temperatures are dependent on the strength of the applied field. It is more usual to consider a fixed temperature, in which case transition (flux penetration) occurs between critical field strengths H_{c1} and H_{c2} (the upper critical field).

Mixed state

Ginzburg–Landau theory defines 2 parameters: The coherence length of a superconductor, related to the mean free path of its charge carriers, and a penetration depth.

The earlier London penetration depth is the penetration distance of a weak magnetic field.

In a Type-II superconductor, the coherence length is smaller than the London penetration depth, meaning that magnetic flux lines can pierce the material at high enough external fields. This is known as the vortex state, as the flux lines run through narrow regions of non superconducting material, surrounded by vortices of supercurrents protecting the rest of the superconductor. The vortices can arrange themselves in a regular structure known as the vortex lattice, also named the Abrikosov vortex, after Alexei Alexeyevich Abrikosov, who was awarded the 2003 Nobel Prize in Physics for his pioneering contributions.

Chapter 9

High-Temperature Superconductivity

High-temperature superconductors (abbreviated **high-T_c** or **HTS**) are materials that have a superconducting transition temperature (T_c) above 30 K (−243.2 °C). From 1960 to 1980, 30 K was thought to be the highest theoretically possible T_c. The first high-T_c superconductor was discovered in 1986 by IBM Researchers Karl Müller and Johannes Bednorz, for which they were awarded the Nobel Prize in Physics in 1987.

Until Fe-based superconductors were discovered in 2008, the term **high-temperature superconductor** was used interchangeably with **cuprate superconductor** for compounds such as bismuth strontium calcium copper oxide (BSCCO) and yttrium barium copper oxide (YBCO).

"High-temperature" has three common definitions in the context of superconductivity:

1. Above the temperature of 30 K that had historically been taken as the upper limit allowed by BCS theory. This is also above the 1973 record of 23 K that had lasted until copper-oxide materials were discovered in 1986.
2. Having a transition temperature that is a larger fraction of the Fermi temperature than for conventional superconductors such as elemental mercury or lead. This definition encompasses a wider variety of unconventional superconductors and is used in the context of theoretical models.
3. Greater than the boiling point of liquid nitrogen (77 K or −196 °C). This is significant for technological applications of superconductivity because liquid nitrogen is a relatively inexpensive and easily handled coolant.

Technological applications benefit from both the higher critical temperature being above the boiling point of liquid nitrogen and also the higher critical magnetic field (and critical current density) at which superconductivity is destroyed. In magnet applications the high critical magnetic field may be more valuable than the high T_c itself. Some cuprates have an upper critical field around 100 teslas. However, cuprate materials are brittle ceramics which are expensive to manufacture and not easily turned into wires or other useful shapes.

Two decades of intense experimental and theoretical research, with over 100,000 published papers on the subject, have discovered many common features in the properties of high-temperature superconductors, but as of 2009, there is no widely accepted theory to explain their properties. Cuprate superconductors (and other unconventional superconductors) differ in many important ways from conventional superconductors, such as elemental mercury or lead, which are adequately explained by the BCS theory. There also has been much debate as to high-temperature superconductivity coexisting with magnetic ordering in YBCO, iron-based superconductors, several ruthenocuprates and other exotic superconductors, and the search continues for other families of materials. HTS are Type-II superconductors, which allow magnetic fields to penetrate their interior in quantized units of flux, meaning that much higher magnetic fields are required to suppress superconductivity. The layered structure also gives a directional dependence to the magnetic field response.

History and progress

- April 1986 - The term *high-temperature superconductor* was first used to designate the new family of cuprate-perovskite ceramic materials discovered by Johannes Georg Bednorz and Karl Alexander Müller, for which they won the Nobel Prize in Physics the following year. Their discovery of the first high-temperature superconductor, LaBaCuO, with a transition temperature of 30 K, generated great excitement.

- LSCO ($La_{2-x}Sr_xCuO_4$) discovered the same year.
- January 1987 - YBCO was discovered to have a T_c of 90 K.
- 1988 - BSCCO discovered with T_c up to 108 K, and TBCCO (T=thallium) discovered to have T_c of 127 K.

- As of 2009, the highest-temperature superconductor (at ambient pressure) is mercury barium calcium copper oxide ($HgBa_2Ca_2Cu_3O_x$), at 135 K and is held by a cuprate-perovskite material, which possibly reaches 164 K under high pressure.
- Recently, iron-based superconductors with critical temperatures as high as 56 K have been discovered. These are often also referred to as high-temperature superconductors.

After more than twenty years of intensive research the origin of high-temperature superconductivity is still not clear, but it seems that instead of *electron-phonon* attraction mechanisms, as in conventional superconductivity, one is dealing with genuine *electronic* mechanisms (e.g. by antiferromagnetic correlations), and instead of s-wave pairing, d-waves are substantial.

One goal of all this research is room-temperature superconductivity. However following numerous announcements of room-temperature superconductivity that were discredited on examination, most condensed matter physicists now treat with extreme skepticism any claims of this nature.

Examples

Examples of high-T_c cuprate superconductors include $La_{1.85}Ba_{0.15}CuO_4$, and YBCO (Yttrium-Barium-Copper-Oxide), which is famous as the first material to achieve superconductivity above the boiling point of liquid nitrogen.

Transition temperatures of well-known superconductors (Boiling point of liquid nitrogen for comparison)

Transition temperature (in kelvins)	Material	Class
133	$HgBa_2Ca_2Cu_3O_x$	Copper-oxide superconductors
110	$Bi_2Sr_2Ca_2Cu_3O_{10}$(BSCCO)	
90	$YBa_2Cu_3O_7$ (YBCO)	
77	Boiling point of liquid nitrogen	
55	SmFeAs(O,F)	Iron-based superconductors
41	CeFeAs(O,F)	
26	LaFeAs(O,F)	
20	Boiling point of liquid hydrogen	
18	Nb_3Sn	Metallic low-temperature superconductors
10	NbTi	
9.2	Nb	
4.2	Hg (mercury)	

Cuprates

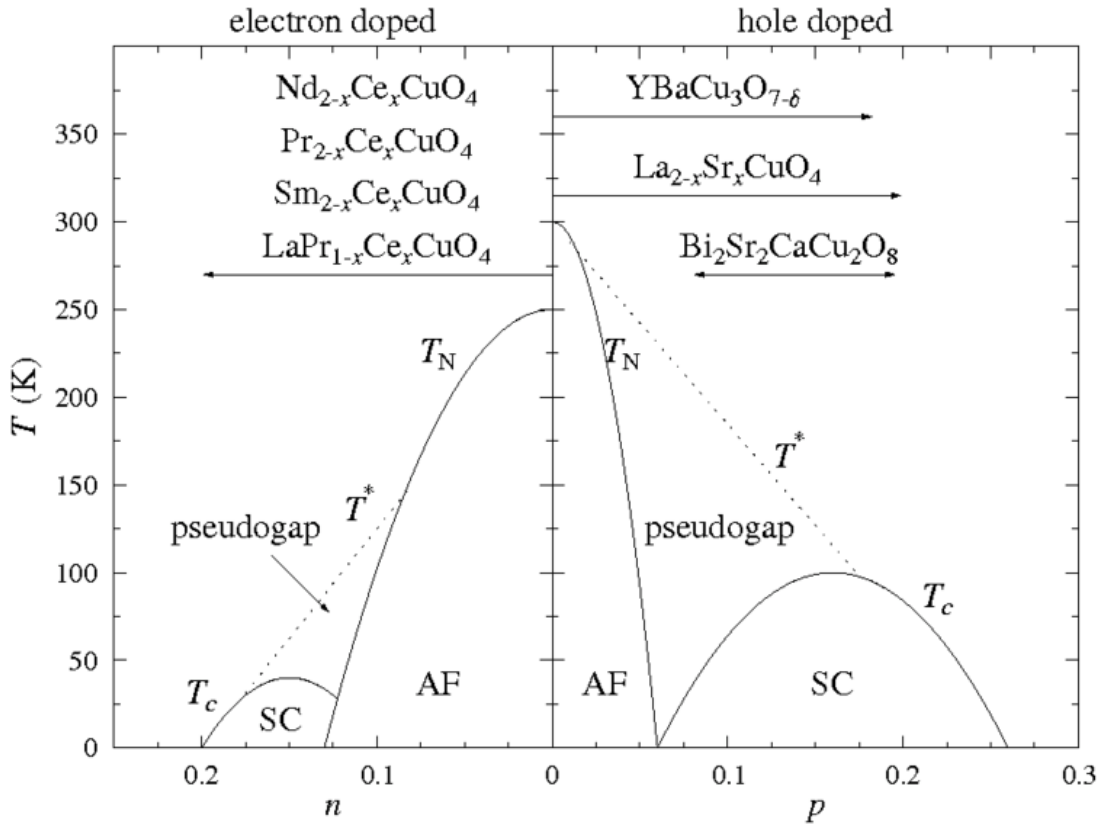

Simplified doping dependent phase diagram of cuprate superconductors for both electron (n) and hole (p) doping. The phases shown are the antiferromagnetic (AF) phase close to zero doping, the superconducting phase around optimal doping, and the pseudogap phase. Doping ranges possible for some common compounds are also shown. After.

Cuprate superconductors are generally considered to be quasi-two-dimensional materials with their superconducting properties determined by electrons moving within weakly coupled copper-oxide (CuO_2) layers. Neighbouring layers containing ions such as lanthanum, barium, strontium, or other atoms act to stabilize the structure and dope electrons or holes onto the copper-oxide layers. The undoped 'parent' or 'mother' compounds are Mott insulators with long-range antiferromagnetic order at low enough temperature. Single band models are generally considered to be sufficient to describe the electronic properties.

The cuprate superconductors adopt a perovskite structure. The copper-oxide planes are checkerboard lattices with squares of O^{2-} ions with a Cu^{2+} ion at the centre of each square. The unit cell is rotated by 45° from these squares. Chemical formulae of superconducting materials generally contain fractional numbers to describe the doping required for superconductivity. There are several families of cuprate superconductors and they can be categorized by the elements they contain and the number of adjacent copper-

oxide layers in each superconducting block. For example, YBCO and BSCCO can alternatively be referred to as Y123 and Bi2201/Bi2212/Bi2223 depending on the number of layers in each superconducting block (n). The superconducting transition temperature has been found to peak at an optimal doping value (p =0.16) and an optimal number of layers in each superconducting block, typically n = 3.

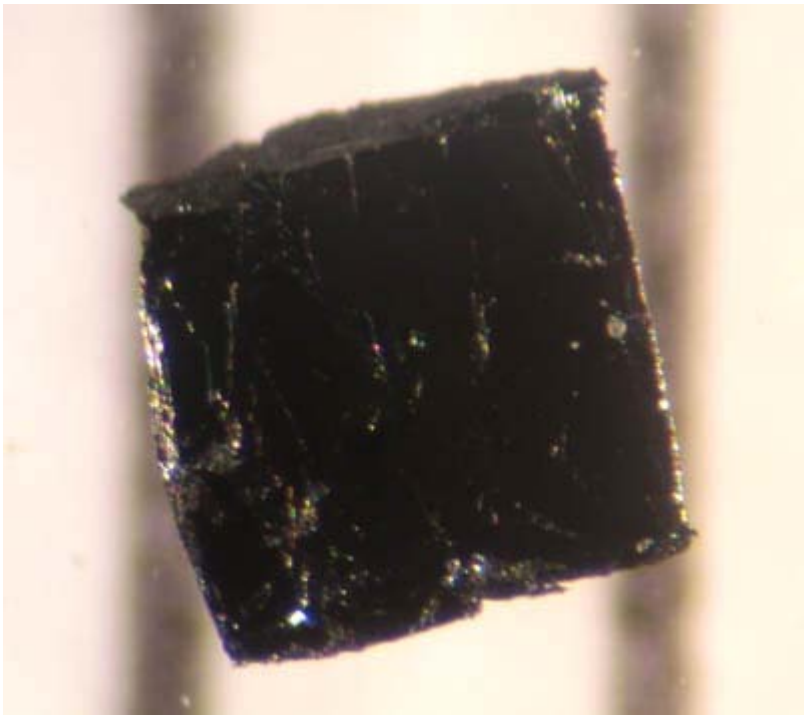

A small sample of the high-temperature superconductor BSCCO-2223.

Possible mechanisms for superconductivity in the cuprates are still the subject of considerable debate and further research. Certain aspects common to all materials have been identified. Similarities between the antiferromagnetic low-temperature state of the undoped materials and the superconducting state that emerges upon doping, primarily the $d_{x^2-y^2}$ orbital state of the Cu^{2+} ions, suggest that electron-electron interactions are more significant than electron-phonon interactions in cuprates – making the superconductivity unconventional. Recent work on the Fermi surface has shown that nesting occurs at four points in the antiferromagnetic Brillouin zone where spin waves exist and that the superconducting energy gap is larger at these points. The weak isotope effects observed for most cuprates contrast with conventional superconductors that are well described by BCS theory.

Similarities and differences in the properties of hole-doped and electron doped cuprates:

- Presence of a pseudogap phase up to at least optimal doping.
- Different trends in the Uemura plot relating transition temperature to the superfluid density. The inverse square of the London penetration depth appears to be proportional to the critical temperature for a large number of underdoped

cuprate superconductors, but the constant of proportionality is different for hole- and electron-doped cuprates. The linear trend implies that the physics of these materials is strongly two-dimensional.

- Universal hourglass-shaped feature in the spin excitations of cuprates measured using inelastic neutron diffraction.
- Nernst effect evident in both the superconducting and pseudogap phases.

Iron-based superconductors

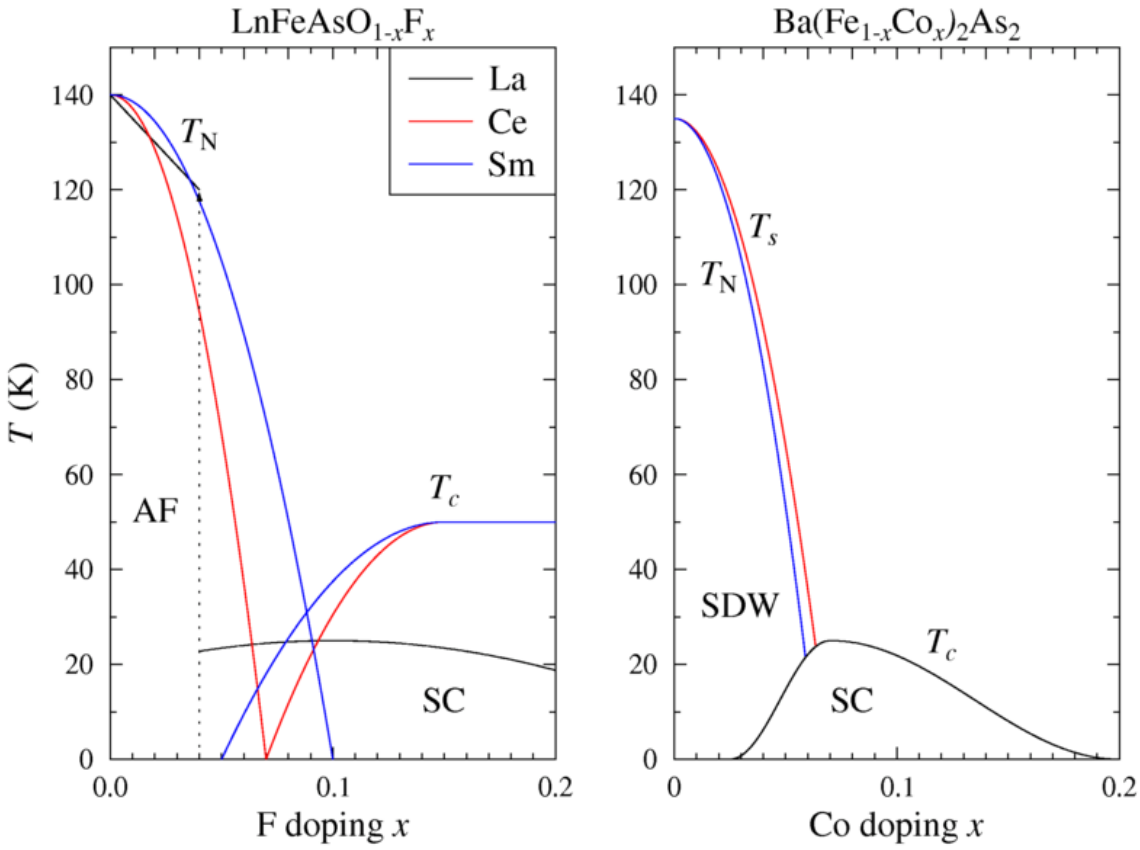

Simplified doping dependent phase diagrams of iron-based superconductors for both Ln-1111 and Ba-122 materials. The phases shown are the antiferromagnetic/spin density wave (AF/SDW) phase close to zero doping and the superconducting phase around optimal doping. The Ln-1111 phase diagrams for La and Sm were determined using muon spin spectroscopy, the phase diagram for Ce was determined using neutron diffraction. The Ba-122 phase diagram is based on.

Iron-based superconductors contain layers of iron and a pnictogen, such as arsenic, phosphorus, or chalcogens. This is currently the family with the second highest critical temperature, behind the cuprates. Interest in their superconducting properties began in 2006 with the discovery of superconductivity in LaFePO at 4 K and gained much greater attention in 2008 after the analogous material LaFeAs(O,F) was found to superconduct at up to 43 K under pressure.

Since the original discoveries several families of iron-based superconductors have emerged:

- LnFeAs(O,F) or $LnFeAsO_{1-x}$ with T_c up to 56 K, referred to as 1111 materials. A fluoride variant of these materials was subsequently found with similar T_c values.
- $(Ba,K)Fe_2As_2$ and related materials with pairs of iron-arsenide layers, referred to as 122 compounds. T_c values range up to 38 K. These materials also superconduct when iron is replaced with cobalt
- LiFeAs and NaFeAs with T_c up to around 20 K. These materials superconduct close to stoichiometric composition and are referred to as 111 compounds.
- FeSe with small off-stoichiometry or tellurium doping.

Most undoped iron-based superconductors show a tetragonal-orthorhombic structural phase transition followed at lower temperature by magnetic ordering, similar to the cuprate superconductors. However, they are poor metals rather than Mott insulators and have five bands at the Fermi surface rather than one. The phase diagram emerging as the iron-arsenide layers are doped is remarkably similar, with the superconducting phase close to or overlapping the magnetic phase. Strong evidence that the T_c value varies with the As-Fe-As bond angles has already emerged and shows that the optimal Tc value is obtained with undistorted $FeAs_4$ tetrahedra. The symmetry of the pairing wavefunction is still widely debated, but an extended s-wave scenario is currently favoured.

Other materials sometimes referred to as high-temperature superconductors

Magnesium diboride is occasionally referred to as a high-temperature superconductor because its T_c value of 39 K is above that historically expected for BCS superconductors. However, it is more generally regarded as the highest T_c conventional superconductor, the increased T_c resulting from two separate bands being present at the Fermi energy.

Fulleride superconductors where alkali-metal atoms are intercalated into C_{60} molecules show superconductivity at temperatures of up to 38 K for Cs_3C_{60}.

Some organic superconductors and heavy fermion compounds are considered to be high-temperature superconductors because of their high T_c values relative to their Fermi energy, despite the T_c values being lower than for many conventional superconductors. This description may relate better to common aspects of the superconducting mechanism than the superconducting properties.

Theoretical work by Neil Ashcroft predicted that solid metallic hydrogen at extremely high pressure should become superconducting at approximately room-temperature because of its extremely high speed of sound and expected strong coupling between the conduction electrons and the lattice vibrations. This prediction is yet to be experimentally verified.

All known high-T_c superconductors are Type-II superconductors. In contrast to Type-I superconductors, which expel all magnetic fields due to the Meissner Effect, Type-II superconductors allow magnetic fields to penetrate their interior in quantized units of flux, creating "holes" or "tubes" of normal metallic regions in the superconducting bulk. Consequently, high-T_c superconductors can sustain much higher magnetic fields.

Ongoing research

The question of how superconductivity arises in high-temperature superconductors is one of the major unsolved problems of theoretical condensed matter physics as of 2010. The mechanism that causes the electrons in these crystals to form pairs is not known. Despite intensive research and many promising leads, an explanation has so far eluded scientists. One reason for this is that the materials in question are generally very complex, multi-layered crystals (for example, BSCCO), making theoretical modelling difficult.

Improving the quality and variety of samples also gives rise to considerable research, both with the aim of improved characterisation of the physical properties of existing compounds, and synthesizing new materials, often with the hope of increasing T_c. Technological research focusses on making HTS materials in sufficient quantities to make their use economically viable and optimizing their properties in relation to applications.

A cable containing Gadolinium has been demonstrated to carry 2800 A at 76 K. The cable has an outside diameter of 7.5mm and a bend radius of 12.5 cm.

Possible mechanism

There have been two representative theories for HTS. Firstly, it has been suggested that the HTS emerges from antiferromagnetic spin fluctuations in a doped system. According to this theory, the pairing wave function of the cuprate HTS should have a $d_{x^2-y^2}$ symmetry. Thus, determining whether the pairing wave function has *d*-wave symmetry is essential to test the spin fluctuation mechanism. That is, if the HTS order parameter (pairing wave function) does not have *d*-wave symmetry, then a pairing mechanism related to spin fluctuations can be ruled out. (Similar arguments can be made for iron-based superconductors but the different material properties allow a different pairing symmetry.) Secondly, there was the **interlayer coupling model**, according to which a layered structure consisting of BCS-type (*s*-wave symmetry) superconductors can enhance the superconductivity by itself. By introducing an additional tunnelling interaction between each layer, this model successfully explained the anisotropic symmetry of the order parameter as well as the emergence of the HTS. Thus, in order to solve this unsettled problem, there have been numerous experiments such as photoemission spectroscopy, NMR, specific heat measurements, etc. But, unfortunately, the results were ambiguous, some reports supported the d symmetry for the HTS whereas others supported the s symmetry. This muddy situation possibly originated from the indirect nature of the experimental evidence, as well as experimental issues such as sample quality, impurity scattering, twinning, etc.

Junction experiment supporting the d symmetry

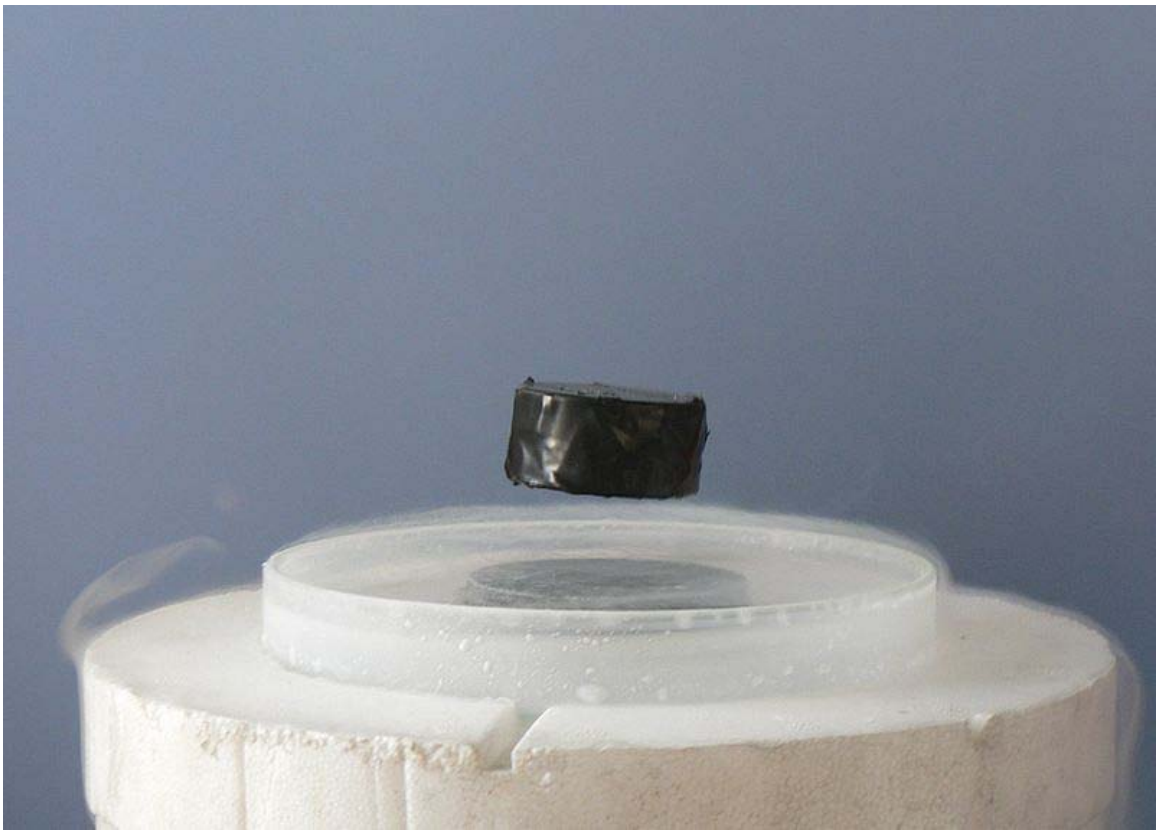

The Meissner effect or a magnet levitating above a superconductor (cooled by liquid nitrogen).

There was a clever experimental design to overcome the muddy situation. An experiment based on flux quantization of a three-grain ring of $YBa_2Cu_3O_7$ (YBCO) was proposed to test the symmetry of the order parameter in the HTS. The symmetry of the order parameter could best be probed at the junction interface as the Cooper pairs tunnel across a Josephson junction or weak link. It was expected that a half-integer flux, that is, a spontaneous magnetization could only occur for a junction of d symmetry superconductors. But, even if the junction experiment is the strongest method to determine the symmetry of the HTS order parameter, the results have been ambiguous. J. R. Kirtley and C. C. Tsuei thought that the ambiguous results came from the defects inside the HTS, so that they designed an experiment where both clean limit (no defects) and dirty limit (maximal defects) were considered simultaneously. In the experiment, the spontaneous magnetization was clearly observed in YBCO, which supported the d symmetry of the order parameter in YBCO. But, since YBCO is orthorhombic, it might inherently have an admixture of s symmetry. So, by tuning their technique further, they found that there was an admixture of s symmetry in YBCO within about 3%. Also, they found that there was a pure $d_{x^2-y^2}$ order parameter symmetry in the tetragonal $Tl_2Ba_2CuO_6$.

Qualitative explanation of the spin-fluctuation mechanism

While, despite all these years, the mechanism of high-T_c superconductivity is still highly controversial, this being due to mostly the lack of exact theoretical computations on such strongly interacting electron systems, most rigorous theoretical calculations, including phenomenological and diagrammatic approaches, converge on magnetic fluctuations as the pairing mechanism for these systems. The qualitative explanation is as follows. (Note that, in the following argument, one can replace “electron” with “hole” and vice versa depending on the actual material.)

In a normal conductor, a hole is created whenever an electron is moved. This causes a resistivity because charge neutrality must be conserved and as electrons move under an electric field, they drag holes behind them through defects and thermal oscillations in the system. In contrast, in a superconductor, one gets an unlimited supply of electrons without creating holes behind. This is through the creation of so-called Cooper pairs in a superconductor. Cooper pairs are pairs of electrons. In a normal conductor, creation of an electron leads to creation of a hole, which conserves the number of particles. But in a superconductor, it's possible to create a Cooper pair without creating holes and therefore not to conserve the number of particles, hence leading to the unlimited supply of electrons.

In a conventional superconductor, Cooper pairs are created as follows. When an electron moves through the system, it creates a depression in the atomic lattice through lattice vibrations known as phonons. If the depression of the lattice is strong enough, another electron can fall into the depression created by the first electron—the so-called water-bed effect—and a Cooper pair is formed. When this effect becomes strong enough, Cooper pairs win over the creation of holes behind the electrons, and the normal conductor turns into a superconductor through an unlimited supply of electrons by the creation of Cooper pairs.

In a high-T_c superconductor, the mechanism is extremely similar to a conventional superconductor. Except, in this case, phonons virtually play no role and their role is replaced by spin-density waves. As all conventional superconductors are strong phonon systems, all high-T_c superconductors are strong spin-density wave systems, within close vicinity of a magnetic transition to, for example, an antiferromagnet. When an electron moves in a high-T_c superconductor, its spin creates a spin-density wave around it. This spin-density wave in turn causes a nearby electron to fall into the spin depression created by the first electron (water-bed effect again). Hence, again, a Cooper pair is formed. Eventually, when the system temperature is lowered, more spin density waves and Cooper pairs are created and superconductivity begins when an unlimited supply of Cooper pairs, denoted as a phase transition, happens. Note that in high-T_c systems, as these systems are magnetic systems due to the Coulomb interaction, there is a strong Coulomb repulsion between electrons. This Coulomb repulsion prevents pairing of the Cooper pairs on the same lattice site. The pairing of the electrons occur at near-neighbor lattice sites as a result. This is the so-called *d*-wave pairing, where the pairing state has a node (zero) at the origin.

Chapter 10

Rapid Single Flux Quantum and Magnetic Flux Quantum

Rapid single flux quantum

In electronics, **rapid single flux quantum** (**RSFQ**) is a digital electronics technology that relies on quantum effects in superconducting devices, namely Josephson junctions, to process digital signals. Josephson junctions are the active elements for RSFQ electronics, like transistors are the active elements for semiconductor electronics. However, RSFQ is not a quantum computing technology in the traditional sense. Even so, RSFQ is very different from the traditional CMOS transistor technology used in every day computers:

- it is based on superconductors, so a cryogenic environment is required;
- the digital information is carried by magnetic flux quanta that are produced by Josephson junctions instead of transistors in semiconductor electronics;
- the magnetic flux quanta are carried by picosecond-duration voltage pulses that travel on superconducting transmission lines, instead of static voltage levels in semiconductor electronics.
- Consequently the area of the quantized voltage pulses that carry single magnetic flux quanta is constant. Depending on the parameters of the Josephson junctions, the pulses can be as narrow as 1 picosecond with an amplitude of about 2 mV, or broader (typically 5-10 picoseconds) with a lower amplitude;
- since pulses usually propagate on superconducting lines, their dispersion is limited and usually negligible if no spectral component of the pulse is above the amplitude of the energy gap of the superconductor;
- in 2010, the typical values of the maximum pulse amplitude, usually called the IcRn product, is of the order of 0.5 to 1 mV. Rn is the normal resistance of the Josephson junction that generates the voltage pulses, while Ic is its critical current.
- In the case of pulses of 5 picoseconds, it is typically possible to clock the circuits at frequencies of the order of 100 GHz (one pulse every 10 picoseconds).

Advantages

- Interoperable with CMOS circuitry, microwave and infrared technology
- Extremely fast operating frequency: from a few tens of gigahertz up to hundreds of gigahertz
- Low power consumption: about 100 000 times lower than CMOS semiconductors circuits
- Existing chip manufacturing technology can be adapted to manufacture RSFQ circuitry
- Good tolerance to manufacturing variations
- RSFQ circuitry is essentially self clocking, making asynchronous designs much more practical.

Disadvantages

- Requires cryogenic cooling; liquid helium is necessary for the most complex circuits, although high-temperature superconductors can also be used for RSFQ, but with low or medium complexity to date. Cryogenic cooling is also an advantage since it allows to work in presence of reduced thermal noise.
- As RSFQ is a disruptive technology, dedicated educational degrees and specific commercial software is still to be developed.

Applications

- Optical and other high-speed network switching devices
- Digital signal processing, even up to radiofrequency signals
- Ultrafast routers
- Software-Defined Radio (SDR)
- High speed analog-to-digital converters
- Petaflop supercomputers

Magnetic flux quantum

	Values (CODATA 2006)	Units
Φ_0	$2.067\ 833\ 667(52)\times10^{-15}$	Wb
K_J	$483\ 597.891(12)\times10^{9}$	Hz/V
K_{J-90}	$483\ 597.9\times10^{9}$	Hz/V

The **magnetic flux quantum** Φ_0 is the quantum of magnetic flux passing through a superconductor. The quantization of magnetic flux is closely related to the Aharonov–

Bohm effect, but was predicted earlier by Fritz London in 1948 using a phenomenological model.

The inverse of the flux quantum, $1/\Phi_0$, is called the **Josephson constant**, and is denoted K_J. It is the constant of proportionality of the Josephson effect, relating the potential difference across a Josephson junction to the frequency of the irradiation. The Josephson effect is very widely used to provide a standard for high precision measurements of potential difference, which (since 1990) have been related to a fixed, "conventional" value of the Josephson constant, denoted K_{J-90}.

Introduction

It is a property of a supercurrent (superconducting electrical current) that the magnetic flux passing through any area bounded by such a current is quantized. The quantum of magnetic flux is a physical constant, as it is independent of the underlying material as long as it is a superconductor. Its value is $\Phi_0 = h/(2e) = 2.067\ 833\ 636 \times 10^{-15}$ Wb.

If the area under consideration consists entirely of superconducting material, the magnetic flux through it will be zero, for supercurrents always flow in such a way as to expel magnetic fields from the interior of a superconductor, a phenomenon known as the Meissner effect. A non-zero magnetic flux may be obtained by embedding a ring of superconducting material in a normal (non-superconducting) medium. There are no supercurrents present at the center of the ring, so magnetic fields can pass through. However, the supercurrents at the boundary will arrange themselves so that the *total* magnetic flux through the ring is quantized in units of Φ_0. This is the idea behind SQUIDs, which are the most accurate type of magnetometer available.

A similar effect occurs when a type II superconductor is placed in a magnetic field. At sufficiently high field strengths, some of the magnetic field may penetrate the superconductor in the form of thin threads of material that have turned normal. These threads, which are sometimes called **fluxons** because they carry magnetic flux, are in fact the central regions ("cores") of vortices in the supercurrent. Each fluxon carries an integer number of magnetic flux quanta.

Quantization of magnetic flux is determined by a geometric unified theory of electromagnetism and gravitation. The electric elementary charge is simultaneously determined by the theory. Furthermore, these charge and flux quanta directly give the fractions which appear in the fractional quantum Hall effect.

Josephson constant

The Josephson constant is the inverse of the quantum of magnetic flux: $K_J = \frac{2e}{h} =$ 483 597.9×10^9 Hz/V. In 1988, the International Committee for Weights and Measures, or

CIPM, recommended that this be considered the exact "conventional" value of the constant, denoted $K_{J\text{-}90}$. The CODATA 2006 value, on the other hand, is K_J = (483 597.891±0.012)×10^9 Hz/V

Measuring the magnetic flux

The magnetic flux quantum may be measured with great precision by exploiting the Josephson effect. In fact, when coupled with the measurement of the von Klitzing constant $R_K = h/e^2$, this provides the most precise values of Planck's constant h obtained to date. This is remarkable since h is generally associated with the behavior of microscopically small systems, whereas the quantization of magnetic flux in a superconductor and the quantum Hall effect are both collective phenomena associated with thermodynamically large numbers of particles.

Chapter 11

Covalent Superconductor

Covalent semiconductors are such solids as diamond, silicon, germanium, silicon carbide and silicon-germanium where atoms are linked by covalent bonds. Most of those materials, at least in their bulk form, are well studied and rarely hit the front pages of the top scientific journals in the last decade. However, issue 23 of volume 93 (2004) of a major physics journal Physical Review Letters contained as many as 4 papers on diamond. Those papers were a reaction to a breakthrough discovery of superconductivity in synthetic diamond grown by high-pressure high-temperature (HPHT) method. The discovery had no practical importance but surprised most scientists as superconductivity has not been considered seriously in covalent semiconductors.

Diamond

Superconductivity in diamond was achieved through heavy p-type doping by boron such that the individual doping atoms started interacting and formed an "impurity band". The superconductivity was of type-II with the critical temperature Tc = 4 K and critical magnetic field Hc = 4 T. Later, Tc ~ 11K has been achieved in homoepitaxial CVD films.

Regarding the origin of superconductivity in diamond, three alternative theories exist at the moment: conventional BCS theory based on phonon-mediated pairing, correlated impurity band theory and spin-flip-driven pairing of holes weakly localized in the vicinity of the Fermi level. Whereas there is no solid experimental support for either model, recent accurate measurements of isotopic shift of the transition temperature Tc upon boron and carbon isotopic substitutions favor the BCS theory.

Silicon

It was suggested that "Si and Ge, which also form in the diamond structure, may similarly exhibit superconductivity under the appropriate conditions", and indeed, discoveries of superconductivity in heavily boron doped Si (Si:B) and SiC:B have quickly followed. Similar to diamond, Si:B is type-II superconductor, but it has much smaller values of Tc = 0.4 K and Hc = 0.4 T. Superconductivity in Si:B was achieved by heavy doping (above

8 at.%), realized through a special non-equilibrium technique of gas immersion laser doping.

Silicon carbide

Superconductivity in SiC was achieved by heavy doping with boron or aluminum. Both the cubic (3C-SiC) and hexagonal (6H-SiC) phases are superconducting and show a very similar Tc of 1.5 K. A crucial difference is however observed for the magnetic field behavior between aluminum and boron doping: SiC:Al is type-II, same as Si:B. On the contrary, SiC:B is type-I. In attempt to explain this difference, it was noted that Si sites are more important than carbon sites for superconductivity in SiC. Whereas boron substitutes carbon in SiC, Al substitutes Si sites. Therefore, Al and B "see" different environment that might explain different properties of SiC:Al and SiC:B.

Carbon nanotubes

Superconductivity in carbon nanotubes has been observed experimentally in 2001. Note however a crucial difference between nanotubes and diamond: Although nanotubes contain covalently bonded carbon atoms, they are closer in properties to graphite than diamond, and can be metallic without doping. Meanwhile, undoped diamond is an insulator.

Intercalated graphite

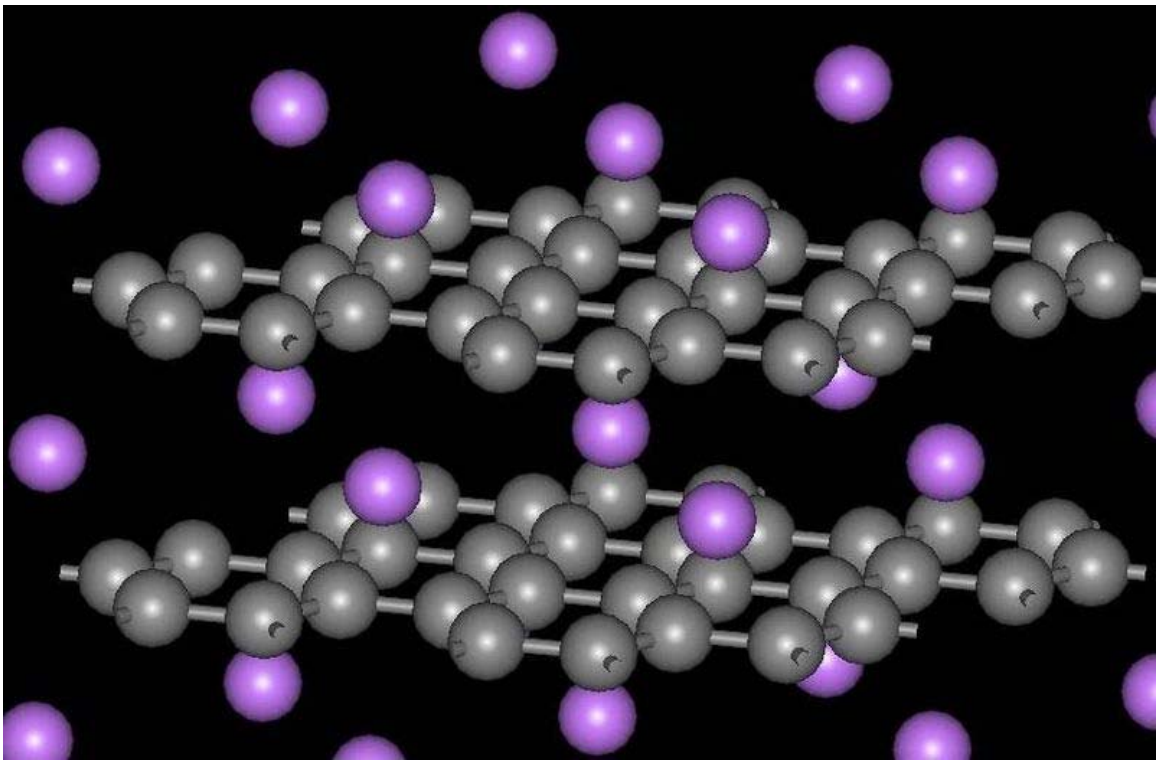

Structure of CaC_6

When metal atoms are inserted (intercalated) between the graphite planes, several superconductors are created with the following transition temperatures:

Material	CaC_6	$Li_3Ca_2C_6$	YbC_6	SrC_6	KC_8	RbC_8	NaC_3	KC_3	LiC_3	NaC_2	LiC_2
Tc (K)	11.5	11.15	6.5	1.65	0.14	0.025	2.3-3.8	3.0	<0.35	5.0	1.9

History

The priority of many discoveries in science is vigorously disputed (see, e.g., Nobel Prize controversies). Another example, after Sumio Iijima has "discovered" carbon nanotubes in 1991, many scientists have pointed out that carbon nanofibers were actually observed decades earlier. The same could be said about superconductivity in covalent semiconductors. Superconductivity in germanium and silicon-germanium was predicted theoretically as early as in the 1960s. Shortly after, superconductivity was experimentally detected in germanium telluride. In 1976, superconductivity with Tc = 3.5 K was observed experimentally in germanium implanted with copper ions; it was experimentally demonstrated that amorphization was essential for the superconductivity (in Ge), and the superconductivity was assigned to Ge itself, not copper.

Chapter 12

London Equations and Fulde-Ferrell-Larkin-Ovchinnikov Phase

London equations

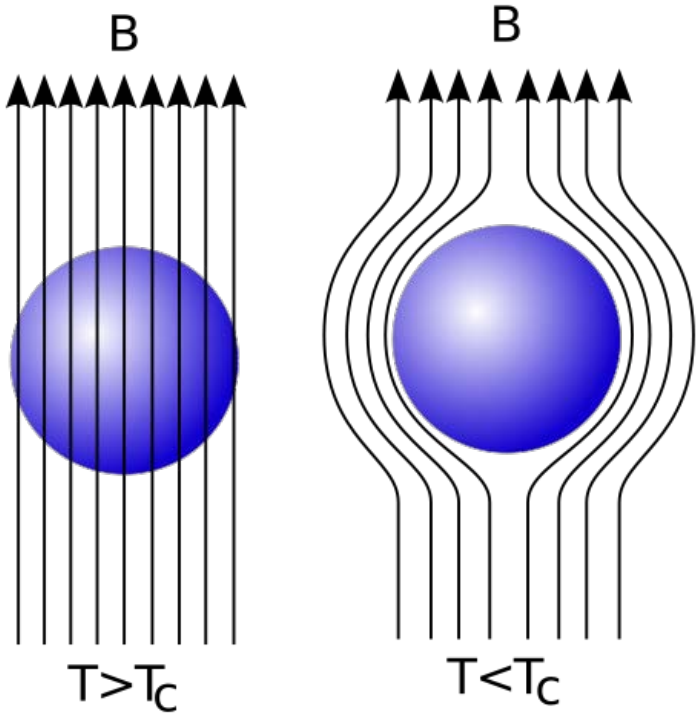

As a material drops below its superconducting critical temperature, magnetic fields within the material are expelled via the Meissner effect. The London equations give a quantitative explanation of this effect.

The **London equations**, developed by brothers Fritz and Heinz London in 1935, relate current to electromagnetic fields in and around a superconductor. Arguably the simplest meaningful description of superconducting phenomena, they form the genesis of almost any modern introductory text on the subject. A major triumph of the equations is their ability to explain the Meissner effect, wherein a material exponentially expels all internal magnetic fields as it crosses the superconducting threshold.

Formulations

There are two London equations when expressed in terms of measurable fields:

$$\frac{\partial \mathbf{j}_s}{\partial t} = \frac{n_s e^2}{m}\mathbf{E}, \qquad \nabla \times \mathbf{j}_s = -\frac{n_s e^2}{mc}\mathbf{B}.$$

Here $\mathbf{j}_s$ is the superconducting current, **E** and **B** are respectively the electric and magnetic fields within the superconductor, e is the charge of an electron & proton, m is electron mass, and n_s is a phenomenological constant loosely associated with a number density of superconducting carriers.

On the other hand, if one is willing to abstract away slightly, both the expressions above can more neatly be written in terms of a single "London Equation" in terms of the vector potential **A**:

$$\mathbf{j}_s = -\frac{n_s e^2}{mc}\mathbf{A}.$$

The last equation suffers from only the disadvantage that it is not gauge invariant, but is true only in the London gauge, where the divergence of **A** is zero.

London Penetration Depth

If the second of London's equations is manipulated by applying Ampere's law,

$$\nabla \times \mathbf{B} = \frac{4\pi \mathbf{j}}{c},$$

then the result is the differential equation

$$\nabla^2 \mathbf{B} = \frac{1}{\lambda^2}\mathbf{B}, \qquad \lambda \equiv \sqrt{\frac{mc^2}{4\pi n_s e^2}}.$$

Thus, the London equations imply a characteristic length scale, λ, over which external magnetic fields are exponentially suppressed. This value is the London penetration depth.

A simple example geometry is a flat boundary between a superconductor within free space where the magnetic field outside the superconductor is a constant value pointed parallel to the superconducting boundary plane in the *z* direction. If *x* leads perpendicular to the boundary then the solution inside the superconductor may be shown to be

$$B_z(x) = B_0 e^{-x/\lambda}.$$

From here the physical meaning of the London penetration depth can perhaps most easily be discerned.

Rationale for the London Equations

Original arguments

While it is important to note that the above equations cannot be derived in any conventional sense of the word, the Londons did follow a certain intuitive logic in the formulation of their theory. Substances across a stunningly wide range of composition behave roughly according to Ohm's law, which states that current is proportional to electric field. However, such a linear relationship is impossible in a superconductor for, almost by definition, the electrons in a superconductor flow with no resistance whatsoever. To this end, the brothers London imagined electrons as if they were free electrons under the influence of a uniform external electric field. According to the Lorentz force law

$$\mathbf{F} = e\mathbf{E} + \frac{e}{c}\mathbf{v} \times \mathbf{B}$$

these electrons should encounter a uniform force, and thus they should in fact accelerate uniformly. This is precisely what the first London equation states.

To obtain the second equation, take the curl of the first London equation and apply Faraday's law,

$$\nabla \times \mathbf{E} = -\frac{1}{c}\frac{\partial \mathbf{B}}{\partial t},$$

to obtain

$$\frac{\partial}{\partial t}\left(\nabla \times \mathbf{j}_s + \frac{n_s e^2}{mc}\mathbf{B}\right) = 0.$$

As it currently stands, this equation permits both constant and exponentially decaying solutions. The Londons recognized from the Meissner effect that constant nonzero solutions were nonphysical, and thus postulated that not only was the time derivative of

the above expression equal to zero, but also that the expression in the parentheses must be identically zero. This results in the second London equation.

Canonical momentum arguments

It is also possible to justify the London equations by other means. Current density is defined according to the equation

$$\mathbf{j}_s = n_s e \mathbf{v}.$$

Taking this expression from a classical description to a quantum mechanical one, we must replace values **j** and **v** by the expectation values of their operators. The velocity operator is given by

$$\mathbf{v} = \frac{1}{m}\left(\mathbf{p} - \frac{e}{c}\mathbf{A}\right).$$

We may then make this replacement in the equation above. However, an important assumption from the microscopic theory of superconductivity is that the superconducting state of a system is the ground state, and according to a theorem of Bloch's, in such a state the canonical momentum **p** is zero. This leaves

$$\mathbf{j}_s = -\frac{n_s e_s^2}{mc}\mathbf{A},$$

which is the London equation according to the second formulation above.

Fulde-Ferrell-Larkin-Ovchinnikov phase

The **Fulde-Ferrell-Larkin-Ovchinnikov (FFLO) phase** can arise in a superconductor in large magnetic field. Among its characteristics are Cooper pairs with nonzero total momentum and a spatially non-uniform order parameter.

History

Two independent publications in the year 1964, one by Peter Fulde and Richard A. Ferrell and the other by Anatoly Larkin and Yuri Ovchinnikov, theoretically predicted a new state in a certain regime of superconductors in high magnetic fields. This particular superconducting state is nowadays known as the Fulde-Ferrell-Larkin-Ovchinnikov state, abbreviated FFLO state (also LOFF state). Since then, experimental observation of the FFLO state has been searched for in different classes of superconducting materials, first

in thin films and later in exotic superconductors such as heavy-fermion and organic superconductors, but so far there is no undisputed experimental evidence. In recent years, the concept of the FFLO state was taken up in the field of atomic physics and experiments to detect the FFLO state in atomic ensembles in optical lattices.

Theory

If a BCS superconductor with a ground state consisting of Cooper pair singlets (and center-of-mass momentum q=0) is subjected to an applied magnetic field, then the spin structure is not affected until the Zeeman energy is strong enough to flip one spin of the singlet and break the Cooper pair, thus destroying superconductivity (paramagnetic or Pauli pair breaking). If instead one considers the normal, metallic state at the same finite magnetic field, then the Zeeman energy leads to different Fermi surfaces for spin-up and spin-down electrons, which can lead to superconducting pairing where Cooper pair singlets are formed with a center-of-mass momentum q which is finite, corresponding to the displacement of the two Fermi surfaces. The non-vanishing q of the Cooper pairs leads to a spatially modulated order parameter (periodic with wave vector q).

Experiment

For the FFLO phase to appear, it is required that Pauli pair breaking is the relevant mechanism to suppress superconductivity (Pauli limiting field, also Chandrasekhar-Clogston limit). In particular, orbital pair breaking (when the vortices induced by the magnetic field overlap in space) has to be weaker, which is not the case for conventional superconductors. Certain unconventional superconductors, on the other hand, may favor Pauli pair breaking: materials with large effective electron mass or layered materials (with quasi-two-dimensional electrical conduction).

Heavy-fermion superconductors

Heavy-fermion superconductivity is caused by electrons with a drastically enhanced effective mass (the heavy fermions, also heavy quasiparticles), which suppresses orbital pair breaking. Furthermore, certain heavy-fermion superconductors, such as $CeCoIn_5$, have a layered crystal structure, with somewhat two-dimensional electronic transport properties. Therefore, detailed studies close to the critical field have been performed on $CeCoIn_5$, and there is evidence that certain regimes in the phase diagram of this material should be interpreted in terms of the FFLO state.

Organic superconductors

Some organic superconductors have very anisotropic conductivity; in particular there are compounds which are good realizations of quasi-two-dimensional electronic transport. Also here there are candidate materials for the FFLO phase, and for the organic superconductors of the κ-$(ET)_2X$ and $\lambda(BETS)_2X$ there is experimental data indicating an FFLO region in the phase diagram of these materials.

Chapter 13

Flux Pumping

Flux pumping is a method for magnetising bulk superconductors to fields in excess of 15 teslas. The method can be applied to any type II superconductor and exploits a fundamental property of superconductors. That is their ability to support and maintain currents on the length scale of the superconductor. Conventional magnetic materials are magnetised on a molecular scale which means that superconductors can maintain a flux density orders of magnitude bigger than conventional materials. Flux pumping is especially significant when one bears in mind that all other methods of magnetising superconductors require application of a magnetic flux density at least as high as the final required field. This is not true of flux pumping.

An electric current flowing in a loop of superconducting wire can persist indefinitely with no power source. In a normal conductor, an electrical current may be visualized as a fluid of electrons moving across a heavy ionic lattice. The electrons are constantly colliding with the ions in the lattice, and during each collision some of the energy carried by the current is absorbed by the lattice and converted into heat, which is essentially the vibrational kinetic energy of the lattice ions. As a result, the energy carried by the current is constantly being dissipated. This is the phenomenon of electrical resistance.

The situation is different in a superconductor. In a conventional superconductor, the electronic fluid cannot be resolved into individual electrons. Instead, it consists of bound *pairs* of electrons known as Cooper pairs. This pairing is caused by an attractive force between electrons from the exchange of phonons. Due to quantum mechanics, the energy spectrum of this Cooper pair fluid possesses an *energy gap*, meaning there is a minimum amount of energy ΔE that must be supplied in order to excite the fluid. Therefore, if ΔE is larger than the thermal energy of the lattice, given by kT, where k is Boltzmann's constant and T is the temperature, the fluid will not be scattered by the lattice. The Cooper pair fluid is thus a superfluid, meaning it can flow without energy dissipation.

In a class of superconductors known as Type II superconductors, including all known high-temperature superconductors, an extremely small amount of resistivity appears at temperatures not too far below the nominal superconducting transition when an electrical current is applied in conjunction with a strong magnetic field, which may be caused by the electrical current. This is due to the motion of vortices in the electronic superfluid,

which dissipates some of the energy carried by the current. If the current is sufficiently small, the vortices are stationary, and the resistivity vanishes. The resistance due to this effect is tiny compared with that of non-superconducting materials, but must be taken into account in sensitive experiments.

Introduction

In the method described here a magnetic field is swept across the superconductor in a magnetic wave. This field induces current according to Faraday's law of induction. As long as the direction of motion of the magnetic wave is constant then the current induced will always be in the same sense and successive waves will induce more and more current.

Traditionally the magnetic wave would be generated either by physically moving a magnet or by an arrangement of coils switched in sequence, such as occurs on the stator of a three-phase motor. Flux Pumping is a solid state method where a material which changes magnetic state at a suitable magnetic ordering temperature is heated at its edge and the resultant thermal wave produces a magnetic wave which then magnetizes the superconductor. A superconducting flux pump should not be confused with a classical flux pump as described in Van Klundert et al.'s review.

The method described here has two unique features:

- At no point is the superconductor driven normal; the procedure simply makes modifications to the critical state.
- The critical state is not modified by a moving magnet or an array of solenoids, but by a thermal pulse which modifies the magnetization, thus sweeping vortices into the material.

The system, as described, is actually a novel kind of heat engine in which thermal energy is being converted into magnetic energy.

Background

Meissner effect

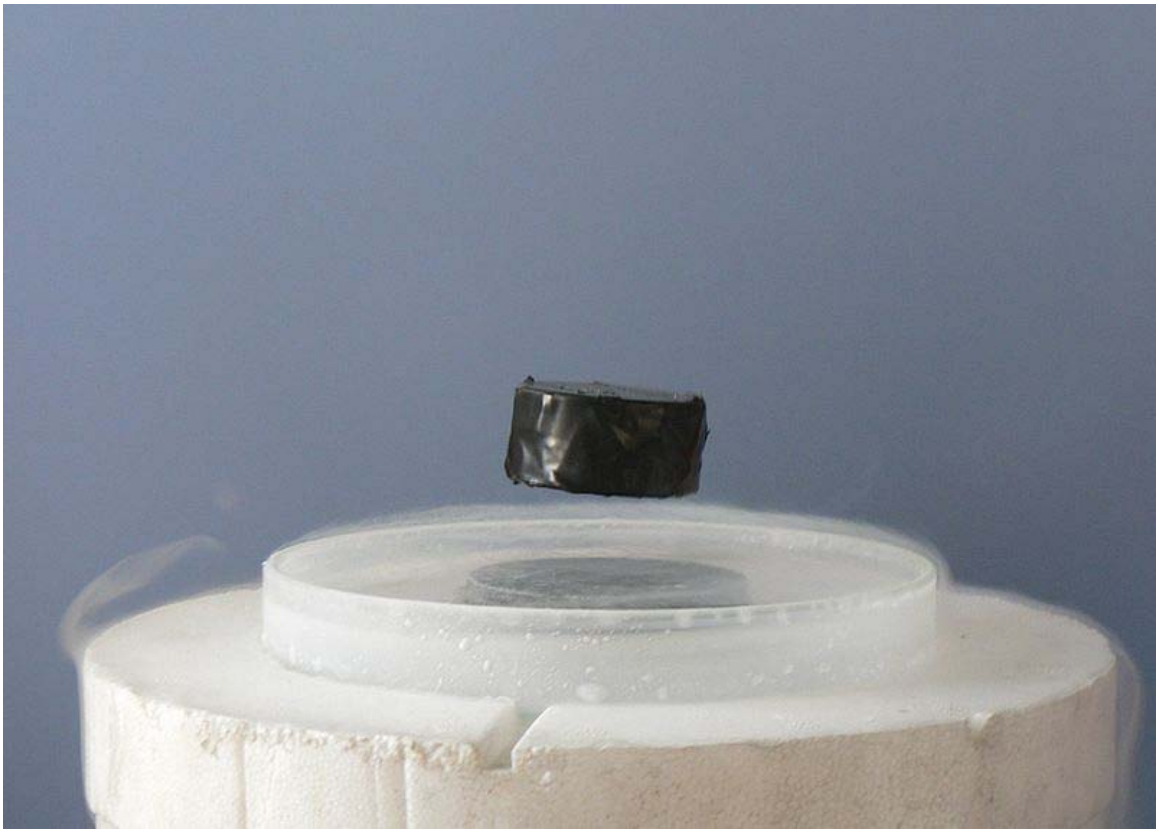

Persistent electric current flows on the surface of the superconductor, acting to exclude the magnetic field of the magnet. This current effectively forms an electromagnet that repels the magnet.

When a superconductor is placed in a weak external magnetic field **H**, the field penetrates the superconductor only a small distance λ, called the **London penetration depth**, decaying exponentially to zero within the bulk of the material. This is called the **Meissner effect**, and is a defining characteristic of superconductivity. For most superconductors, the London penetration depth is on the order of 100 nm.

The Meissner effect is sometimes confused with the kind of diamagnetism one would expect in a perfect electrical conductor: according to Lenz's law, when a *changing* magnetic field is applied to a conductor, it will induce an electrical current in the conductor that creates an opposing magnetic field. In a perfect conductor, an arbitrarily large current can be induced, and the resulting magnetic field exactly cancels the applied field.

The Meissner effect is distinct from this because a superconductor expels *all* magnetic fields, not just those that are changing. Suppose we have a material in its normal state, containing a constant internal magnetic field. When the material is cooled below the

critical temperature, we would observe the abrupt expulsion of the internal magnetic field, which we would not expect based on Lenz's law.

The Meissner effect was explained by the brothers Fritz and Heinz London, who showed that the electromagnetic free energy in a superconductor is minimized provided

$$\nabla^2 \mathbf{H} = \lambda^{-2} \mathbf{H}$$

where **H** is the magnetic field and λ is the London penetration depth.

This equation, which is known as the London equation, predicts that the magnetic field in a superconductor decays exponentially from whatever value it possesses at the surface.

In 1962, the first commercial superconducting wire, a niobium-titanium alloy, was developed by researchers at Westinghouse, allowing the construction of the first practical superconducting magnets. In the same year, Josephson made the important theoretical prediction that a supercurrent can flow between two pieces of superconductor separated by a thin layer of insulator. This phenomenon, now called the Josephson effect, is exploited by superconducting devices such as SQUIDs. It is used in the most accurate available measurements of the magnetic flux quantum $\Phi_0 = \frac{h}{2e}$, and thus (coupled with the quantum Hall resistivity) for Planck's constant *h*. Josephson was awarded the Nobel Prize for this work in 1973.

E-J Power Law

The most popular model used to describe superconductivity is the Bean or Critical State model and variations such as the Kim-Anderson model. However the Bean model assumes zero resistivity and that current is always induced at the critical current. A more useful model for engineering applications is the so-called E_J power law in which the Field and the current are linked by the following equations:

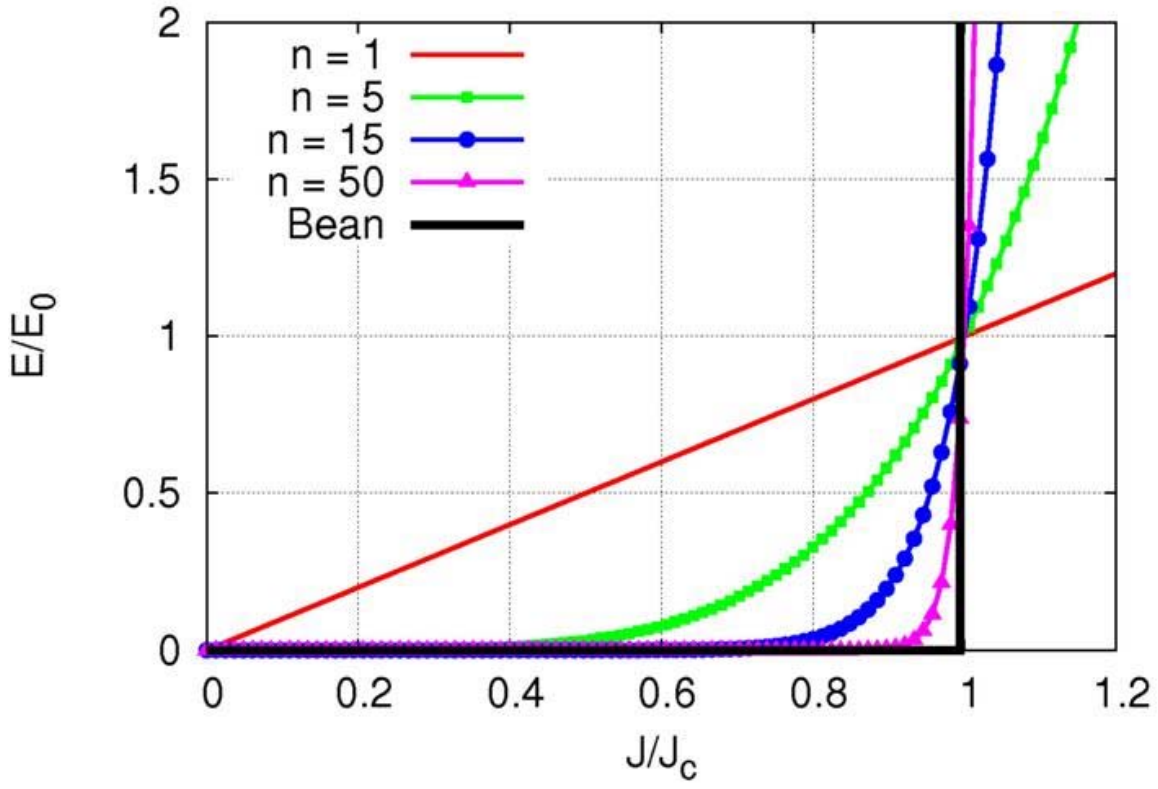

$$\rho = \frac{dE}{dJ}$$

$$\mathbf{E} = \mathbf{E_0} * (\frac{J}{J_c})^n$$

$$\rho(J) = \frac{E_0 * n * (\frac{J}{J_c})^{n-1}}{J_c}$$

In these equations if n = 1 then the conductor has linear resistivity such as is found in copper. The higher the n-value the closer we get to the critical state model. Also the higher the n-value then the "better" the superconductor as the lower the resistivity at a certain current. The E_J power law can be used to describe the phenomenon of flux-creep in which a superconductor gradually loses its magnetisation over time. This process is logarithmic and thus gets slower and slower and ultimately leads to very stable fields.

Theory

The potential of bulk melt-processed YBCO single domains to trap significant magnetic fields at cryogenic temperatures makes them particularly attractive for a variety of engineering applications including superconducting magnets, magnetic bearings and motors. It has already been shown that large fields can be obtained in single domain samples at 77 K. A range of possible applications exist in the design of high power density electric motors.

Before such devices can be created a major problem needs to be overcome. Even though all of these devices use a superconductor in the role of a permanent magnet and even though the superconductor can trap potentially huge magnetic fields (greater than 10 T) the problem is the induction of the magnetic fields. There are four possible known methods:

1. Cooling in field;
2. Zero field cooling, followed by slowly applied field;
3. Pulse magnetization;
4. Flux pumping;

Any of these methods could be used to magnetise the superconductor and this may be done either in situ or ex situ. Ideally the superconductors are magnetised in situ.

There are several reasons for this: first, if the superconductors should become demagnetised through (i) flux creep, (ii) repeatedly applied perpendicular fields or (iii) by loss of cooling then they may be re-magnetized without the need to disassemble the machine. Secondly, there are difficulties with handling very strongly magnetized material at cryogenic temperatures when assembling the machine. Thirdly, ex situ methods would require the machine to be assembled both cold and pre-magnetized and would offer significant design difficulties. Until room temperature superconductors can be prepared, the most efficient design of machine will therefore be one in which an in situ magnetizing fixture is included!

The first three methods all require a solenoid which can be switched on and off. In the first method an applied magnetic field is required equal to the required magnetic field, whilst the second and third approaches require fields at least two times greater. The final method, however, offers significant advantages since it achieves the final required field by repeated applications of a small field and can utilise a permanent magnet.

If we wish to pulse a field using, say, a 10 T magnet to magnetize a 30 mm × 10 mm sample then we can work out how big the solenoid needs to be. If it were possible to wind an appropriate coil using YBCO tape then, assuming an Ic of 70 A and a thickness of 100 μm, we would have 100 turns and 7000 A turns. This would produce a B field of approximately $7000/(20 \times 10{-}3) \times 4\pi \times 10{-}7 = 0.4$ T. To produce 10 T would require pulsing to 1400 A! An alternative calculation would be to assume a Jc of say $5 \times 108\mathrm{Am}{-}1$ and a coil 1 cm^2 in cross section. The field would then be $5 \times 108 \times 10{-}2 \times (2 \times 4\pi \times 10{-}7) = 10$ T. Clearly if the magnetisation fixture is not to occupy more room than the puck itself then a very high activation current would be required and either constraint makes in situ magnetization a very difficult proposition. What is required for in situ magnetisation is a magnetisation method in which a relatively small field of the order of milliteslas repeatedly applied is used to magnetize the superconductor.

Applications

Superconducting magnets are some of the most powerful electromagnets known. They are used in MRI and NMR machines, mass spectrometers, and the beam-steering magnets used in particle accelerators. They can also be used for magnetic separation, where weakly magnetic particles are extracted from a background of less or non-magnetic particles, as in the pigment industries.

Other early markets are arising where the relative efficiency, size and weight advantages of devices based on HTS outweigh the additional costs involved.

Promising future applications include high-performance transformers, power storage devices, electric power transmission, electric motors (e.g. for vehicle propulsion, as in vactrains or maglev trains), magnetic levitation devices, and fault current limiters.

Chapter 14

Scanning SQUID Microscope

A **Scanning SQUID Microscope** is a sensitive near-field imaging system for the measurement of weak magnetic fields by moving a Superconducting Quantum Interference Device (SQUID) across an area. The microscope can map out buried current-carrying wires by measuring the magnetic fields produced by the currents, or can be used to image fields produced by magnetic materials. By mapping out the current in an integrated circuit or a package, short circuits can be localized and chip designs can be verified to see that current is flowing where expected.

High temperature scanning SQUID microscope

Scanning SQUID microscope

A high temperature Scanning SQUID Microscope using a YBCO SQUID is capable of measuring magnetic fields as small as 20 pT (about 2 million times weaker than the earth's magnetic field). The SQUID sensor is sensitive enough that it can detect a wire even if it is carrying only 10 nA of current at a distance of 100 μm from the SQUID sensor with 1 second averaging. The microscope uses a patented design to allow the sample under investigation to be at room temperature and in air while the SQUID sensor is under vacuum and cooled to less than 80 K using a cryo cooler. No Liquid Nitrogen is used. During non-contact, non-destructive imaging of room temperature samples in air, the system achieves a raw, unprocessed spatial resolution equal to the distance separating the sensor from the current or the effective size of the sensor, whichever is larger. To best locate a wire short in a buried layer, however, a Fast Fourier Transform (FFT) back-evolution technique can be used to transform the magnetic field image into an equivalent map of the current in an integrated circuit or printed wiring board. The resulting current map can then be compared to a circuit diagram to determine the fault location. With this post-processing of a magnetic image and the low noise present in SQUID images, it is

possible to enhance the spatial resolution by factors of 5 or more over the near-field limited magnetic image. The system's output is displayed as a false-color image of magnetic field strength or current magnitude (after processing) versus position on the sample. After processing to obtain current magnitude, this microscope has been successful at locating shorts in conductors to within ±3 μm at a sensor-current distance of 150 μm.

SQUID operation

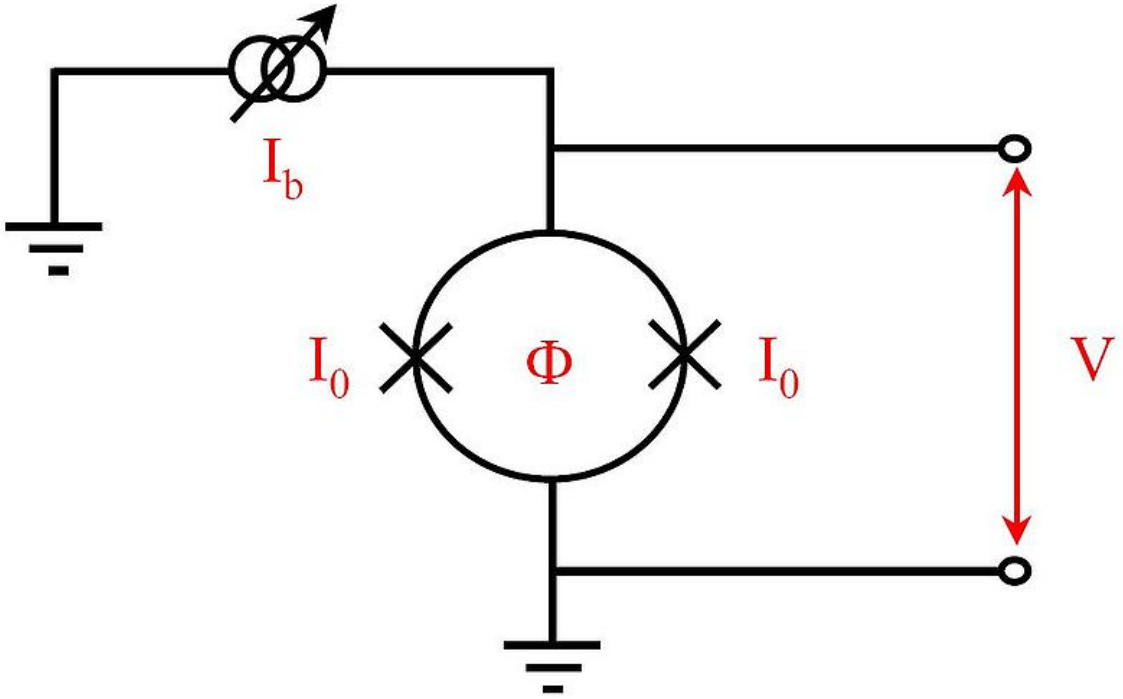

Figure 1: Electrical schematic of a SQUID where I_b is the bias current, I_0 is the critical current of the SQUID, Φ is the flux threading the SQUID and V is the voltage response to that flux.

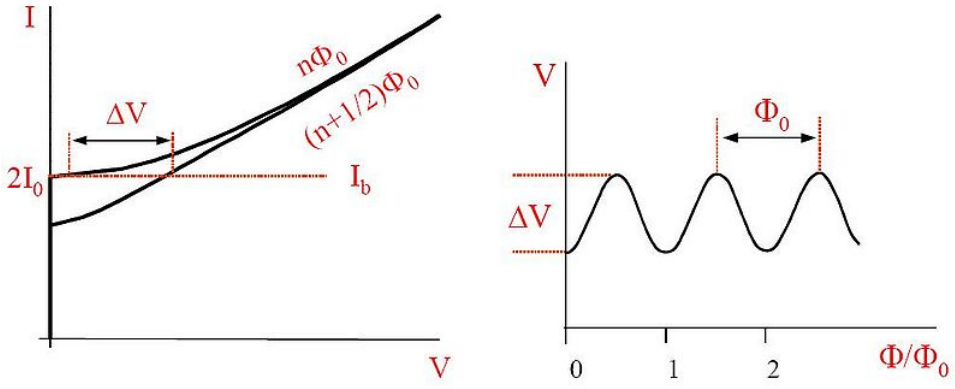

Figure 2 a) Plot of current vs. voltage for a SQUID. Upper and lower curves correspond to $n\Phi_0$ and $(n+1/2)\Phi_0$ respectively. Figure 2 b) Periodic voltage response due to flux through a SQUID. The periodicity is equal to one flux quantum, Φ_0

As the name implies, SQUIDs are made from superconducting material. As a result, they need to be cooled to cryogenic temperatures of less than 90 K (liquid nitrogen temperatures) for high temperature SQUIDs and less than 9 K (liquid helium temperatures) for low temperature SQUIDs. For magnetic current imaging systems, a small (about 30 μm wide) high temperature SQUID is used. This system has been designed to keep a high temperature SQUID, made from $YBa_2Cu_3O_7$, cooled below 80K and in vacuum while the device under test is at room temperature and in air. A SQUID consists of two Josephson tunnel junctions that are connected together in a superconducting loop (see Figure 1). A Josephson junction is formed by two superconducting regions that are separated by a thin insulating barrier. Current exists in the junction without any voltage drop, up to a maximum value, called the critical current, I_o. When the SQUID is biased with a constant current that exceeds the critical current of the junction, then changes in the magnetic flux, Φ, threading the SQUID loop produce changes in the voltage drop across the SQUID (see Figure 1). Figure 2(a) shows the I-V characteristic of a SQUID where ΔV is the modulation depth of the SQUID due to external magnetic fields. The voltage across a SQUID is a nonlinear periodic function of the applied magnetic field, with a periodicity of one flux quantum, $\Phi_0=2.07\times10^{-15}$ Tm^2 (see Figure 2(b)). In order to convert this nonlinear response to a linear response, a negative feedback circuit is used to apply a feedback flux to the SQUID so as to keep the total flux through the SQUID constant. In such a flux locked loop, the magnitude of this feedback flux is proportional to the external magnetic field applied to the SQUID. Further description of the physics of SQUIDs and SQUID microscopy can be found elsewhere.

Magnetic field detection using SQUID

$$d\vec{B} = \frac{\mu_0}{4\pi} \frac{I d\vec{\ell} \times \vec{r}}{r^2}$$

Figure 3: Biot-Savart Law (B is the magnetic induction, Idℓ is an element of the current, the constant μ_0 is the permeability of free space, and r is the distance between the current and the sensor)

Magnetic current imaging uses the magnetic fields produced by currents in electronic devices to obtain images of those currents. This is accomplished though the fundamental physics relationship between magnetic fields and current, the Biot-Savart Law (Figure 3). As a result, the current can be directly calculated from the magnetic field knowing only the separation between the current and the magnetic field sensor. The details of this

mathematical calculation can be found elsewhere, but what is important to know here is that this is a direct calculation that is not influenced by other materials or effects, and that through the use of Fast Fourier Transforms these calculations can be performed very quickly. A magnetic field image can be converted to a current density image in about 1 or 2 seconds.

Applications using a Scanning SQUID Microscope

Scanning SQUID Microscope can detect all types of shorts and conductive paths including Resistive Opens (RO) defects such as cracked or voided bumps, Delaminated Vias, Cracked traces/mouse bites and Cracked Plated Through Holes (PTH). It can map power distributions in packages as well as in 3D Integrated Circuits (IC) with Through-Silicon Via (TSV), System in Package (SiP), Multi-Chip Module (MCM) and stacked die. SQUID scanning can also isolate defective components in assembled devices or Printed Circuit Board (PCB).

Short Localization in Advanced Wirebond Semiconductor Package

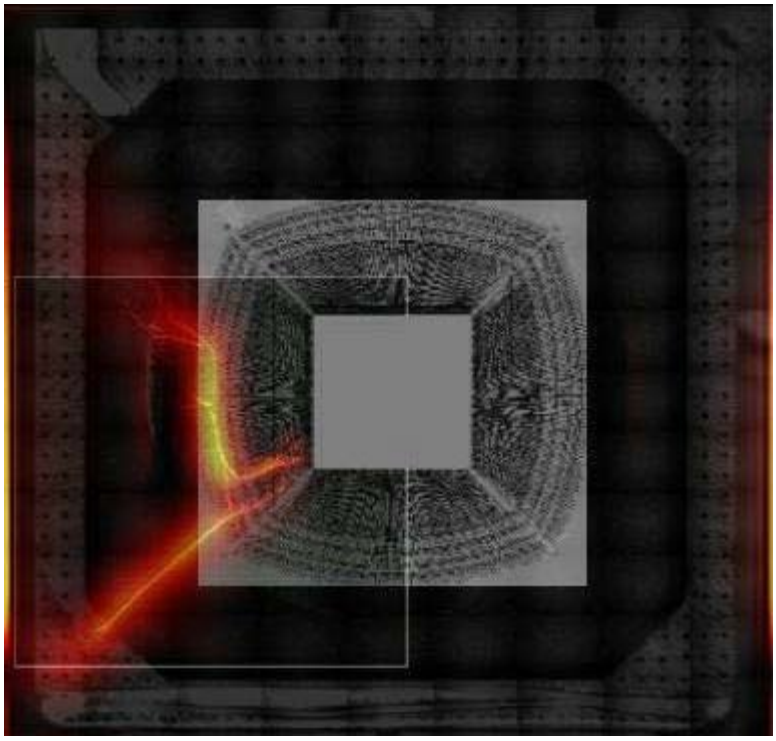

Current Image overlaid the optical image of the part and the layout of the part

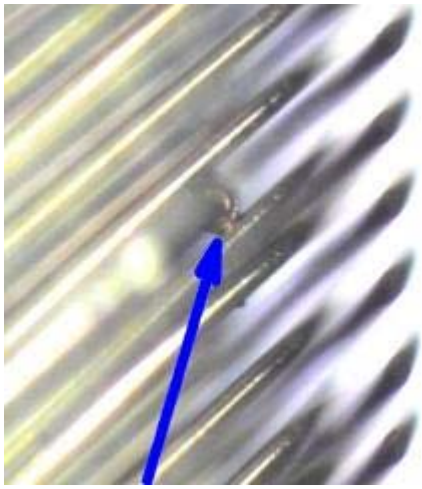

Optical image of the decapped wire bonds that are lifted from the die and touching another wire bond

Advanced wire-bond packages, unlike traditional Ball Grid Array (BGA) packages, have multiple pad rows on the die and multiple tiers on the substrate. This package technology has brought new challenges to failure analysis. To date, Scanning Acoustic Microscopy (SAM), Time Domain Reflectometry (TDR) analysis, and Real-Time X-ray (RTX) inspection were the non-destructive tools used to detect short faults. Unfortunately, these techniques do not work very well in advanced wire-bond packages. Because of the high density wire bonding in advanced wire-bond packages, it is extremely hard to localize the short with conventional RTX inspection. Without detailed information as to where the short might occur, attempting destructive decapsualtion to expose both die surface and bond wires is full of risk. Wet chemical etching to remove mold compound in a large area often results in over-etching. Furthermore, even if the package is successfully decapped, visual inspection of the multi-tiered bond wires is a blind search.

The Scanning SQUID Microscopy (SSM) data are current density images and current peak images. The current density images give the magnitude of the current, while the current peak images reveal the current path with a ± 3 μm resolution. Obtaining the SSM data from scanning advanced wire-bond packages is only half the task; fault localization is still necessary. The critical step is to overlay the SSM current images or current path images with CAD files such as bonding diagrams or RTX images to pinpoint the fault location. To make alignment of overlaying possible, an optical two-point reference alignment is made. The package edge and package fiducial are the most convenient package markings to align to. Based on the data analysis, fault localization by SSM should isolate the short in the die, bond wires or package substrate. After all non-destructive approaches are exhausted, the final step is destructive deprocessing to verify SSM data. Depending on fault isolation, the deprocessing techniques include decapsulation, parallel lapping or cross-section.

Short in multi-stacked packages

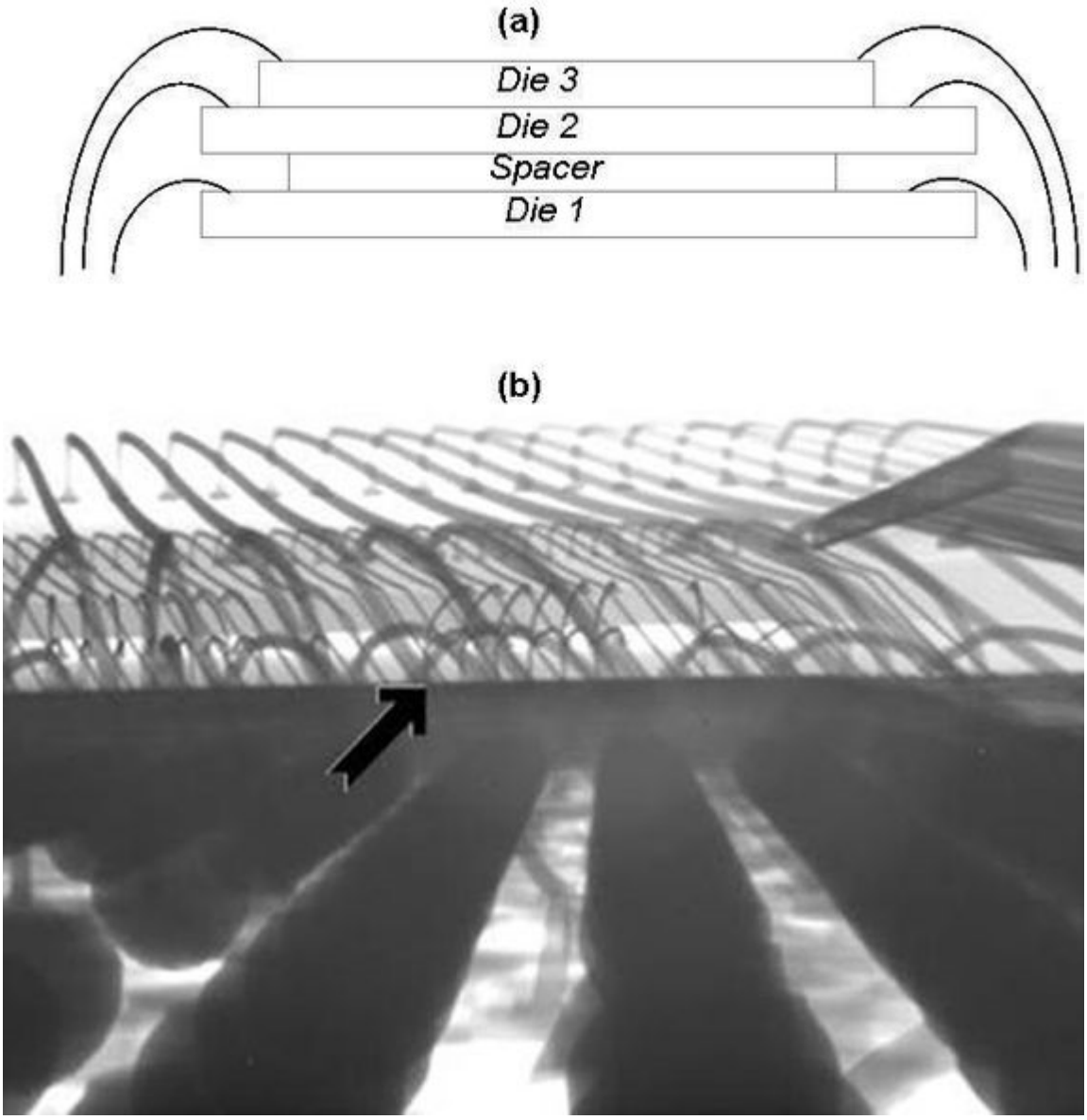

Figure 1(a) Schematic showing typical bond wires in a triple-stacked die package, Figure 1(b) x-ray lateral view of actual triple-stacked die package.

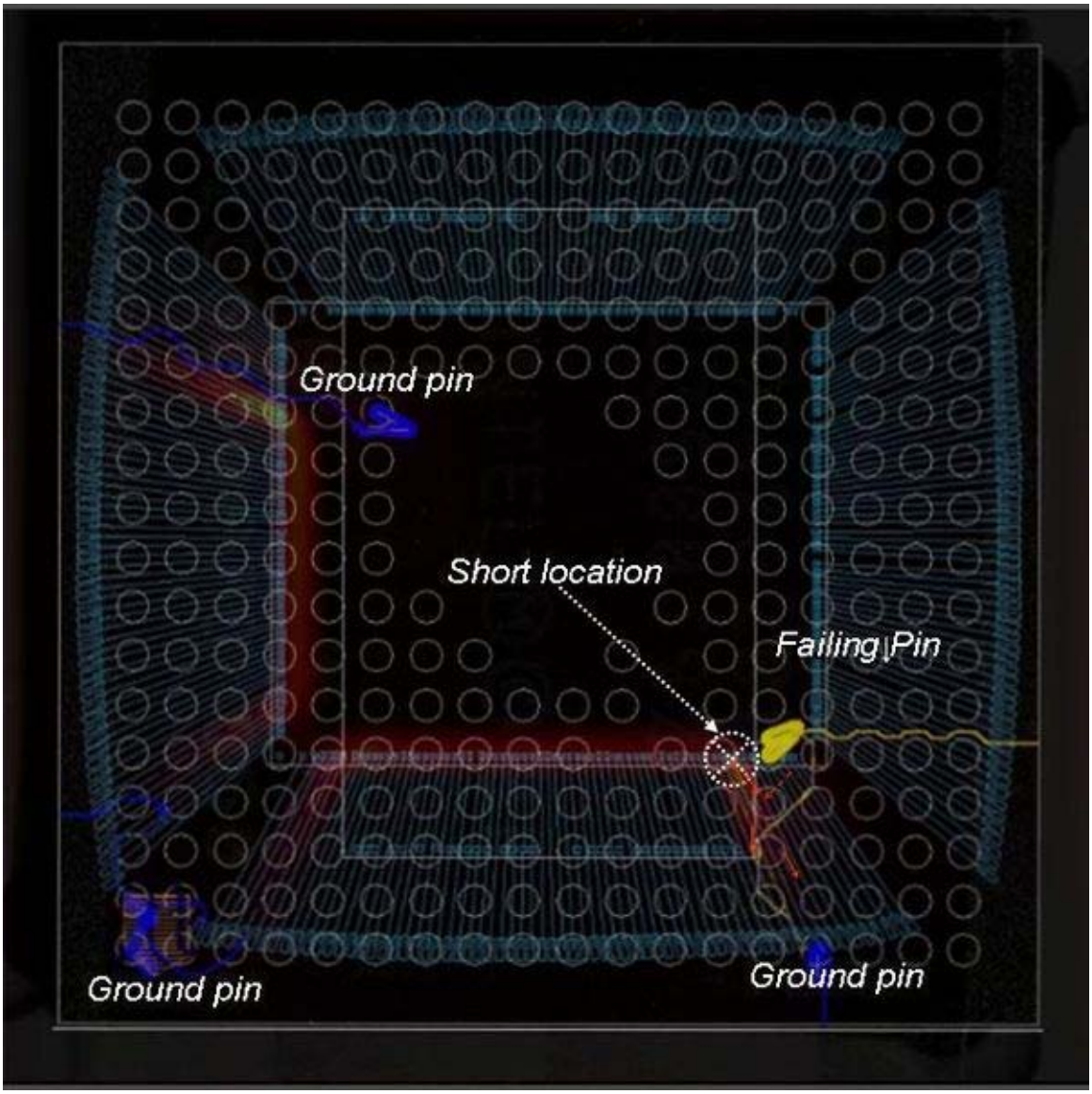

Figure 2: Overlay of current density, optical, and CAD images in triple-stacked die package with electric short failure mode.

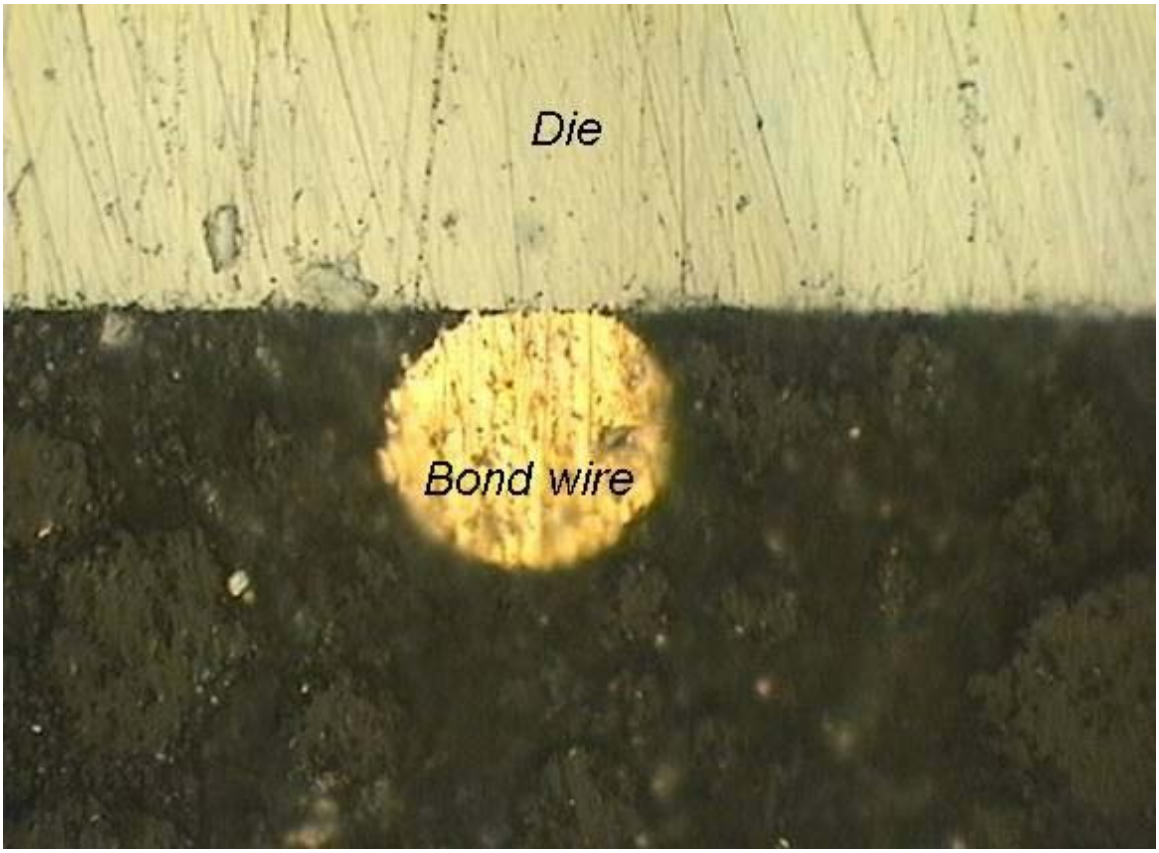

Figure 3: Cross sectional image showing a bond wire touching the die causing signal to ground leakage.

Electric shorts in multi-stacked die packages can be very difficult to isolate non-destructively; especially when a large number of bond wires are somehow shorted. For instance, when an electric short is produced by two bond wires touching each other, x-ray analysis may help to identify potential defect locations; however, defects like metal migration produced at wirebond pads, or bond wires somehow touching any other conductive structures, may be very difficult to catch with non-destructive techniques that are not electrical in nature. Here, the availability of analytical tools that can map out the flow of electrical current inside the package provide valuable information to guide the failure analyst to potential defect locations.

Figure 1a shows the schematic of our first case study consisting of a triple-stacked die package. The x-ray image of figure 1b is intended to illustrate the challenge of finding the potential short locations represented for failure analysts. In particular, this is one of a set of units that were inconsistently failing and recovering under reliability tests. Time domain reflectometry and X-ray analysis were performed on these units with no success in isolating the defects. Also there was no clear indication of defects that could potentially produce the observed electrical short failure mode. Two of those units were analyzed with SSM.

Electrically connecting the failing pin to a ground pin produced the electrical current path shown in figure 2. This electrical path strongly suggests that the current is somehow flowing through all the ground nets though a conductive path located very close to the wirebond pads from the top down view of the package. Based on electrical and layout analysis of the package, it can be inferred that current is either flowing through the wirebond pads or that the wirebonds are somehow touching a conductive structure at the specified location. After obtaining similar SSM results on the two units under test, further destructive analysis focused around the small potential short region, and it showed that the failing pin wirebond is touching the bottom of one of the stacked dice at the specific XY position highlighted by SSM analysis. The cross section view of one of those units is shown in figure 3.

A similar defect was found in the second unit.

Short between pins in molding compound package

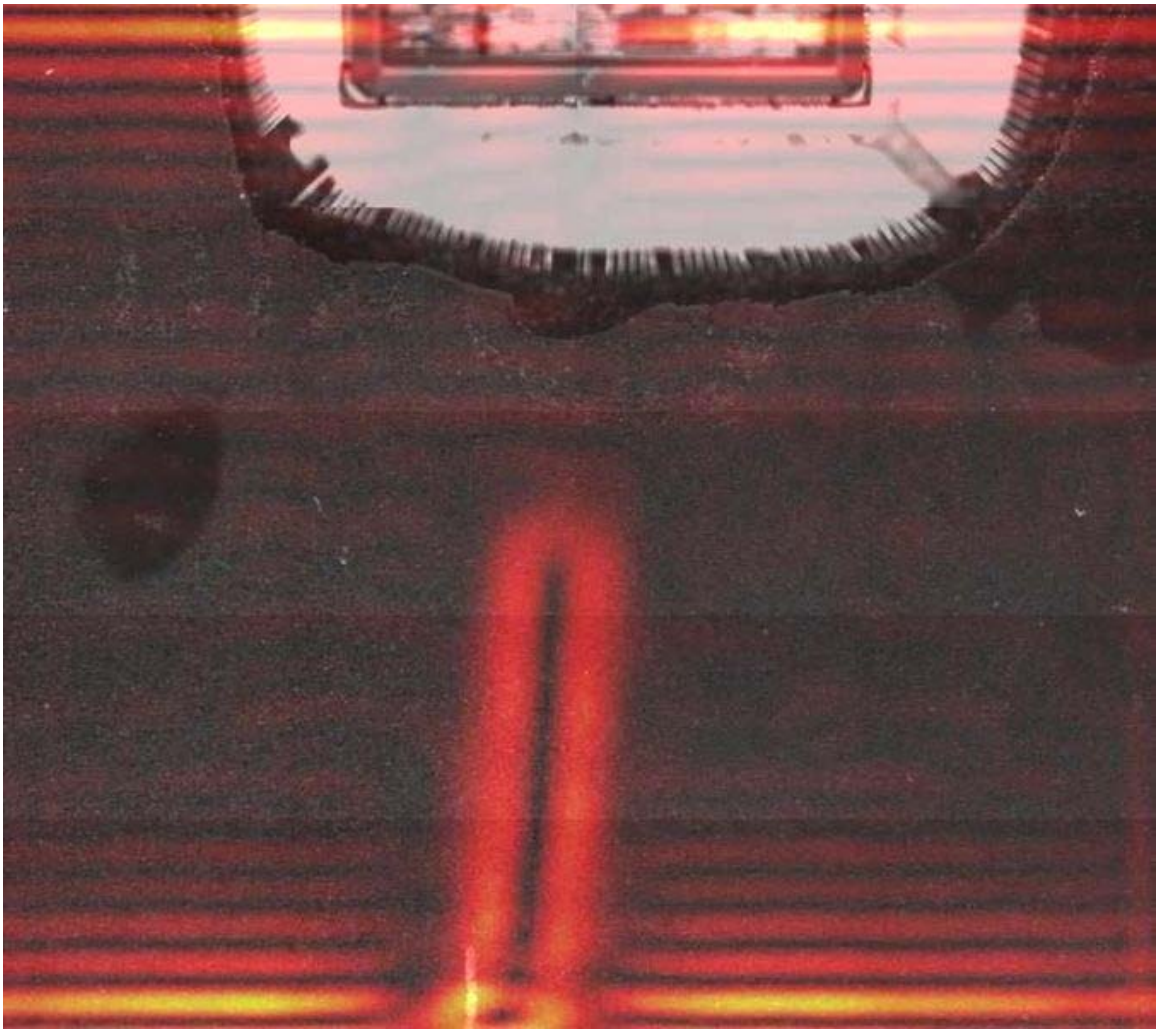

Figure 1 SQUID image of package indicating location of short.

Figure 2: High-resolution radiographic image of filament, measured at 2.9 micrometres wide. Image shows filament running under both shorted leads.

The failure in this example was characterized as an eight-ohm short between two adjacent pins. The bond wires to the pins of interest were cut with no effect on the short as measured at the external pins, indicating that the short was present in the package. Initial attempts to identify the failure with conventional radiographic analysis were unsuccessful. Arguably the most difficult part of the procedure is identifying the physical location of the short with a high enough degree of confidence to permit destructive techniques to be used to reveal the shorting material. Fortunately, two analytical techniques are now available that can significantly increase the effectiveness of the fault localization process.

Superconducting Quantum Interference Device (SQUID) Detection

One characteristic that all shorts have in common is the movement of electrons from a high potential to a lower one. This physical movement of the electrical charge creates a small magnetic field around the electron. With enough electrons moving, the aggregate magnetic field can be detected by superconducting sensors. Instruments equipped with

such sensors can follow the path of a short circuit along its course through a part. The SQUID detector has been used in failure analysis for many years, and is now commercially available for use at the package level. The ability of SQUID to track the flow of current provides a virtual roadmap of the short, including the location in plan view of the shorting material in a package. We used the SQUID facilities at Neocera to investigate the failure in the package of interest, with pins carrying 1.47 milliamps at 2 volts. SQUID analysis of the part revealed a clear current path between the two pins of interest, including the location of the conductive material that bridged the two pins. The SQUID scan of the part is shown in Figure 1.

Low-power radiography

The second fault location technique will be taken somewhat out of turn, as it was used to characterize this failure after the SQUID analysis, as an evaluation sample for an equipment vendor. The ability to focus and resolve low-power x-rays and detect their presence or absence has improved to the point that radiography can now be used to identify features heretofore impossible to detect. The equipment at Xradia was used to inspect the failure of interest in this analysis. An example of their findings is shown in Figure 2. The feature shown (which is also the material responsible for the failure) is a copper filament approximately three micrometres wide in cross-section, which was impossible to resolve in our in-house radiography equipment.

The principal drawback of this technique is that the depth of field is extremely short, requiring many ‘cuts’ on a given specimen to detect very small particles or filaments. At the high magnification required to resolve micrometre-sized features, the technique can become prohibitively expensive in both time and money to perform. In effect, to get the most out of it, the analyst really needs to know already where the failure is located. This makes low-power radiography a useful supplement to SQUID, but not a generally effective replacement for it. It would likely best be used immediately after SQUID to characterize morphology and depth of the shorting material once SQUID had pinpointed its location.

Short in a 3D Package

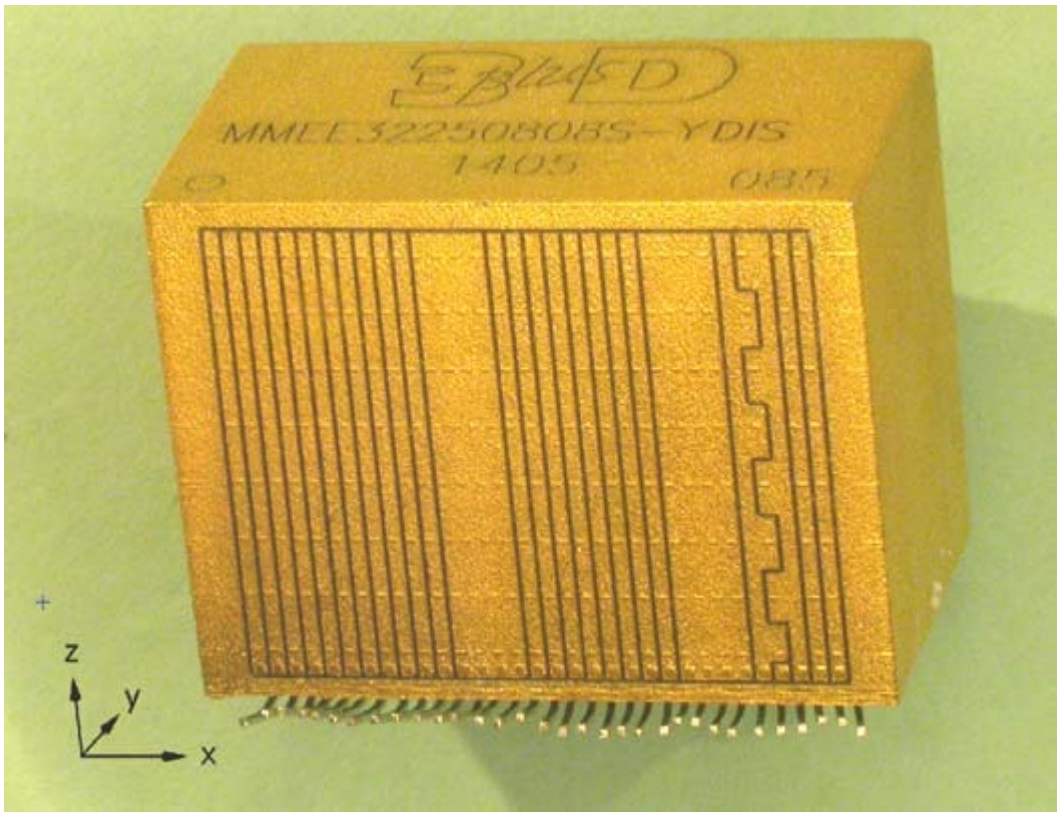

Figure 1: An external view of the EEPROM module shows the coordinate axis used while performing orthogonal magnetic current imaging. These axes are used to define the scanning planes in the body of the paper.

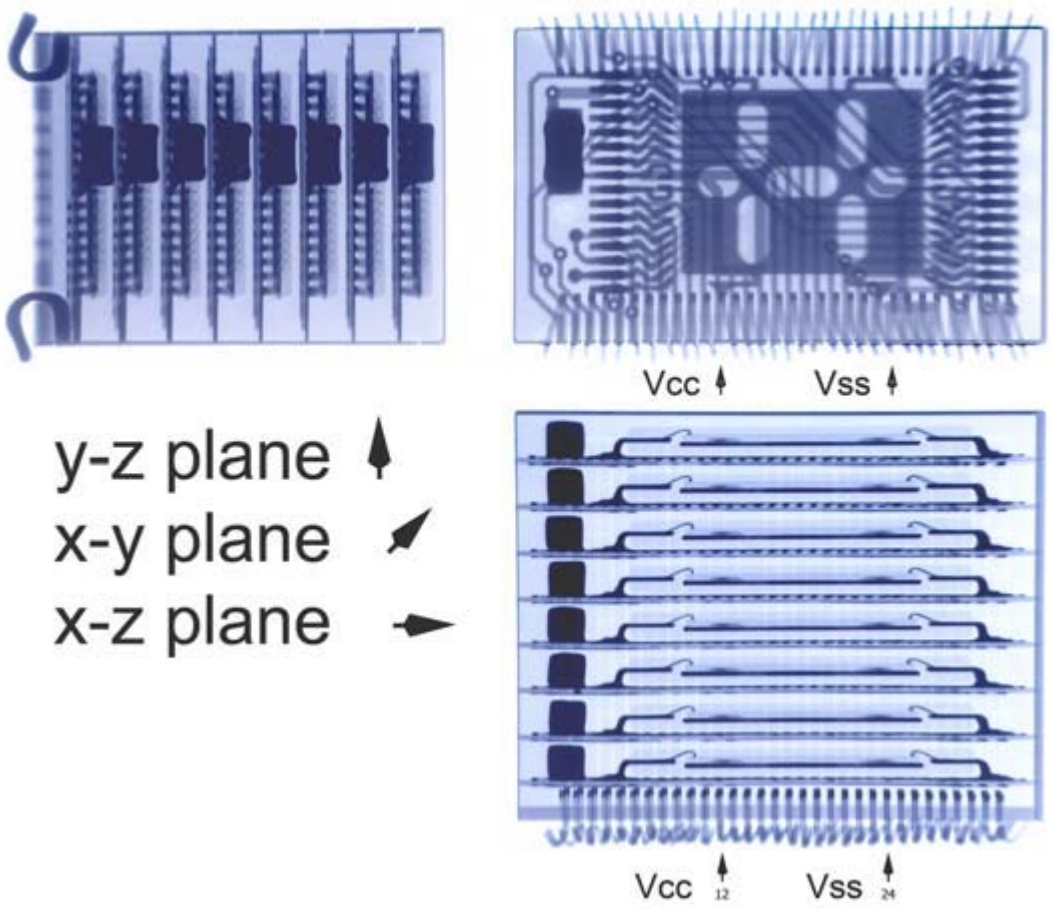

Figure 2: Radiography, showing three orthogonal views of the part, reveals internal construction of the module.

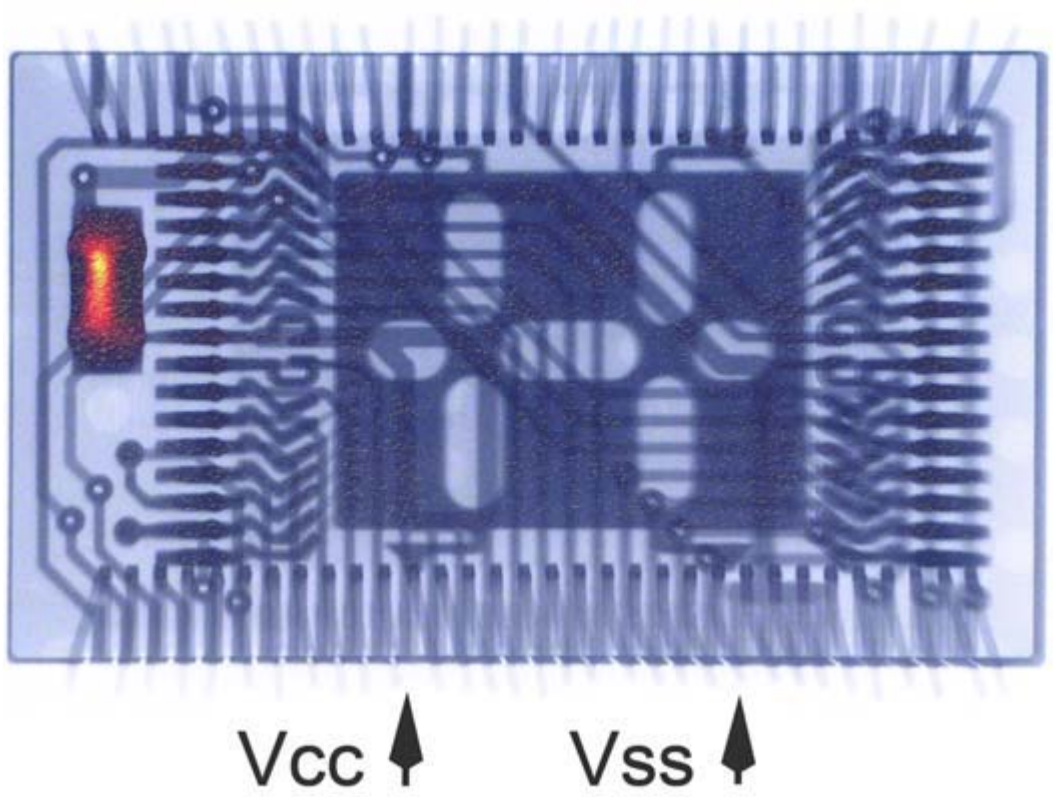

Figure 3: A magnetic current image overlay on an x-ray image of the EEPROM module. Thresholding was used to show only the strongest current at the capacitor of the TSOP08 mini-board. Arrows indicate Vcc and Vss pins. This image is in the x-y plane.

Initial Failure Analysis Examination of the module shown in Figure 1 in the Failure Analysis Laboratory found no external evidence of the failure. Coordinate axes of the device were chosen as shown in Figure 1. Radiography was performed on the module in three orthogonal views: side, end, and top-down; as shown in Figure 2. For purposes of this paper the top-down x-ray view shows the x-y plane of the module. The side view shows the x-z plane, and the end view shows the y-z plane. No anomalies were noted in the radiographic images. Excellent alignment of components on the mini-boards permitted an uncluttered top-down view of the mini-circuit boards. The internal construction of the module was seen to consist of eight, stacked mini-boards, each with a single microcircuit and capacitor. The mini-boards connected with the external module pins using the gold-plated exterior of the package. External inspection showed that laser-cut trenches created an external circuit on the device, which is used to enable, read, or write to any of the eight EEPROM devices in the encapsulated vertical stack. Regarding nomenclature, the laser-trenched gold panels on the exterior walls of the package were labeled with the pin numbers. The eight miniboards were labeled TSOP01 through TSOP08, beginning at the bottom of the package near the device pins.

Pin-to-pin electrical testing confirmed that Vcc Pins 12, 13, 14, and 15 were electrically common, presumably through the common exterior gold panel on the package wall.

Likewise, Vss Pins 24, 25, 26, and 27 were common. Comparison to the xray images showed that these four pins funneled into a single wide trace on the mini-boards. All of the Vss pins were shorted to the Vcc pins with a resistance determined by the I-V slope at approximately 1.74 ohms, the low resistance indicating something other than an ESD defect. Similarly electrical overstress was considered an unlikely cause of failure as the part had not been under power since the time it was qualified at the factory. The three-dimensional geometry of the EEPROM module suggested the use of magnetic current imaging (MCI) on three, or more flat sides in order to construct the current path of the short within the module. As noted, the coordinate axes selected for this analysis are shown in Figure 1.

Magnetic Current Imaging SQUIDs are the most sensitive magnetic sensors known. This allows one to scan currents of 500 nA at a working distance of about 400 micrometres. As for all near field situations, the resolution is limited by the scanning distance or, ultimately, by the sensor size (typical SQUIDs are about 30 μm wide), although software and data acquisition improvements allow locating currents within 3 micrometres. To operate, the SQUID sensor must be kept cool (about 77 K) and in vacuum, while the sample, at room temperature, is raster-scanned under the sensor at some working distance z, separated from the SQUID enclosure by a thin, transparent diamond window. This allows one to reduce the scanning distance to tens of micrometres from the sensor itself, improving the resolution of the tool.

The typical MCI sensor configuration is sensitive to magnetic fields in the perpendicular z direction (i.e., sensitive to the in-plane xy current distribution in the DUT). This does not mean that we are missing vertical information; in the simplest situation, if a current path jumps from one plane to another, getting closer to the sensor in the process, this will be revealed as stronger magnetic field intensity for the section closer to the sensor and also as higher intensity in the current density map. This way, vertical information can be extracted from the current density images. Further details about MCI can be found elsewhere.